

INVESTIGATION ON THE EFFECTS OF IONIC LIQUID
AND IONIC MIXTURE IN BIODEGRADABLE POLYMER
ELECTROLYTES

R.SHANTI D/O RAJANTHARAN

MASTER OF SCIENCE

FACULTY OF ENGINEERING AND SCIENCE
UNIVERSITI TUNKU ABDUL RAHMAN
FEBRUARY 2011

**INVESTIGATION ON THE EFFECTS OF IONIC LIQUID AND IONIC
MIXTURE IN BIODEGRADABLE POLYMER ELECTROLYTES**

By

R. SHANTI D/O RAJANTHARAN

A thesis submitted to the Department of Science,
Faculty of Engineering and Science,
Universiti Tunku Abdul Rahman,
in partial fulfillment of the requirements for the degree of
Master of Science
February 2011

ABSTRACT

INVESTIGATION ON THE EFFECTS OF IONIC LIQUID AND IONIC MIXTURE IN BIODEGRADABLE POLYMER ELECTROLYTES

R. Shanti D/O Rajantharan

Four different series of biodegradable polymer electrolytes based on two different types of natural polymers namely corn starch (CS) and cellulose acetate (CA) were successfully synthesized by solution casting technique. Natural polymers are highly crystalline in nature thus to suppress this region, the polymers were embedded with a common ionic salt known as bis(trifluoromethanesulfonyl)imide (LiTFSI) in the polymer matrix with either 1-allyl-3-methylimidazolium chloride ([Amim] Cl) or deep eutectic solvent (DES), the mixture of choline chloride and urea in specific ratio. The effectiveness between the ionic liquid and ionic mixture in suppressing the crystalline region were visualized by various physical and electrochemical analyses.

The initial development of polymer electrolytes was completed upon incorporation of DES in both the CS and CA matrix with the presence of LiTFSI and was labeled as System I and II respectively. The highest ionic conductivity for both the systems falls at 10^{-3} S cm⁻¹. To further improve the ionic conductivity the other two remaining systems, CS: LiTFSI and CA: LiTFSI based polymer electrolytes were prepared by plasticizing with

[Amim] Cl and was labeled as System III and IV respectively.

Incorporation of [Amim] Cl in the polymer electrolytes improves the ionic conductivity until it hits 10^{-2} S cm⁻¹ which was higher in one order compared to the DES-plasticized systems. This was attributed to the high chloride ion concentration possessed by [Amim] Cl that imparts an unusual solvent property which further boosts the amorphocity of the matrix and induces an enhancement in the ionic conductivity.

Based on the overall results, systems containing corn starch exhibits slightly lower maximum ionic conductivity compared to CA based polymer electrolytes. The reason is CS are highly in crystalline nature compared to CA due to the presence of branched amylopectin which is hard to be diffused and hence restricts the ionic transport mechanism.

ACKNOWLEDGEMENTS

I would like to grab this golden opportunity to overstate my sincere gratitude to my supervisors, Drs. Ramesh T. Subramaniam (ex-supervisor) and Morris A G Ezra for helping me to complete the writing of this dissertation as well as the challenging research that lies behind it. I really appreciate their enthusiasm, inspiration, and his great efforts to explain things concise and precise concerning to my project. Also, throughout my thesis-writing period, they have provided encouragement, sound advice, good teaching, good company, and lots of good ideas. My supervisors have an indispensable role in preparing this thesis by providing lots of sufficient good ideas.

I am indebted to UTAR and UM as it provided me with instruments, apparatus and facilities, as well as a stimulating and conducive working environment for the completion of my research work. On the other hand, I would like to express my appreciation to all the laboratory officers, lab assistants and my team mates for assisting me in many different ways. Without the continuous support from them, it will be a hard time for me to complete my research work fruitfully.

In addition, I wish to extend my deepest appreciation to my entire family members for their continuous support, love and encouragement to persuade my interest in this research and achieve the partial fulfilment of the requirements for the degree program.

APPROVAL SHEET

This thesis entitled “**INVESTIGATION ON THE EFFECTS OF IONIC LIQUID AND IONIC MIXTURE IN BIODEGRADABLE POLYMER ELECTROLYTES**” was prepared by R. SHANTI D/O RAJANTHARAN and submitted as partial fulfillment of the requirements for the degree of Master of Science at Universiti Tunku Abdul Rahman.

Approved by:

(Asst. Prof. Dr. MORRIS A G EZRA)

Date:.....

Assistant Professor/Supervisor

Department of Electrical and Electronic Engineering

Faculty of Engineering and Science

Universiti Tunku Abdul Rahman

**UNIVERSITI TUNKU ABDUL RAHMAN
FACULTY OF ENGINEERING AND SCIENCE**

Date: _____

PERMISSION SHEET

It is hereby certified that **R. SHANTI D/O RAJANTHARAN** (ID No: **09UEM09086**) has completed this thesis entitled “INVESTIGATION ON THE EFFECTS OF IONIC LIQUID AND IONIC MIXTURE IN BIODEGRADABLE POLYMER ELECTROLYTES” under the supervision of DR MORRIS A G EZRA from the Department of Electrical and Electronic Engineering, Faculty of Engineering and Sciences.

I understand that University will upload softcopy of my thesis in pdf format into UTAR Institutional Repository, which will be made accessible to UTAR community and public.

Yours truly,

(R. SHANTI D/O RAJANTHARAN)

DECLARATION

I hereby declare that the dissertation is based on my original work except for quotations and citations which have been duly acknowledged. I also declare that it has not been previously or concurrently submitted for any other degree at UTAR or other institutions.

R.SHANTI D/O RAJANTHARAN

Date:

TABLE OF CONTENTS

| | Page |
|--|--------------|
| ABSTRACT | ii |
| ACKNOWLEDGEMENTS | iv |
| APPROVAL SHEET | v |
| PERMISSION SHEET | vi |
| DECLARATION | vii |
| LIST OF PUBLICATIONS | xi |
| LIST OF TABLES | xii |
| LIST OF FIGURES | xiv |
| LIST OF ABBREVIATIONS | xviii |
| | |
| CHAPTER | |
| | |
| 1.0 INTRODUCTION | 1 |
| 1.1 Separator in batteries | 1 |
| 1.2 Polymer | 4 |
| 1.3 Overall view | 7 |
| 1.4 Problem statement | 7 |
| 1.5 Research objectives | 8 |
| 1.6 Scope of research | 8 |
| 1.6.1 Preparation method | 8 |
| 1.6.2 Characterisations | 10 |
| | |
| 2.0 LITERATURE REVIEW | 12 |
| 2.1 Introduction to polymer electrolytes | 12 |
| 2.1.1 Gel polymer electrolytes | 15 |
| 2.1.2 Thin film polymer electrolytes | 17 |
| 2.2 Advantages of polymer electrolytes | 17 |
| 2.3 Limitations of polymer electrolytes | 19 |
| 2.4 Methods of enhancing ionic conductivity | 20 |
| 2.4.1 Polymer blending | 20 |
| 2.4.2 Mixed salts system | 21 |
| 2.4.3 Addition of plasticisers | 23 |
| 2.5 Corn starch | 26 |
| 2.6 Cellulose acetate | 29 |
| 2.7 Lithium bis(trifluoromethanesulfonyl)imide | 31 |
| 2.8 Deep eutectic solvent | 35 |
| 2.9 1-Allyl-3-methylimidazolium chloride | 39 |

| | | |
|------------|--|-----------|
| 3.0 | MATERIALS AND METHODS | 43 |
| 3.1 | Materials | 43 |
| 3.2 | Synthesis of deep eutectic solvent (DES) | 43 |
| 3.3 | Preparation of polymer electrolytes | 44 |
| | 3.3.1 CS based polymer electrolytes | 45 |
| | 3.3.2 CA based polymer electrolytes | 45 |
| 3.4 | Physical appearance of the developed polymer electrolytes | 46 |
| 3.5 | Instrumentations | 47 |
| | 3.5.1 Alternating current (AC) impedance spectroscopy | 48 |
| | 3.5.2 Ubbelohde capillary viscometer | 50 |
| | 3.5.3 Horizontal attenuated total reflectance- Fourier transform infrared (HATR-FTIR) | 51 |
| | 3.5.4 X-ray diffractometry (XRD) | 52 |
| | 3.5.5 Scanning electron microscopy (SEM) | 53 |
| | 3.5.6 Atomic force microscopy (AFM) | 54 |
| | 3.5.7 Thermogravimetric analysis (TGA) | 54 |
| 4.0 | RESULTS AND DISCUSSION: SYSTEM I | 55 |
| 4.1 | Conductivity studies at room temperature | 55 |
| 4.2 | Scanning electron microscopy (SEM) | 58 |
| 4.3 | Horizontal attenuated total reflectance- Fourier transform infrared (HATR-FTIR) | 61 |
| 4.4 | Frequency dependence of loss tangent studies | 65 |
| 4.5 | Temperature dependent conductivity studies | 68 |
| 4.6 | Thermogravimetric analysis | 70 |
| 5.0 | RESULTS AND DISCUSSION: SYSTEM II | 73 |
| 5.1 | Conductivity studies at room temperature | 73 |
| 5.2 | Relative viscosity studies | 76 |
| 5.3 | Frequency dependence of loss tangent studies | 79 |
| 5.4 | Scanning electron microscopy (SEM) | 82 |
| 5.5 | Horizontal attenuated total reflectance- Fourier transform infrared (HATR-FTIR) | 85 |
| 5.6 | X-ray diffractometry (XRD) | 91 |
| 5.7 | Temperature dependent conductivity studies | 95 |
| 5.8 | Conductivity retained studies | 97 |
| 5.9 | Thermogravimetric analysis | 99 |

| | | |
|------------|--|------------|
| 6.0 | RESULTS AND DISCUSSION: SYSTEM III | 102 |
| 6.1 | Conductivity studies at room temperature | 102 |
| 6.2 | Relative viscosity studies | 104 |
| 6.3 | Frequency dependence of loss tangent studies | 107 |
| 6.4 | Temperature dependent conductivity studies | 110 |
| 6.5 | Horizontal attenuated total reflectance- Fourier transform infrared (HATR-FTIR) | 113 |
| 6.6 | Thermogravimetric analysis | 118 |
| 7.0 | RESULTS AND DISCUSSION: SYSTEM IV | 121 |
| 7.1 | Conductivity studies at room temperature | 121 |
| 7.2 | Relative viscosity studies | 124 |
| 7.3 | Atomic force microscopy (AFM) | 126 |
| 7.4 | Temperature dependent conductivity studies | 128 |
| 7.5 | Conductivity retained studies | 131 |
| 7.6 | Horizontal attenuated total reflectance- Fourier transform infrared (HATR-FTIR) | 133 |
| 7.7 | X-ray diffractometry (XRD) | 140 |
| 7.8 | Frequency dependence of loss tangent studies | 142 |
| 7.9 | Thermogravimetric analysis | 145 |
| 8.0 | RESULTS AND DISCUSSION: COMPARISON | 148 |
| 8.1 | Comparison of CS: LiTFSI matrix plasticised with DES and [Amim] Cl | 148 |
| 8.2 | Comparison of CA: LiTFSI matrix plasticised with DES and [Amim] Cl | 150 |
| 8.3 | Comparison between CS and CA based polymer electrolytes | 152 |
| 9.0 | CONCLUSIONS | 153 |
| | REFERENCES | 155 |

LIST OF PUBLICATIONS

- International Journals
 - S. Ramesh, R. Shanti & R. Durairaj (2010). *Journal of Non-Crystalline Solid*, 357, 1357-1363. [Journal Impact factor: 1.252 (Tier 1)]
 - S. Ramesh, R. Shanti, Ezra Morris & R. Durairaj. Utilisation of corn starch in the production of “green” biodegradable polymer electrolytes. (communicated to *Materials Research Innovations*)

- International Conferences
 - S. Ramesh & R. Shanti (2010). Enhancement in the performance of corn starch based polymer electrolytes incorporating deep eutectic solvent for use in “green” polymer batteries. International Chemical Congress of Pacific Basin Societies, Hawaii, USA, 15-20 December 2010.
 - S. Ramesh, R. Shanti, Ezra Morris & R. Durairaj (2010). Utilisation of corn starch in the production of “green” biodegradable polymer electrolytes. Proceedings of 3rd International Conference on Functional Materials and Devices (ICFMD), Kuala Terengganu, Malaysia, 14-17 June 2010.

- National Conference
 - S. Ramesh, R. Shanti & Chin Siew Fai (2010). Conductivity and FTIR studies of low molecular weight poly (vinyl chloride) (PVC) based polymer electrolytes. Proceedings of Malaysian Science Technology Congress (MSTC), Kuala Lumpur, Malaysia, 9-11 November 2010.

LIST OF TABLES

| Table | | Page |
|--------------|--|-------------|
| 1.1 | Summary of the developed four systems | 9 |
| 3.1 | Composition ratio of polymer electrolytes in all four systems with the respective designations | 44 |
| 3.2 | Physical appearance of casted polymer electrolytes for four different systems | 46 |
| 3.3 | Instruments used in characterising the four developed systems | 47 |
| 4.1 | Band assignments and wavenumbers exhibited by pure constituents namely CS, LiTFSI and DES | 61 |
| 4.2 | Relaxation frequencies of samples with different DES content | 66 |
| 4.3 | Activation energies of samples calculated using Arrhenius equation | 69 |
| 4.4 | The maximum decomposition temperatures and percentages of total weight loss for pure CS, DES-0, DES-20 and DES-80 | 71 |
| 5.1 | Band assignments and wavenumbers of some important peaks in FTIR spectra exhibited by pure CA, pure LiTFSI and pure DES | 85 |
| 5.2 | Maximum decomposition temperatures and percentages of total weight loss for pure CA, CA-0, CA-40 and CA-60 by TGA analysis | 100 |
| 6.1 | Relaxation frequencies for samples with different [Amim] Cl content | 108 |
| 6.2 | The activation energies (E_a) exhibited by polymer electrolytes with different [Amim] Cl concentration | 111 |
| 6.3 | Band assignments and wavenumbers exhibited by pure CS, pure LiTFSI and pure [Amim] Cl | 114 |
| 6.4 | The maximum decomposition temperatures and percentages of total weight loss for pure CS, CS-0, CS-20 and CS-80 | 119 |

| | | |
|-----|--|-----|
| 7.1 | The activation energies (E_a) exhibited by polymer electrolytes with different [Amim] Cl concentration | 130 |
| 7.2 | Band assignments and wavenumbers exhibited by pure CA, pure LiTFSI and pure [Amim] Cl | 133 |
| 7.3 | Relaxation frequencies of samples with different [Amim] Cl content | 143 |
| 7.4 | Maximum decomposition temperatures and percentages of total weight loss for pure CA, IL-0, IL-40 and IL-80 by TGA analysis | 146 |

LIST OF FIGURES

| Figures | | Page |
|---------|---|------|
| 2.1 | Structure of CS containing two different chains | 26 |
| 2.2 | Structure of CA | 29 |
| 2.3 | Structure of LiTFSI | 32 |
| 2.4 | Resonance states of the TFSI anion | 32 |
| 2.5 | Dissociation of LiTFSI forming its respective cation and anion | 33 |
| 2.6 | Molecular formulas of choline chloride and urea | 37 |
| 2.7 | Structure of [Amim] Cl | 40 |
| 3.1 | A typical complex impedance plot | 48 |
| 4.1 | The dependence of log ionic conductivity (σ) values of CS: LiTFSI: DES polymer electrolytes at room temperature | 55 |
| 4.2 | SEM micrographs of CS: LiTFSI: DES matrix when different concentration of DES is incorporated in (a) DES-20, (b) DES-30 and (c) DES-40, with the bar length of 1 μm = 0.1 cm for the image dimension 26.0 cm x 19.5 cm | 58 |
| 4.3 | FTIR spectra of (a) pure CS, (b) pure LiTFSI, (c) DES-0, (d) pure DES and (e) DES-80 | 62 |
| 4.4 | The changes in intensity of C-SO ₂ -N band for (a) pure LiTFSI and (b) DES-0 | 63 |
| 4.5 | Variation of $\tan \delta$ as a function of angular frequency for samples DES-20 (\square), DES-40 (\diamond) and DES-60 (Δ) at room temperature | 65 |
| 4.6 | Variation of $\tan \delta$ as a function of angular frequency for sample DES-80 at room temperature | 65 |
| 4.7 | Arrhenius plots of log ionic conductivity against reciprocal temperature for samples DES-20 (\blacktriangle), DES-40 (\blacklozenge), DES-60 (\blacksquare) and DES-80 (x) | 68 |

| | | |
|------|--|-----|
| 4.8 | Thermogravimetric curves for pure CS (\diamond), DES-0 (\square), DES-20 (Δ) and DES-80 (\times) | 70 |
| 5.1 | Variation of log ionic conductivity (σ) as a function of DES concentration at room temperature | 73 |
| 5.2 | The dependence of relative viscosity (η_{rel} , \blacklozenge) and fluidity (ϕ , \blacktriangle) upon DES concentration at room temperature | 76 |
| 5.3 | Variation of $\tan \delta$ as a function of angular frequency for samples CS-0 (\diamond), CA-40 (\square), CA-50 ($+$) and CA-60 (\times) | 79 |
| 5.4 | SEM micrographs of samples (a) CA-0, (b) CA-40, (c) CA-50 and (d) CA-60 obtained at room temperature, with the bar length of $1 \mu\text{m} = 0.2 \text{ cm}$ for the image dimension $27.0 \text{ cm} \times 20.3 \text{ cm}$ | 82 |
| 5.5 | FTIR spectra of (a) pure CA, (b) pure LiTFSI and (c) CA-0 | 86 |
| 5.6 | The changes in intensity of C=O symmetric band for (a) pure CA and (b) CA-0 | 87 |
| 5.7 | FTIR spectra of (a) CA-0, (b) pure DES, (c) CA-40 and CA-60 | 88 |
| 5.8 | XRD patterns of pure CA that present in two different states (a) powder and (b) thin film forms | 91 |
| 5.9 | XRD patterns of (a) pure CA-thin film, (b) CA-0, (c) CA-40, (d) CA-60 and pure LiTFSI in the inset | 92 |
| 5.10 | Arrhenius plots of log ionic conductivity (σ) against reciprocal temperature for samples CA-40 (\blacklozenge) and CA-60 (\blacksquare) | 95 |
| 5.11 | Variation of log ionic conductivity as a function of storage time for samples CA-0 (\blacktriangle), CA-20 (\bullet), CA-40 (\blacksquare) and CA-60 (\blacklozenge) at room temperature | 97 |
| 5.12 | Thermogravimetric curves of pure CA (\times), CA-0 (\blacklozenge), CA-40 (\blacksquare) and CA-60 (\blacktriangle) | 99 |
| 6.1 | Variation of log ionic conductivity (σ) values of CS: LiTFSI: [Amim] Cl polymer electrolytes as a function of [Amim] Cl concentration | 102 |

| | | |
|-----|--|-----|
| 6.2 | Variation of relative viscosity (η_{rel}) of CS: LiTFSI: [Amim] Cl polymer electrolytes as a function of [Amim] Cl concentration at room temperature | 105 |
| 6.3 | Variation of $\tan \delta$ with angular frequency at room temperature for samples CS-20 (Δ), CS-40 (\diamond), CS-60 (\square) and CS-80 (in the inset) | 107 |
| 6.4 | Arrhenius plots of log ionic conductivity (σ) against reciprocal temperature for samples CS-20 (\diamond), CS-40 (\blacksquare), CS-60 (\blacktriangle) and CS-80 (x) | 110 |
| 6.5 | FTIR spectra of (a) pure CS, (b) pure LiTFSI and (c) CS-0 | 113 |
| 6.6 | The changes in intensity of C-SO ₂ -N band for (a) pure LiTFSI and (b) CS-0 | 115 |
| 6.7 | FTIR spectra of (a) CS-0, (b) pure [Amim] Cl, (c) CS-20 and (d) CS-80 | 116 |
| 6.8 | Thermogravimetric curves for pure CS (\diamond), CS-0 (\blacksquare), CS-20 (\blacktriangle) and CS-80 (x) | 118 |
| 7.1 | The variation of ionic conductivity as a function of [Amim] Cl concentration at room temperature | 121 |
| 7.2 | Variation of relative viscosity (η_{rel}) as a function of [Amim] Cl concentration at room temperature | 124 |
| 7.3 | AFM images for samples (a) IL-40, (b) IL-50, (c) IL-60 and (d) IL-80 | 126 |
| 7.4 | Arrhenius plots of log ionic conductivity (σ) against reciprocal temperature for samples IL-20 (\diamond), IL-40 (\blacksquare), IL-60 (\blacktriangle) and IL-80 (x) | 128 |
| 7.5 | Variation of log ionic conductivity with storage time for samples IL-0 (\diamond), IL-40 (\blacktriangle) and IL-80 (\blacksquare) at room temperature | 131 |
| 7.6 | FTIR spectra of (a) pure CA, (b) pure LiTFSI and (c) IL-0 | 135 |
| 7.7 | The changes in intensity of C=O symmetric band for (a) pure CA and (b) IL-0 | 136 |
| 7.8 | FTIR spectra of (a) IL-0, (b) pure [Amim] Cl, (c) IL-40 and (d) IL-80 | 137 |

| | | |
|------|--|-----|
| 7.9 | The diffraction patterns of (a) pure CA (thin film), (b) IL-0, (c) IL-40, (d) IL-80 and pure LiTFSI in the inset | 140 |
| 7.10 | Variation of $\tan \delta$ with angular frequency for IL-0 (\diamond), IL-40 (Δ) and IL-80 (x) at room temperature | 142 |
| 7.11 | Thermogravimetric curves for pure CA (\diamond), IL-0 (\square), IL-40 (Δ) and IL-80 (x) | 145 |
| 8.1 | Variation of logarithm ionic conductivity of CS: LiTFSI matrix as a function of plasticiser content for DES (\blacklozenge) and [Amim] Cl (\blacksquare) | 148 |
| 8.2 | Variation of logarithm ionic conductivity of CA: LiTFSI matrix as a function of plasticiser content for DES (\blacksquare) and [Amim] Cl (\blacklozenge) | 150 |

LIST OF ABBREVIATIONS

| | |
|----------------------|---|
| [Amim] Cl | 1-allyl-3-methylimidazolium chloride |
| <i>A</i> | Area of the disc electrodes in cm ² |
| CA | Cellulose acetate |
| <i>C_p</i> | Parallel equivalent static capacitance / Specific heat capacity |
| CS | Corn starch |
| DES | Deep eutectic solvent |
| FTIR | Fourier transform infrared |
| <i>G</i> | Conductance in S cm ⁻¹ |
| IL | Ionic liquid |
| <i>L</i> | Thickness of the thin film in cm |
| Li ⁺ | Lithium conducting ion |
| LiTFSI | Lithium bis(trifluoromethanesulfonyl)imide |
| PEO | Poly(ethylene oxide) |
| PMMA | Poly(methyl methacrylate) |
| PVA | Poly(vinyl alcohol) |
| PVAc | Poly(vinyl acetate) |
| <i>R_b</i> | Bulk impedance in Ohm |
| Rms | Root mean square |
| RTIL | Room temperature ionic liquid |
| SPE | Solid polymer electrolytes |
| Tan δ | Dissipation loss tangent |
| <i>T_d</i> | Decomposition temperature |

| | |
|--------------|------------------------------------|
| TGA | Thermal gravimetric analysis |
| η | Viscosity |
| η_{rel} | Relative viscosity |
| σ | Conductivity in S cm ⁻¹ |
| ω | Angular frequency in Hz |

CHAPTER 1

INTRODUCTION

1.1 Separator in batteries

Batteries are one of the core applications that extensively being developed under the energy storage technology. This energy storage device is capable in conducting the current due to the presence of two primary functional components which are the anode consisting of lithium intercalated graphite with a low electrochemical potential and a transition-metal oxide cathode with high potential which both can reversibly intercalate and release lithium ions (Li^+). Although the presence of the two active solid electrodes are essential in producing the current yet these two different charged electrodes are prohibited to have direct electronic contact.

The direct contact between the electrodes causes excessive free ionic transport which consequently results in short-circuit. Thus, separation between the electrodes is crucial but right after that there are no possibilities in ion migration from anode to cathode attributed to empty spacing. In order to resolve this obstacle, a separator is sandwiched between the two different charged electrodes. The placement of the separator prevents direct physical contact between the electrodes and at the same time it being the medium that facilitates the free ionic transport and isolating electronic flow (Zhang, 2006). The initial scientific term adopted for this separator is electrolyte.

Electrolyte is a substance concentrated with free ionic species, which behaves as an electrically conductive medium. There are a few types of electrolytes present and each of the type distinguished based on its physical states. The typical electrolyte is addressed as ionic solutions based on the distribution of free ions in a solution medium, commonly appear as the solutions of acids, bases or salts whereas molten and solid electrolytes are referred to the membrane where the free conducting ions are being dispersed in a solid matrix. Eventually, some gases may also behave as electrolytes under conditions of high temperature or low pressure. The similar natured substance also can be obtained upon dissolution of biological and synthetic polymer, termed as polyelectrolytes, which contain multiple charged moieties.

In earlier years, the conventional electrolytes used as a separator in batteries were fabricated through the dissolution of various inorganic salts such as lithium hexafluorophosphate (LiPF_6), lithium tetrafluoroborate (LiBF_4) or lithium perchlorate (LiClO_4) in an organic solvent medium. This type of ionic solution was classified as liquid electrolyte. The dissociation of the individual constituents in an organic solvent forming free ions was attributed to the thermodynamic interaction between the solvent and solutes, in a process called solvation. The presence of free ions in the liquid medium conducts an electric current. The urge for better development of liquid electrolytes was consistently being worked out with the incorporation of plasticisers namely, ethylene carbonate (EC), dimethyl carbonate (DMC), and diethyl carbonate (DEC).

Some listed disadvantages of liquid electrolyte, limit its utilisation as a separator in batteries. The most prominent property of an electrolyte is chemically and electrochemically stable towards the electrodes since both of these components have direct surface contact. In contrast to liquid electrolyte, the occurrence of corrosion reactions between the separator and electrodes evident its failure to function continuously as a separator and the lack of this property limits the life period of the batteries. Additionally, this separator must also be mechanically strong in order to withstand the high tension during the battery assembly operation. Eventually, this property can be ignored in liquid counterparts attributed to its physical state. Another shortcoming is the leakage of the harmful aqueous electrolytes from the battery which questions the safety and this leads to a requirement of special sealing or packaging techniques which are neither practical nor economical.

The performance of battery depends on other properties of electrolytes in terms of the energy density, power density and cycle life. The limitation in the spaced occupied in battery is also a prominent factor that influences the excellence of energy storage device. For high energy and power densities, the electrolyte is required to present in a very thin and highly porous form while persisting an appreciable mechanical stability. Here with, efforts were devoted to replace the conventional liquid electrolytes with other upgraded forms with the aid of various classes of polymers to be used as the insulating medium. In earlier years, typical electrolytes were improved to gel polymer electrolytes (GPEs), consequently to composite polymer electrolytes (CPEs) and finally in the form of solid polymer electrolytes (SPEs) to be utilized in the

electrochemical devices. The profound function of electrolytes have dragged most of its utilisation in almost all the solid state devices including fuel cells, solar cells, electrochromic windows and solar-state batteries (Shriver *et al.*, 1981; Armand, 1986; Rajendran *et al.*, 2004; Siva Kumar *et al.*, 2006).

1.2 Polymer

In overcoming the limitations of the conventional liquid electrolyte properties, an effort was derived by using polymers as a medium to hold on the conducting free ions within the matrix formed. Polymer can be referred as macromolecules having high molar masses composed of a large number of repeating structural units. These repeating units were connected to each other by covalent chemical bonding, forming a long chain. The term ‘polymer’ was originated from the Greek word whereby the word *poly* correlates to ‘many’ whereas *mer* refers to ‘part’.

Polymer encompasses a large class of natural and synthetic materials with wide variety of properties which are ubiquitous in everyday life routine. Some examples of naturally occurring polymers are listed as deoxyribonucleic acid (DNA), proteins, starches, cellulose, latex and nucleic acids. Apart from that, the synthetic polymers derived from the natural type are produced commercially on a very large scale such as polystyrene (PS), plastic and nylon.

Polymers were selected as the matrix in developing the separator due to some of its unique features. The most profound characteristic is the

presence of polar functional groups in the polymer chain, forms partial bonding with the lithium conducting ions (Li^+), aid in transporting the mobile free ions from negatively charged electrodes to the positively charged. The ease in tailoring the insulating properties of polymer making it as a semi-conductor via simple blending of additives is another promising feature.

Previously the development of polymer electrolytes were mainly based on synthetic polymers and currently being adversely swapped with the biodegradable type through the employment of natural polymers. This effort was deliberated in order to overcome the environmental problem associated with the previous invention and at the same time to come out with something more greener to the surroundings. Natural polymers are abundantly present in nature from the beginning, some of the examples are cellulose, starch, gelatin, chitin and etc. Instead of the abundance present, natural polymers do possess some other outstanding criteria: 1) sustainable owing to its renewable nature that does not deplete as the petrochemical source, 2) cheap in cost since it is naturally occurring polymer and 3) biodegradable nature that makes it more environmental-friendly (Viera *et al.*, 2007; Xu *et al.*, 2004).

The selection of natural polymer in the development of conducting medium needs a lot of consideration since it is highly crystalline in nature. The crystallinity of polymer is characterised by their degree of crystallinity which ranges from zero for a completely non-crystalline polymer to one for a theoretical completely crystalline polymer. Polymers with the degree of crystallinity approaching zero or one will be transparent, while polymers with

intermediate degrees of crystallinity appears as opaque due to light scattering by crystalline or glassy regions. Thus for many polymers, reduced crystallinity may also be associated with increased transparency.

In order to select the best polymer host in the fabrication of high conducting polymer electrolytes, focused was paid to the totally amorphous polymers. Although this employment gives a high conducting medium but eventually this natured polymers are generally less tough or more scientifically referred as mechanically unstable (will easily break upon bending) and possess low impact-resistant compared to the microcrystalline containing polymers. Since the mechanical stability and impact-resistant have the same weight as the conductivity properties in the development of polymer electrolytes, thus an acceptable degree of crystallinity in the polymer is required, in order to exert an appreciable ionic conductivity with the combination of other desired properties.

1.3 Overall view

In this research, greener alternatives were driven to fabricate biodegradable polymer electrolytes by employing two different types of natural polymers namely, corn starch (CS) and cellulose acetate (CA). This contraption was developed to be used in electrochemical devices such listed are fuel cells, solar cells, electrochromic windows, solar-state batteries and especially in lithium polymer cells. This type of electronic devices require successively high ionic conducting medium that enables it to function at ambient temperature.

1.4 Problem statement

It is well established that lithium ion (Li^+) coordination takes place predominantly in the amorphous domain but since natural polymers are highly in crystalline, therefore CS and CA alone cannot be a suitable medium in developing high conducting polymer electrolytes. Hence, fascinating alternatives were engaged to disrupt the crystalline elastomeric phase in natural polymers by incorporating with either two different types of bio based materials, namely DES (ionic mixture) or [Amim] Cl (ionic liquid) in the matrix formed by CS/CA and LiTFSI. The addition of either DES or [Amim] Cl tailors the insulating properties of CS and CA allowing greater enhancement in the ionic conductivity. The utilisation of DES and [Amim] Cl sustains the biodegradable properties of natural polymers.

1.5 Research objectives

The aim of this research is to synthesise four different systems of biodegradable polymer electrolytes by utilising bio based materials which are more environmental friendly. The four systems are as shown below:

- 1) CS + LiTFSI + DES
- 2) CA + LiTFSI + DES
- 3) CS + LiTFSI + [Amim] Cl
- 4) CA + LiTFSI + [Amim] Cl

Ionic solvent either DES or [Amim] Cl is used to plasticise the matrix formed by CS/CA: LiTFSI. The developed systems were then characterised in terms of electrical, structural and thermal properties to study the influence of DES/ [Amim] Cl content in the polymer electrolytes properties.

1.6 Scope of research

In order to accomplish the set of objectives, the following scope of work has been drawn.

1.6.1 Preparation method

In this study, four different systems of polymer electrolytes were synthesised by dispersing an appropriate amount of either DES or [Amim] Cl into the polymer matrix formed by CS/CA and LiTFSI. The first two systems were developed individually by CS and CA host polymer with the combination of both LiTFSI and DES, which are labeled as Systems I and II,

respectively. Another remaining two systems are similar to the previous contraction only differentiated by the ionic solvent type, [Amim] Cl and labeled as System III and IV, respectively.

The four systems were summarized in Table 1.1. The nature of samples in System I present in both forms, thin film membrane at lower concentration of DES and consequently forms gel-like samples at higher plasticisation. CS system plasticised with [Amim] Cl produced gel-like samples through out the entire composition. Samples with CA as the host polymer present in transparent thin film membrane.

Table 1.1: Summary of the developed four systems

| | |
|---|---|
| System I: | System II: |
| <ul style="list-style-type: none"> • CS • LiTFSI • DES | <ul style="list-style-type: none"> • CA • LiTFSI • DES |
| System III: | System IV: |
| <ul style="list-style-type: none"> • CS • LiTFSI • [Amim] Cl | <ul style="list-style-type: none"> • CA • LiTFSI • [Amim] Cl |

1.6.2 Characterisations

The variation in the polymer electrolytes properties upon plasticising with different amount of either DES or [Amim] Cl were evaluated by subjecting to several different types of characterisation techniques that being tested on its electrical, structural and thermal properties.

The preliminary characterisation technique is alternating current (AC) impedance spectroscopy that was used to test on the polymer electrolytes electrical properties. This measurement was taken at room temperature, various temperature ranges and over a specified storage time. Similar characterisation technique was used to study the frequency dependence of loss tangent.

Additional techniques such are relative viscosity and fluidity, horizontal attenuated total reflectance-Fourier transform infrared (HATR-FTIR) spectroscopy, x-ray diffractometry (XRD) and morphology studies either using scanning electron microscopy (SEM) or atomic force microscopy (AFM) were used to study the structural properties of the developed polymer electrolytes. These scrutinises evident the occurrence of complexation that causes structural disorderliness upon the suppression of crystallinity in CS/CA matrix. Some of the above mentioned scrutinies were not performed on gel-like samples since its physical state is not compatible to be tested with the employed instrument.

The characterization of the polymer electrolytes is then followed by an important aspect from industrial point of view: thermal properties accounting to its heat-resistivity and thermal stability. This characterisation was performed by thermogravimetric analysis (TGA).

CHAPTER 2

LITERATURE REVIEW

2.1 Introduction to polymer electrolytes

Polymer electrolyte is a solvent-free membrane developed from the dissolution of some additives in a high molecular weight polar polymer matrix. This is an ionically conducting phase that widely used as a separator in numerous consumers electronic devices. The development of polymer electrolyte was revealed as the best approach in rendering the traditional electrolyte system. This attributes to its capability in retaining the intrinsic phenomenon needed by a conducting medium in which exhibits the liquid-like conductivity without motion of solvent which consequently appears to be safe. Additionally, the ease in manufacturing the polymer electrolytes into various convenient shapes makes it to appear as promising alternatives.

During the 20th century, extensive types of ionically conducting synthetic polymers were used as structural materials or as electric insulators. In later part, these natured polymers were subsequently tailored as ion conductors by incorporating with appropriate additives. The initial development of polymer electrolyte was worked out by embedding ionic salts in the insulating polymer matrix (Fenton *et al.*, 1973), where a macroscopic solid state is achieved by entanglement or cross-linking. This type of polymer electrolytes are classified as the first generation solid polymer electrolytes.

The first fabrication of solid electrical conductor polymer/salt complex was evolved by a polymer chemist named Peter V. Wright in 1975, utilising poly (ethylene oxide) (PEO) as a host polymer. From the practical standpoint, PEO is not itself an ideal electrolyte, thus proper manipulations was needed to prevent its crystallization and to extent the elastomeric phase which is favorable to high ionic conductivity. Herewith, the first effort to tailor the insulating property of PEO was done by incorporating with two different types of ionic salt namely, sodium and potassium thiocyanates in order to develop a high conducting polymer electrolytes (Wright, 1975).

In later part, several different types of ionic salts namely, lithium perchlorate (LiClO_4), lithium hexafluoroarsenate (LiAsF_6) and lithium trimethanesulfonate (LiCF_3SO_3) were studied replacing the earlier reported ionic salt owing for better development. The employed lithium salts were found to dissolve in the solvating polymer matrix through direct interaction between the cation and electron pairs, as a result of the favorable competition between the solvation energy and lattice energy of the salt. The developed polymer electrolytes were found to behave as a conductor only at the temperature ranging from 60-80°C. Apart from the above mentioned ionic salt, RbSCN, RbI, CsSCN, CsI and $\text{Hg}(\text{ClO}_4)_2$ do been employed to fabricate low temperature amorphous polymer electrolyte systems with PEO.

In progressive years, other structurally similar polymers were extensively studied such as poly (propylene oxide) (PPO) together with other classes of conductive polymers in 1980s. In the year of 1983, some detailed

mechanistic studies were executed and was found that the ionic motion in salt-polymer membrane was not due to charges hopping from site to site. Apparently, it was attributed to the continuous motion occurring in the amorphous elastomeric phase of the polymer material (Berthier *et al.*, 1983; Minier *et al.*, 1984). In here, it was very clear that the conductivity nature of the polymer electrolytes strongly influenced by two major factors which are the presence of amorphous elastomeric fraction and ionic mobility. The ionic mobility is strongly dependent on the ion association, ion-polymer interactions and local relaxations of the polymer.

In later part, PEO was used again to develop a conducting medium but at this point of time the crystallinity of the polymer matrix were suppressed by few other alternatives such as by plasticising with a low molecular weight polar molecule or forming block or comb copolymers. The resultant polymer electrolytes exhibit better ion conduction with the combination of other outstanding properties. This type of development falls under the category of second generation polymer electrolytes. The most commonly used low molecular weight aprotic plasticizers are propylene carbonate (PC) and ethylene carbonate (EC) that having high dielectric constants and low vapour pressure.

The shortcomings of the above mentioned two generations were driven to the third generation. In which, the inherent crystallinity of polymers were suppressed by plasticising salts or ceramic fillers. This new approach was found to improve the electrochemical and mechanical characteristics of the

second generation polymer electrolytes (Appetecchi and Passerini, 2000).

The appealing properties of polymer electrolytes that well fit as a separator for electronic devices urge to a continuous development by using various types of polymers. Previously, most of the research were diversely worked out by employing numerous types of synthetic polymers such listed are poly(vinyl chloride) (PVC), poly(methyl methacrylate) (PMMA), poly(vinylidene fluoride) (PVdF), poly(acrylonitrile) (PAN) and etc. In current years, natural polymers create its own platform in conjunction with the synthetic polymers and some examples of commonly used natural polymers are cellulose acetate, gelatin, corn starch and so forth.

In this research work, two different physical states of polymer electrolytes were developed, gel-like and thin film. The detailed explanation of both mentioned physical states were conversed in the following sub section.

2.1.1 Gel polymer electrolytes

Gels are generally delineated as “polymers and their swollen matters with three dimensional network structures that are insoluble in any solvents” and gels exist under special condition which is not found in solid, liquid and gasses (Osada and Kajiwara, 2001). Polymer gel primarily consist of a polymer network and solvents in which the polymer network envelopes the liquid and prevents it from escaping or in other word we can classify the polymer network as a container that can hold a large amount of solvent.

The characterization of this natured sample falls in between the solid and liquid, their properties vary from viscous liquids to hard solids. The properties of polymer gel depend upon the structure of the polymer network that makes up the gel as well as the interaction of the network and the solvent. Since the polymer networks are solvated by a large amount of trapped solvent thus gels generally possess high mobility.

Since the first report on high conductivity in lithium ion conducting polymer gel electrolytes (Feuillade and Perche, 1975), the polymer gel appears as a promising alternative in producing high mobility membrane or medium in the development of polymer electrolytes. The interest in these materials is due to their potential applications in solid state batteries, electrochromic devices, fuel cells, supercapacitors and etc (Abraham and Alamgir, 1994).

Generally, gel-type polymer electrolytes were obtained from heavily plasticised polymers. This fabrication caught most of the researcher attention in line to some of their unique properties like high value of conductivity at room temperature (10^{-2} – 10^{-4} S/cm), ease in preparation, wide range of composition and hence wider control of properties, good adhesive properties suitable for lamination, good thermal/electrochemical stability etc.

The preparation of CS based gel polymer electrolytes always been done by gelatinising the CS as the first step prior to the immobilization of the additives either salt, plasticizers or fillers (Ning *et al.*, 2009).

2.1.2 Thin film polymer electrolytes

Thin film polymer electrolytes are another alternative derived to substitute the conventional fabrication. This invention is of current interest due to its capability in exhibiting high ionic conductivity and the absence of organic solvent makes it safer to use. This natured conducting medium is built of host polymers that are insulator and upon the dissolution of additives (ionic salts, fillers, plasticizers and etc.) its insulating properties were tailored to semi-conductor which holds the free conducting ions within the matrix formed. Generally, thin film polymer electrolytes exhibit slightly lower ionic conductivity as compared to gel type attribute to its low solvent retention property. But, careful selection of additives easily suppresses the mentioned limitation. The profound mechanical properties that usually own by thin film make it suitable to be used as a separator in electronic devices. Despite that, the ease in preparation method and good thermal stability also make this fabrication more appealing.

2.2 Advantages of polymer electrolytes

Polymer electrolytes are widely used in the applications of electronic devices. This utilisation was stimulated by a number of listed advantages that potentially offered by solid and gel polymer electrolytes when compared to their liquid counterparts: (1) excellent processability and flexibility that could enable the fabrication of ultrathin lithium cells so that high energy and power density could be achieved for versatile applications, (2) safer due to the absence of flammable organic solvents and the much lower reactivity of

macromolecules toward lithium, (3) the possible prevention of the growth of lithium dendrite crystals upon cycling, (4) the high dimensional stability that could lead to the elimination of a separator, so further improvement in both energy density and manufacturing cost could be achieved due to the simplified cell configuration and enhanced packing efficiency. SPEs do possess other advantages such as being low profile, solvent free condition, flexible, light weight and also less chance for electrolytes leakage (Ramesh and Arof, 2001).

Since most of the inventions are extensively worked out for the purpose of commercialisation, thus the development of SPEs will be more compelling due to the ease in manufacturing into shapes which were not found in the conventional liquid containing systems. The convenience in reshaping the polymer electrolytes to the desired preference appeals as an important feature among the mobile phone manufacturers who are constantly working on smaller, thinner and lighter phones that well fit the consumer expectations. Any reasonable size can be produced economically in a very high volume.

An appreciable rigidity of SPEs enables it to form good interface contacts with electrode materials and more importantly, maintain these contacts under stress such as the volume changes associated with cell charging and discharging. Despite of this, SPEs are chemically and electrochemically stable towards the electrodes owing to its solvent free condition. This is another important feature that increases the span life of the storage device. Generally, ionic conduction in SPEs is dominated by the amorphous elastomeric phase (Furusawa *et al.*, 2008).

In this dissertation we are involved in the development of polymer electrolytes utilising natural polymers. The biodegradable nature of the conducting matrix formed makes it more appealing since it is greener to the environment. In site of that, the employment of natural polymers as the host polymer potential in reducing the cost of production in commercial wise which are very much desired by the manufacturers. The cost of production is reduced since it is a renewable resource that naturally available in the surroundings. The utilisation of bio based materials in suppressing the high degree of crystallinity in natural polymer sustains the biodegradable nature.

2.3 Limitations of polymer electrolytes

There are several limitations of polymer electrolytes when reviewed as industrial applications. The profound shortcoming is attributed to its low ionic conductivity which is not compatible for practical applications (Song *et al.*, 1999). This limitation completely drags out the utilisation of polymer electrolytes as the separator since it is a crucial aspect of battery electrolyte. In addition, SPEs have considerably lower energy density and cycle count compared to lithium-ion battery which utilizes electrolyte conducting medium. In current years, the low ionic conductivity of SPEs is easily tailored upon numerous alternatives.

2.4 Methods of enhancing ionic conductivity

Numerous manipulations were derived by number of researchers to enhance the ionic conductivity of polymer electrolytes at ambient temperature, that adaptable to use in consumers electronic devices. The improvement in ionic conductivity was done by means of polymer blending (Yue *et al.*, 2003; Wu *et al.*, 2009; Takegawa *et al.*, 2010), mixed salt system (Ramesh and Arof, 2000), addition of plasticisers (Wang *et al.*, 2005; Pradhan *et al.*, 2005; Ning *et al.*, 2009) and etc.

2.4.1 Polymer blending

Blending of two or more different polymers is an easy method to develop high conducting polymer electrolytes (Morita *et al.*, 1996; Kim *et al.*, 2001) at room temperature. In addition, the ease in controlling the physical properties within the compositional regime is also found to be an appealing factor. The conductivity enhancement through this contraption was induced by the increase in the amorphous elastomeric phase which is responsible in facilitating the lithium conducting ions (Li^+). This method also has significant effect on the thermal and mechanical properties of the polymer electrolytes (Rajendran *et al.*, 2001).

The low ion conduction of natural polymer was feasibly overcome by developing polymeric electrolytes containing the mixture of cellulose, gelatin and starch. An approximate ionic conductivity value of $10^{-5} \text{ S cm}^{-1}$ was

obtained at room temperature, which is very close to the ionic conductivity required for practical purposes (Wu *et al.*, 2009). The resultant polymer electrolytes not only possess good ionic conductivity but also combined with transparency and good adhesion. Thus, it appears as a promising material to be used as solid electrolyte in electrochromic devices.

This polymer blending technique also improves the properties of chitosan film that lack of water resistance and poor mechanical properties by blending with two thermally gelatinised corn starches (Xu *et al.*, 2005). The blending with corn starch component not only appears to be environmental friendly yet attained the desired properties.

Subramaniam *et al.* (2008) studied the performance of perfluorosulfonic acid polymer (Nafion) that was blended with two different types of host polymers namely, cellulose acetate and micro porous polytetrafluoroethylene (PTFE) separately. The electrochemical performance of solid-state EDLCs constructed of Nafion/ PTFE was profound compared to Nafion/ CA membrane. This development was used as an electrolyte in the solid-state EDLC.

2.4.2 Mixed salts system

Polymer electrolyte that composed of double or mixed salt system can enhance the ionic conductivity. In a study carried out by Ramesh and Arof (2000), found that mixed salt system containing mixed cations and mixed

anions exhibits better ionic conductivity than single salt systems. This is because the addition of second component will hinder the formation of aggregates and clusters, thus increasing the mobility of the ionic carriers.

The mixed-salt systems was studied for three poly (ethylene oxide)-inorganic salt complexes: PEO-LiCF₃SO₃-NaI ([EO]/[Li]/[Na] = 8/1/1), PEO-LiCF₃SO₃ ([EO]/[Li] = 4), and PEO-NaI ([EO]/[Na] = 4) (Maccallum *et al.*, 1988). The mixed-salt systems were found to have larger amorphous phase content than either of the single-salt systems and more potential charge carriers. The mixing of salts suppresses the crystalline nature in the polymer matrix and contributes to a dramatic effect upon the lithium motion and microviscosity of the amorphous phase. The similar enhancement in the volume of available amorphous phase upon mixing of salt was studied on the matrix formed between PEO, lithium triflate (LiTf) and sodium iodide (NaI). The increment in the amorphous elastomeric phase improves the ionic conductivity through the reduction in microviscosity which consequently enhances the mobility of lithium ions.

In this research, only one type of ionic salt was incorporated and it serves as an alternative to tailor the insulating property of natural polymer. The anion in the ionic salt induces structural disorderliness whereas the cation involved in enhancing the ionic conductivity.

2.4.3 Addition of plasticisers

Plasticizers are small molecules, that when added to a polymer it will mix between the long polymeric chains affecting the interaction between those chains. As such, plasticisers are the key part of many compounds and can significantly alter the properties of a polymer, both in terms of the processability and the final product. Plasticizers will increase the flexibility, workability and ionic conductivity of the polymer electrolytes.

Most commonly used plasticisers for recent developments in polymer electrolytes are low molecular weight ethylene carbonate (EC) (Wang *et al.*, 2005), propylene carbonate (PC) (Wang *et al.*, 2005) and poly(ethylene glycol) (PEG) (Pradhan *et al.*, 2005). This aprotic solvent suppresses the crystalline region through the complete dissolution of the charge carriers and provides a mobile medium for ions mobility so as to enhance the ionic conductivity of the resultant polymer electrolytes.

Over years, it has been known as one of the most effective ways to improve the ionic conductivity of such polymer electrolytes. The features of selecting a suitable plasticiser includes its higher dielectric constant than that of the pure polymer used, low volatility, low freezing point and high boiling point and its inert nature towards the electrodes (Kumar and Sekhon, 2004).

The key function on the plasticization of the matrix composed of poly(vinyl alcohol) (PVA), potassium hydroxide (KOH), α -Al₂O₃ with propylene

carbonate (PC) were verified by the enhancement in the ionic conductivity by three orders of magnitude to the reading of approximate 10^{-4} S cm⁻¹ compared to the non-plasticised sample (Mohamad and Arof, 2007). Other supporting evidence on the reliability of plasticiser in enhancing the ionic conductivity can be visualised from the system composed of gelatin as a host polymer with two variables namely LiBF₄ and glycerol (Vieira and Pawlicka, 2009). From this analysis it was identified that the effect of glycerol (plasticizer) in enhancing the ionic conductivity is more prominent than the effect obtained by varying the lithium salt content or the effect of the interaction of both variables. The highest conducting sample was identified for sample with the highest content of glycerol and lithium salt with the conductivity value of 2.29×10^{-5} S cm⁻¹.

Apart from the previous worked out method, similar plasticiser were mixed with a type of ionic liquid namely [Amim] Cl to prepare a mixture of plasticisers to plasticise corn starch. Commonly, ionic liquid have extended function of the plasticiser. This finding compensate with the obtained result in which the conductivity was enhanced with increase in [Amim] Cl concentration with the highest conductivity value of $10^{-1.6}$ S cm⁻¹ for TPS with 30 wt. % [Amim] Cl (Ning *et al.*, 2009).

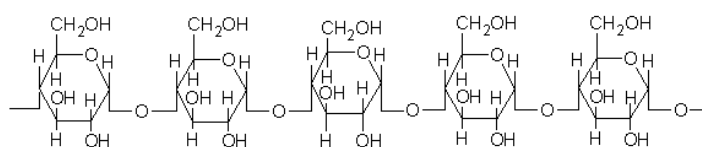
In this dissertation, two different types of ionic solvent having plasticising effect were studied for its workability. One of it is [Amim] Cl and another type is DES which is a type of ionic mixture that shares the similar functions of the ionic liquid. Both of the type falls under the scope of plasticiser since it is capable in transforming the crystalline domain in the

polymer host into amorphous elastomeric phase and additionally facilitates ionic dissociation of dopant salts. The highly ionic nature of ionic liquid is what differentiates itself from other plasticiser, to be a better kind of 'plasticizer'. Other advantages of the utilised ionic liquid and ionic mixture will be conversed in latter subsection.

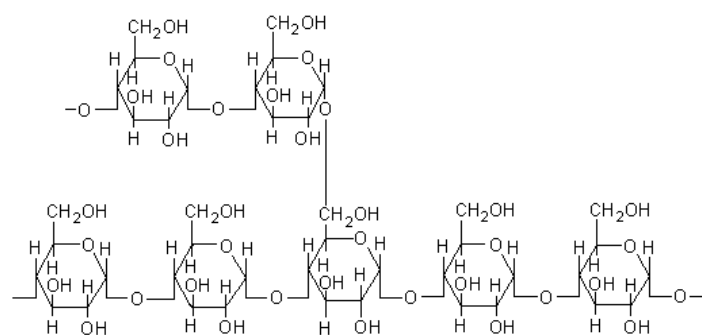
2.5 Corn starch

Corn starch (CS) falls under the category of carbohydrate, consisting of a large number of glucose units joined together by glycosidic bonds. This is a type of renewable source that commonly used to fabricate biodegradable polymer electrolytes owing to its low cost, widely available and relatively easy to handle. In addition, their superior mechanical and electrical properties (Finkenstadt and Willett, 2005) make CS to appear as a promising host polymer. CS can be easily processed as a membrane by dissolving in distilled water ignoring the usage of organic solvents which are not greener to the environment.

CS is a semi-crystalline polymer composed of both linear amylose and branched amylopectin chain (Beninca *et al.*, 2008). The molecular structure of amylose and amylopectin were shown in Figure 2.1 below:



Amylose-linear polysaccharide



Amylopectin-highly branched

Figure 2.1: Structure of CS containing two different chains

Generally, the proportion of these two types of chains will be in the ratio of 20 to 25% amylose and 75 to 80% amylopectin. Amylose is a smaller molecule compared to amylopectin, which both were arranged in starch granules. The amylose molecule is responsible in exhibiting an appreciable ionic conductivity property as the results of the disruption in its structure whereas the superior mechanical property is obtained from the amylopectin chains due to its highly crystalline nature.

The development of CS based polymer electrolytes is always initiated by the gelation of CS powder in distilled water at temperature of 75 °C. This step makes the starch granules to swollen and underwent disruption into smaller aggregates or particles (Takeda *et al.*, 1993; Wang *et al.*, 2009). At this point of time, amylose will be leached out from the starch granules, evident the diffusion only in the amylose chain while persisting the amylopectin chain. The leached smaller amylose molecules form a network that holds water which increases the mixture's viscosity.

The disruption of starch granules induces an increase in the amorphous elastomeric fraction that being the path for the mobility of free ions to conduct ionic conductivity. Regardless to the binding of water molecules in the network formed between the amylose provides a dilute medium that eases the free ions mobility in the polymer electrolytes that consequently enhances the ionic conductivity. The gelation procedure yields a viscous solution which then gelatinised upon cooling, to form semisolid gels that has the ability to form strong adhesive films when dried.

The ratio of amylose in CS are very much lesser compared to amylopectin chain therefore, further structural alternation is needed to develop high conducting polymer membranes. The selection of proper method in disrupting the amylopectin chain is crucial since it is arranged as double helices in branching nature (Beninca *et al.*, 2008; Atwell *et al.*, 1988), making it to present in a highly crystalline form. The only alternative to disrupt this chain is through the incorporation of highly negative charged anions.

The initial approach in developing CS based polymer electrolytes was done through the incorporation of ionic salt, which provides ionic species both anion and cation upon dissolution in the CS matrix. The anions are responsible in inducing the structural disorderliness in the CS matrix for the purpose of enhancing the ionic conductivity. Some examples of ionic salts that been used to evaluate the performance of CS based polymer electrolytes are lithium chloride (LiCl), sodium chloride (NaCl) and potassium chloride (KCl). The addition of this type of alkali metal chlorides improves both the mechanical and conductivities of polymer electrolytes.

A satisfying enhancement in the ionic conductivity was observed when *N, N*-dimethylacetamide (DMAc) with certain concentration of LiCl was used to plasticise starch by melting extrusion. This membrane has a potential application as solid biopolymer electrolytes. The maximum ionic conductivity of $10^{-0.5} \text{ S cm}^{-1}$ was achieved for this contraption when incorporate with 18 wt. % of LiCl (Ning *et al.*, 2009).

In current years, the high degree of crystallinity in CS was suppressed by employing ionic liquid which have similar function of plasticiser. This type of incorporation is believed to be the best approach in converting the crystalline phase in CS to amorphous. A research was carried out to study the efficiency of [Amim] Cl/glycerol mixture in suppressing the crystallinity of CS. This fabrication exhibits ionic conductivity as high as $10^{-1.6}$ S cm⁻¹ at 14.5 wt. % water content when incorporated with only [Amim] Cl of 30 wt. % (Ning *et al.*, 2009).

2.6 Cellulose acetate

Cellulose acetate (CA) is a well known biopolymers derived from the naturally occurring organic compound namely cellulose. Commercial production of this compound is usually performed by treating cellulose in the form of wood pulp with various chemicals. Chief among these is acetic acid. Acetic anhydride is also usually used in the treatment, along with sulfuric acid. This process is called acetylation, and on a molecular level, the hydrogen atoms of the cellulose molecules are being replaced by acetyl groups, a carbon-based molecular group. The molecular structure of cellulose acetate was shown in Figure 2.2.

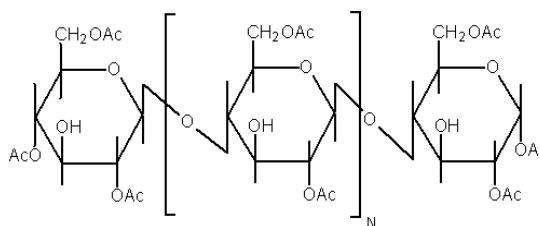


Figure 2.2: Structure of CA

CA is being used in high volume in many applications such as a component in some adhesives, film base in photography and even in separation processes (e.g. filtering, reverse osmosis) (Rodrigues Filho *et al.*, 2008). This is because CA is a renewable resource, capable in reducing the cost of production as being the main concern in the commercialising world. Additionally, good chemical stability combined with high transparency and good toughness in preparing thin membranes make CA to be more appealing in developing a conducting medium in the field of polymer electrolytes. However, CA host polymer never intensively been used to develop polymer electrolytes to be use in electrochemical devices. This is because, natural polymers are highly in crystalline phase concentration which makes it incapable in producing high conducting medium that being the main requirement in developing polymer electrolytes.

In contrast to cellulose, CA possesses a much less crystalline structure. This is because, the acetate (-Ac) group connected to the oxygen (-O) atom in CA is comparably bigger in atomic size than the hydrogen (-H) atom found in the cellulose structure. Since, -Ac are greater in size thus, it cannot well fit into the lattice as the -H atom. Hence, the ester cellulose will be in less highly coordinating form. This condition allows the CA to have better solubility in common organic solvents such as acetone as an initial step to fabricate thin film. The presences of an acceptable degree of crystallinity in CA act as a mechanical support whereas the amorphous phase aids the ion conduction.

Even though the level of crystallinity in CA are comparably lower than its original form, yet it still possess low ionic conductivity when being developed in thin film form, thus limits their use in practical purposes (Croce *et al.*, 2006). The mentioned limitations were overcome by number of means. The initial worked out method was through blending of ionic salt with CA. This approach shows a positive feedback on the increase in the polymer matrix's amorphous fraction which then improves the free volume, local viscosity and ultimately, the ionic conductivity. One of the utilised ionic salt is lithium perchlorate (LiClO_4). The ionic conductivity of this combination was found to enhance as increase in LiClO_4 concentration till the maximum conductivity value is achieved upon the addition of 16 wt. % of LiClO_4 with the value of $4.9 \times 10^{-3} \text{ S cm}^{-1}$ at room temperature (Selvakumar and Krishna Bhat, 2008). The undeniable outstanding properties of CA were drawn to the development of electrolytes with the combination of perfluorosulfonic acid polymer (Nafion) to be used in solid-state EDLCs (Subramaniam *et al.*, 2008). This type of host polymer also captured many researchers attention in developing porous structures (Fischer *et al.*, 2006; Reverchon and Cardea, 2007).

2.7 Lithium bis(trifluoromethanesulfonyl)imide

Lithium salts capture the attention of most researchers due to its small ionic radius, greatest electrochemical potential and largest energy content. The profound function of small ionic radii is to exert good salt dissolution when bonded with larger size of anion and at the same time the small size of

Li^+ ions can move more freely with high mobility. The lithium salt that has been used in this research work is lithium bis(trifluoromethanesulfonyl)imide (LiTFSI) with the molecular structure as shown in Figure 2.3.

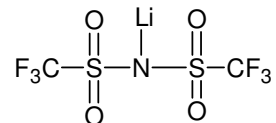


Figure 2.3: Structure of LiTFSI

This type of ionic salt is first reported by Foropoulos and DesMarteau in 1984 (Foropoulos and DesMarteau, 1984) and of special interest due to its large electronegativity, low lattice energy and delocalization of charge (Ramesh and Lu, 2008). The formal negative charge of this “new generation” anion is well delocalised attributed to the strong electron-withdrawing nature of the triflic groups and the conjugation between them and the lone electron pair on the nitrogen. The resonance structure of the anions (TFSI⁻) was shown in Figure 2.4.

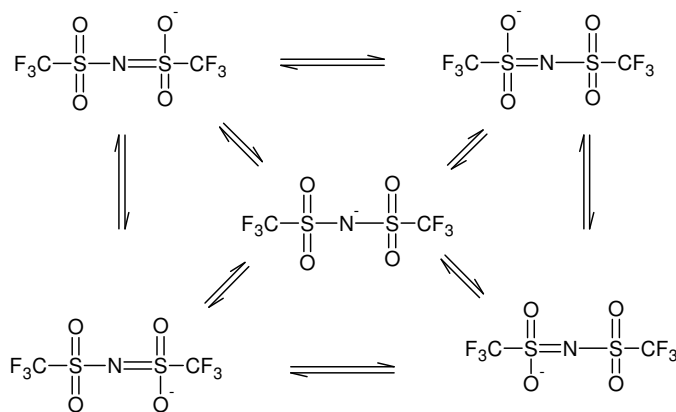


Figure 2.4: Resonance states of the TFSI anion

The high delocalised anionic charge in TFSI anion promotes high degree of dissociation of LiTFSI in the polymer matrix and allows the two different

charges of ions to remain in its ionic state as being depicted below (Webber, 1991):

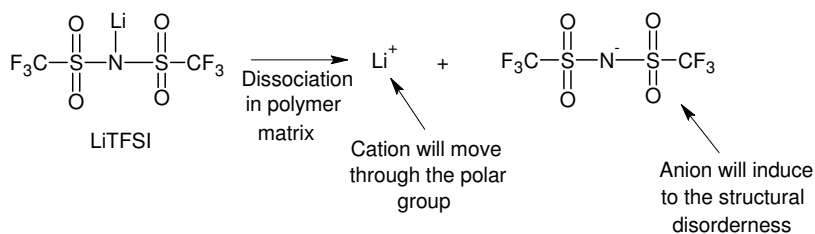


Figure 2.5: Dissociation of LiTFSI forming its respective cation and anion

In addition, the solvated ions also have the ability to move within the non-aqueous media with high mobility.

As well established, the ionic conductivity of a polymer electrolyte is very much dependent on the mobility of lithium conducting ions (Li^+) which occurs via forming coordination with the polar functional group in polymer that capable in donating electrons such as oxygen, nitrogen and etc. The presence of anion (TFSI) will contribute to the structural disorderness in the polymer matrix through breaking the hydrogen bond in polar functional group. This in turn, increases the availability of amorphous phase that ease the Li^+ ions motion which tailors the insulating property of polymer.

The excellent miscibility of LiTFSI promotes its vast utilisation in developing solid polymer electrolytes as proposed by Armand *et al.* (1986). Besides that, LiTFSI have potential to substitute some commonly used lithium salts such as replacing the poor conducting LiTf, the hazardous LiClO_4 , the thermally unstable LiBF_4 and LiPF_6 , and the toxic LiAsF_6 in lithium battery applications. Apart from this, LiTFSI proved to be safe, thermally stable since

it melts at higher temperature of 236 °C without decomposing (a rarity among lithium salts) and does not decompose until 360°C. Its highly conducting nature also makes it to be more appealing in order to develop polymer electrolytes that can well fit in current applications.

Electrochemical stability test carried out on a GC electrode reveals that the anion (TFSI⁻) is stable against oxidation although its oxidation limit is lower than those for LiBF₄ and LiPF₆, but still high enough to be practiced. The morphology of cycling lithium in LiTFSI based electrolytes is apparently superior to that in other salt-based electrolytes (Naoi *et al.*, 1999). Additionally, both the anion and cation obtained upon miscibility of LiTFSI in the matrix are inert towards other cell components such as separator, electrode substrate and cell packaging materials.

Holding on the profound properties of LiTFSI as mentioned above came to light on its suitability to be used as a dopant salt in polymer electrolytes. Its function in tailoring the insulating property of polymer can also be enhanced when present in the combination of other additives such as plasticisers, fillers and etc.

2.8 Deep eutectic solvent

Deep eutectic solvent abbreviated as DES is a type of ionic solvent composed of a mixture forming a eutectic with a melting point much lower than either of their individual components. The lower melting point of DES was induced by the hydrogen bond that combines two organic molecules forming super-molecules. This hydrogen bond decreases the electrostatic attraction between the hydrogen and organic molecules leading to a decrease in the melt point. Since it was made from a mixture thus, the term ionic mixture were adopted although it shares many similar characteristics of ionic liquid. The eutectic mixtures are liquids containing both ions and neutral molecules.

This type of ionic mixture is a new series of ionic liquid that currently gaining interest due to many outstanding features compared to the traditional imidazolium-based ionic liquids. Those properties are as listed below (Hou *et al.*, 2008; Jhong *et al.*, 2009; Zhang *et al.*, 2009):

- very cheap due to low cost of raw materials
- simple preparation procedures: the components of eutectic can be easily mixed and converted to ionic liquid without further purification steps and no medium being required during the synthesis
- safe to be use because most of the formulations are non-toxic
- biodegradable nature making it to be more environmental friendly

- good biocompatibility since quaternary ammonium salts such as choline chloride was used as an additive in chicken feed
- very low volatile organic compound (VOC) compared to ordinary solvent
- sustainable
- non-flammable and
- non-reactive to water.

Additionally, the unusual solvent property of DES believed to render the solubility problem associated to the utilisation of high crystalline natural polymer in developing high conducting polymer electrolytes which previously appears as the major limitations. The unusual solvent property of DES was attributed to the high chloride ion concentration and a specific activity borne by the ionic mixture which is capable in breaking the extensive hydrogen bonding network between the atoms that connected to the polar functional group, in this case it referred to the polar functional group in polymer. DES also found to be an effective solvent for a number of hydrolase-catalyzed reactions, including transesterification, epoxide hydrolysis, and ring-opening polymerisation. The above mentioned properties of DES makes it as a promising and inexpensive replacement for both volatile organic solvent (VOS) and ILs. The DES is known as 'green solvent' due to its safer reaction proceeds in the environment which is totally different from the traditional solvents.

DES is a physical mixture formed between variety of quaternary ammonium salts and hydrogen bond donors (Abbott *et al.*, 2003). This type of ionic mixture classified as the first generation eutectic solvent. The most commonly used quaternary ammonium salts in synthesizing DES are choline iodide, choline chloride and chlorcholine chloride, which react with any compound from amides, amines, carboxylic acids alcohols, and metal halides.

The physical properties of DES are significantly affected by the structure of the hydrogen bond donors since its characteristic govern by the hydrogen bond between the molecules. The phase behavior of the mixture can be simply modeled by taking into account the mole fraction of the hydrogen bond donors. The physical properties such as viscosity, conductivity, and surface tension of the DES are similar to ambient temperature ionic liquids. It shows that the conductivity and viscosity of these liquids is controlled by ion mobility and the availability of voids of suitable dimensions, and this is consistent with the fluidity of other ionic liquids and molten salts.

In this research, DES were synthesized from the mixture of choline chloride (2-hydroxyethyl-trimethylammonium chloride) and urea ($\text{NH}_2\text{C}=\text{ONH}_2$) in 1:2 mole ratios. The deep eutectic phenomenon was first described in the year of 2003 for the similar mixture. The respective chemical structure of the raw materials was shown in Figure 2.6 below:

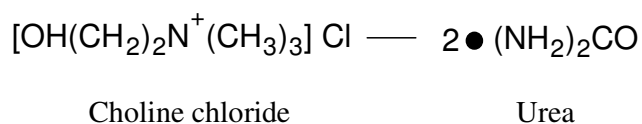


Figure 2.6: Molecular formulas of choline chloride and urea

The halide ion from choline chloride (Cl^-) forms hydrogen bonding with urea. The synthesised DES possess a very low melting point as low as $12\text{ }^\circ\text{C}$ which is far lower than their individual components, the melting temperature of choline chloride and urea are $302\text{ }^\circ\text{C}$ and $133\text{ }^\circ\text{C}$, respectively.

Since eutectic mixture has a very low melting point, thus the heating process during synthesising the DES assured that the solution is concentrated by ionic species at the end of the synthesising process. Due to this nature, some studies disclose that DES itself is conductive as high as 1 mS cm^{-1} at $30\text{ }^\circ\text{C}$ (Abbott *et al.*, 2003). The high ionic conductivity of DES attributed to their high mobility and high concentration of carrier ions make it to be a promising additive to be used in suppressing the insulating properties of natural polymers.

Another appealing property of DES is its highly viscous nature which is greater compared to ionic liquid. This makes the DES to possess a very low volatility whereby the incorporated DES in the polymer matrix will have either a very slow or negligible evaporation compared to other commonly used plasticisers such as ethylene carbonate (EC), propylene carbonate (PC) and etc. This clarifies that the performance of DES plasticised polymer electrolytes can be sustained over a long range of storage time which consequently enhances the performance and life time of the batteries.

In recent years, most of the applications of DES were focused on the development of electrolyte to be used widely in electrochemical devices such

as dye-sensitized solar cells (DSSCs). The DES being incorporated owing to its high conducting features as a result of the very high concentration of mobile ionic species. A similar approach was carried out by using a eutectic mixture composed of glycerol and choline chloride in developing the electrolyte for dye-sensitized solar cells (DSSCs) (Jhong *et al.*, 2009).

Apart from that, the unusual solvent property of DES aid in dissolving the natural polymers, mainly for cellulose and in some cases the DES been used as a medium for converting compounds such as fructose. DES also successfully assessed for electrodeposition of different metals (Cr, Mn, Cu, Ag) (Bakkar and Neubert, 2007) and alloys (Zn/Cr, Zn/Sn) on different substrates (Abbott *et al.*, 2007; Dale *et al.*, 2007); in electropolishing (Abbott *et al.*, 2006); and in electrowinning of metals from complex oxide matrices (Abbott *et al.*, 2005; Abbott *et al.*, 2006). Additionally, the benefits of DES cause it to even penetrate into the field of biology, where the eutectic mixtures were used as catalyst. This eutectic mixture is a promising green solvent for poorly soluble compounds in preclinical studies. In spite of that, DES also plays an important role in separation and purification of organic compounds and do involve in organic reaction.

2.9 1-Allyl-3-methylimidazolium chloride

In recent years, ionic liquid (IL) gains its surety to be utilised as an additive in many applications attributed to the urge of replacing the conventional volatile solvents which are hazardous to both human and

environment (Forsyth and MacFarlane, 2003). In this dissertation, a room temperature ionic liquid (RTIL), [Amim] Cl is used to suppress the high crystallinity in natural polymers. The molecular structure of [Amim] Cl is as shown in Figure 2.7.

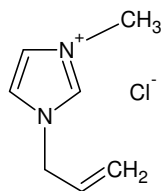


Figure 2.7: Structure of [Amim] Cl

RTIL are literally salts that remain in liquid state over a wide range of temperature, including room temperature. This feature is important for the application of electric battery. RTIL melts without decomposing or vaporising whereas it forms an ionic solid which may neither in crystalline nor glassy form upon cooling. This liquid substance is concentrated with ions and short-lived ion pairs in excessive amount, which is not found in any other additives. This nature makes RTIL as electrically conducting fluids (electrolytes). Other common adopted terms for RTIL are liquid electrolytes, ionic melts, ionic fluids, fused salts, liquid salts, or ionic glasses.

Apart from the safety purpose, [Amim] Cl do possess long listed properties such as 1) non-measurable vapour pressure, 2) non-flamability, 3) low viscosity, 4) good thermal stability, 5) wide chemical and electrochemical window and 6) promising electrical conductivity (Ning *et al.*, 2009). Those mentioned properties are the crucial requirements to develop the desired polymer electrolytes.

In addition, the unusual solvent property of [Amim] Cl makes it more appealing (Cuissinat *et al.*, 2008). The utilisation of natural polymer in this research strongly needs a good solvent to overcome the highly crystalline region which are greater compared to the one found in synthetic polymers. Thus, [Amim] Cl seems to be the best alternative to overcome the solvating problem of natural polymers. This unusual solvent property was attributed to high chloride ion concentration and a specific activity borne by [Amim] Cl which is capable in breaking the extensive hydrogen bonding network in the polymer backbone. This solvent property contributes to great suppression of the crystalline region in the polymer and the breaking of hydrogen bonding network allows more oxygen to be unoccupied which then available for Li⁺ co-ordination (Swatloski *et al.*, 2002). These features encourage the utilisation of ionic liquid as a liquid component in a gel polymer electrolyte system instead of organic solvent electrolyte.

This type of ionic liquid is also recognised as “green solvents” due to its safer reaction proceeds in the environment which is totally different from the traditional solvents. Since it is a recyclable solvent, it therefore reduces the load on the environment from the viewpoint of green chemistry. The good solvent property of [Amim] Cl enables it to be use as the solvent for diverse kind of materials. Some of the examples of natural polymers that were dissolved in this solvent are cellulose, corn starch and etc.

Moreover, the incorporation of [Amim] Cl in polymer electrolytes also displays high ionic conductivity as a result of their high mobility and high

concentration of carrier ions. This was evident based on the exerted ionic conductivity of $10^{-1.6}$ S cm⁻¹ when incorporate 30 wt. % of [Amim] Cl in the matrix formed by corn starch (Ning *et al.*, 2009).

Researchers have identified RTIL as another alternative to replace water as the electrolyte in metal-air batteries. RTIL have great appeal because they evaporate at much lower rates than water, increasing battery life time by drying slower. This property also overcomes the solvent leakage problem that usually being accounted in batteries which are found to be very much unsafe as in conventional electrolytes.

In this research, [Amim] Cl is used to dissolve the employed natural polymers since its solvating power is much greater than the used solvent. The well dissociation of natural polymer allows more coordinating sites to be available for Li⁺ co-ordination. The polar groups in [Amim] Cl also aid in free ions transportation by proving a binding site for the Li⁺ ion co-ordination. As a result, the incorporation of [Amim] Cl enhances the ionic conductivity of polymer electrolytes while sustaining the biodegradable properties of the matrix formed by natural polymers.

CHAPTER 3

MATERIALS AND METHODS

3.1 Materials

Corn starch (CS) and cellulose acetate (CA, $M_w = 61000$ g/mol) were purchased from Aldrich. The lithium bis(trifluoromethanesulfonyl)imide, LiTFSI were procured from Fluka. The starting materials of deep eutectic solvent (DES) namely, choline chloride and urea were obtained from Sigma. 1-allyl-3-methylimidazolium chloride ([Amim] Cl) with the purity of 99 % was purchased from Aldrich. Distilled water and N, N-dimethylformamide (DMF) attained from R & M Chemicals were used to dissolve all the starting materials upon developing CS and CA based polymer electrolytes, respectively.

3.2 Synthesis of deep eutectic solvent (DES)

An appropriate amount of choline chloride and urea with the ratio of 1:2 were placed in a small clean beaker. The mixture of two individual solids were heated up under stirring condition using a hot plate until it dissolves completely and appear as a colourless viscous solution.

3.3 Preparation of polymer electrolytes

All the polymer electrolytes were prepared by solution casting technique. Table 3.1 summarises the composition ratio of four systems with its respective designations. The employment of two different polymers yields a slight difference in the sample preparation method as will be conversed in the subsequent sub section.

Table 3.1: Composition ratio of polymer electrolytes in all four systems with the respective designations

| Composition (wt. %) | | | Designation for systems | | | |
|---------------------|--------|-------------------|-------------------------|--------------|--------------|--------------|
| CS/CA | LiTFSI | DES/ [Amim] Cl | I | II | III | IV |
| 70 | 30 | 0 | DES-0 | CA-0 | CS-0 | IL-0 |
| 63 | 27 | 10 | DES-10 | CA-10 | CS-10 | IL-10 |
| 56 | 24 | 20 | DES-20 | CA-20 | CS-20 | IL-20 |
| 49 | 21 | 30 | DES-30 | CA-30 | CS-30 | IL-30 |
| 42 | 18 | 40 | DES-40 | CA-40 | CS-40 | IL-40 |
| 35 | 15 | 50 | DES-50 | CA-50 | CS-50 | IL-50 |
| 28 | 12 | 60 | DES-60 | CA-60 | CS-60 | IL-60 |
| 21 | 9 | 70 | DES-70 | CA-70 | CS-70 | IL-70 |
| 14 | 6 | 80 | DES-80 | - | CS-80 | IL-80 |
| 7 | 3 | 90 | DES-90 | - | - | - |

Some sampling of polymer electrolytes were not done up to 90 wt. % plasticisation owing to a very low mechanical properties that is not beneficial in the application of polymer electrolytes. The designations of highest conducting compositions for all the four systems were bolded.

3.3.1 CS based polymer electrolytes


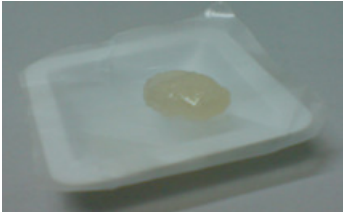



The initial step in developing biodegradable polymer electrolytes was by dissolving an appropriate amount of CS powder in 15 ml of distilled water which produces a milky solution. This solution was then gelatinised at the temperature of 75 °C under constant stirring. This step yields a transparent viscous solution. After the heating process, the solution was cooled at ambient temperature under constant stirring for about 30 minutes. Follow up with an appropriate addition of LiTFSI and DES/[Amim] Cl into the viscous solution and again the solution was allowed to stir for another hour to allow good miscibility between the added chemical constituents. The homogeneous polymer electrolytes were then casted by spreading the viscous solution on a clean Teflon plate and dried in the oven at 55 °C for 8 hours.

3.3.2 CA based polymer electrolytes

The polymer electrolytes were attained by dissolving an appropriate amount of CA, LiTFSI and DES/[Amim] Cl in 10 ml of DMF and the solution was left to stir overnight at room temperature. The overnight stirring produces a colourless homogeneous solution which was then casted by spreading the suspension on a clean Petri dish and left to dry in the oven at 55 °C for 8 hours. This procedure yields a mechanically stable and free standing transparent film.

3.4 Physical appearance of the developed polymer electrolytes

Table 3.2: Physical appearance of casted polymer electrolytes for four different systems

| System | Physical appearance | |
|------------|--|---|
| I |  0 – 40 wt. % |  50 – 90 wt. % |
| II |  0 – 70 wt. % | |
| III |  0 – 80 wt. % | |
| IV |  0 – 80 wt. % | |

3.5 Instrumentations

In this research work, seven different types of instruments were hands on to characterise the developed polymer electrolytes. Those listed are Alternating current (AC) impedance spectroscopy, Horizontal attenuated total reflectance-Fourier transform infrared (HATR-FTIR), Ubbelohde capillary viscometer, X-ray diffractometry (XRD), Scanning electron microscopy (SEM), Atomic force microscopy (AFM) and Thermogravimetric analysis (TGA). The above stated instruments were not consistently used to characterise all the four systems since some of the instruments only limits to thin film testing and unable to test the gel-like polymer electrolytes. The employed instruments to characterise each of the systems were summarised in Table 3.3.

Table 3.3: Instruments used in characterising the four developed systems

| System | Instrument | | | | | | |
|------------|---------------------------|-----------|--------------------------------|-----|-----|-----|-----|
| | AC Impedance spectroscopy | HATR-FTIR | Ubbelohde capillary viscometer | SEM | AFM | XRD | TGA |
| I | √ | √ | - | √ | - | - | √ |
| II | √ | √ | √ | √ | - | √ | √ |
| III | √ | √ | √ | - | - | - | √ |
| IV | √ | √ | √ | - | √ | √ | √ |

3.5.1 Alternating current (AC) impedance spectroscopy

This is the main analysis carried out to test the ionic conductivity of the synthesised polymer electrolytes. As the initial step, the thickness of the polymer electrolytes were measured using a micrometer screw gauge prior performing the ionic conductivity measurements. The thickness of sample is one of the important parameter that needs to take into account since it has a significant effect on the ionic conductivity of polymer electrolytes.

The conductivity measurements were performed for each developed polymer electrolytes by impedance spectrometer using a HIOKI Model 3532-50 Hi-Tester. All the measurements were taken over the frequency ranging from 50 Hz to 5 MHz with the polymer electrolytes sandwiched in between two stainless steel blocking electrodes which having an area of 4.9807 cm². The Cole-Cole impedance plot was attained upon the completion of the analysis. An example of the typical complex impedance plot (Z'' vs. Z') was shown in Figure 3.1.

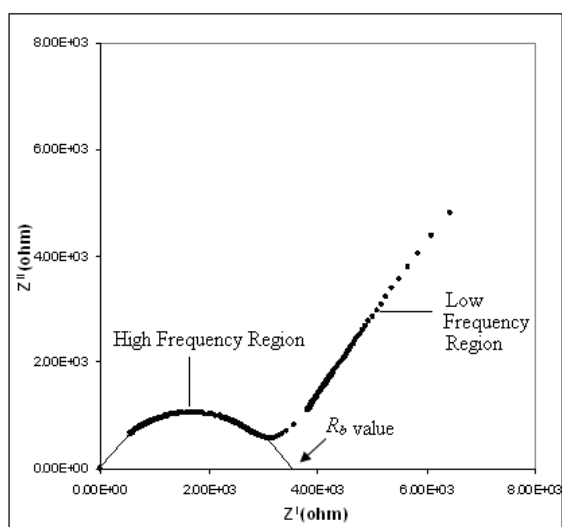


Figure 3.1: A typical complex impedance plot

The shape of graph may not be exactly the same for all the tested samples since this measurement is strongly dependent on the nature of the tested samples.

The complex impedance plot composed of two parts, which is real (Z') and imaginary part (Z''). The Z' is plotted on the x-axis whereas the Z'' is plotted on the y-axis. The complex impedance plot has one major shortcoming, where there is no frequency indication for all the data point plotted. Therefore, we have annotated that low frequency data are on the right side of the plot and higher frequency is on the left side, as indicated in Figure 3.1.

The obtained impedance plot was then used to find out the bulk resistance (R_b) value by drawing a semicircle on the plot using a compass. The Z' value where the semicircle cuts represents the R_b value, where $Z''= 0$. Therefore, the Z' real and Z'' imaginary axis must be of equal scale as the radius of the circle has to be the same. The ionic conductivity value was calculated upon substituting the R_b value in the expression below:

$$\sigma = \frac{L}{R_b A} \quad (3.1)$$

where σ is the conductivity in $S\ cm^{-1}$, L refers to the thickness of sample in cm, R_b is the bulk electrical resistance in Ω and A represent the surface area of the stainless-steel blocking electrodes in cm^2 .

This scrutiny is performed to monitor the variation of ionic conductivity when the ratio of either DES or [Amim] Cl is being varied in CS/CA: LiTFSI based polymer electrolytes. The similar conductivity measurements at room temperature is used to plot the dissipation tangent loss graph which sheds some light on the motions of Li^+ ions within the polymer matrix. Additionally, the ion transport mechanism of polymer electrolytes were deduced by measuring the ionic conductivities over a certain range of temperatures. Similar characterization technique was used to monitor the ionic conductivity borne by polymer electrolytes over the storage time of 30 days with an interval of 10 days at room temperature. This analysis was performed to understand the influence of ionic solvent ratio either DES or [Amim] Cl in retaining the ionic conductivity properties over storage time. The conductivity retained analysis is only performed for thin film samples.

3.5.2 Ubbelohde capillary viscometer

Relative viscosity measurements provide an insight on the structural arrangement of polymer electrolytes that influences the fluidity of Li^+ ions when the amount of DES/ [Amim] Cl is manipulated. This result is useful since it compensate with the ionic conductivity measurements, thus this can be a great alternative in double confirming the exerted ionic conductivity trend.

The relative viscosities (η_{rel}) of polymer electrolytes were obtained by Ubbelohde capillary viscometer using a small adapter assembly. The temperature of the liquid samples was maintained at room temperature by the aid of a Julabo water circulator. This measurement was done by taking into

account the flow time of the samples to flow from one calibrated point to another in the unit of seconds (s). The measured flow time value was then be substituted in the equation below to calculate the relative viscosity of the samples:

$$\eta_{rel} = t_{solution} / t_{solvent} \quad (3.2)$$

where η_{rel} signify the relative viscosity, $t_{solution}$ and $t_{solvent}$ represents the flow time of sample solution and solvent, respectively.

The ion fluidity value was determined through a simple calculation involving the relative viscosity of the polymer electrolytes using the expression below:

$$\varphi = 1 / \eta_{rel} \quad (3.3)$$

where φ represents the ion fluidity. Both relative viscosity and ion fluidity are unitless parameters. The information that been obtained from this analysis clearly shows the relationship that exist between the polymer electrolytes viscosity with the ionic conductivity that is related to the ions migration.

3.5.3 Horizontal attenuated total reflectance-Fourier transform infrared (HATR-FTIR)

The structural disorderliness in CS/CA: LiTFSI based polymer electrolytes upon plasticisation with DES/ [Amim] Cl was induced from the possible complexation between the chemical constituents. The occurrence of complexation was determined by HATR-FTIR.

Horizontal Attenuated Total Reflectance-Fourier Transform Infrared (HATR-FTIR) studies were carried out using Perkin-Elmer FTIR Spectrometer, Spectrum RX1, with the aid of HATR accessory. The FTIR spectra were recorded in the transmittance mode in the wave region ranging from 4000 to 600 cm^{-1} with the resolution of 4 cm^{-1} .

The FTIR-HATR spectra vary as a result of mixing different composition ratios and occurrence of complexation between the constituents (Rajendran and Uma, 2000). The occurrence of complexation were perceived in both crystalline and amorphous phase based on the changes on the cage peaks in terms of the frequency shifting, relative intensity, shape, absence of the existing peak and even through the observation of new peaks.

3.5.4 X-ray diffractometry (XRD)

The X-Ray Diffraction (XRD) patterns were analysed by the aid of Siemens D-5000 Diffraction System using Cu-K_α radiation with the wavelength of 1.5406 Å. The respective XRD pattern was recorded for the Bragg angles (2θ) ranging from 5 ° to 80 ° at room temperature. This characterisation technique is performed for phase identification that is important in understanding the ionic conductivity of the polymer electrolytes.

3.5.5 Scanning electron microscopy (SEM)

Morphology features of the polymer electrolytes are very much related to the ionic conductivity performance as it is the interface between the two active solid electrodes, permitting the migration of Li^+ ions. This study was relied in order to examine the morphology changes on the surface of the polymer electrolytes with the addition of LiTFSI and DES/ [Amim] Cl. This scrutiny also aid to figure out the possible structural disorderliness, validated in terms of the increase in free volume within the polymer matrix which represents the amorphous fraction. In spite of this, the anomalies in ionic conductivity attributed to the conglomeration forming neutral ion multiples also been proved from the morphology study.

The morphology images of selected polymer electrolytes were captured using Leica's SEM with the model S440 at 6 kV. The micrographs for CS and CA based polymer electrolytes were captured with the magnification factor of 500 X and 1000 X, respectively. Prior capturing the surface image, a thin layer of gold was coated on the thin film samples as a step to prevent electrostatic charging when the samples surface being subjected with a high-energy beam of electrons. This testing is only limited to thin film samples.

3.5.6 Atomic force microscopy (AFM)

This is another advance technique used to study the surface nature of polymer electrolytes in which the morphology images were obtained by the aid of AFM Dimension 3000 bridge interfaced to a computer for data acquisition. Small sizes of thin films were subjected to this analysis by using the silicon made tip and all the images were captured in air under contact mode. This characterisation technique is greatly preferred since it capable in quantitatively measures the surface roughness of polymer electrolytes which cannot be obtained by any other advanced microscopes.

3.5.7 Thermogravimetric analysis (TGA)

This analysis accounts to the thermal properties of polymer electrolytes which includes heat-resistivity and thermal stability. The knowledge on the samples heat-resistivity and thermal stability were obtained by referring to the maximum decomposition temperature (T_d) and percentage of total weight loss (wt. %) respectively with the aid of TGA thermograms.

The thermal properties of polymer electrolytes were scrutinised by the aid of Mettler Toledo analyzer consists of a TGA/SDTA851^e main unit and STARe software. All the selected polymer electrolytes were analysed at the temperature ranging from 25 °C to 550 °C with the heating rate of 10 °C min⁻¹ under nitrogen atmosphere. This analysis was performed for all the developed systems.

CHAPTER 4

RESULTS AND DISCUSSION: SYSTEM I

4.1 Conductivity studies at room temperature

Figure 4.1 depicts the variation of ionic conductivity when the concentration of DES in CS: LiTFSI: DES polymer electrolytes is increased from 0 wt. % to 90 wt. %. The ionic conductivity plot was sub divided into four regions to ease discussion on the exerted ionic conductivity trend.

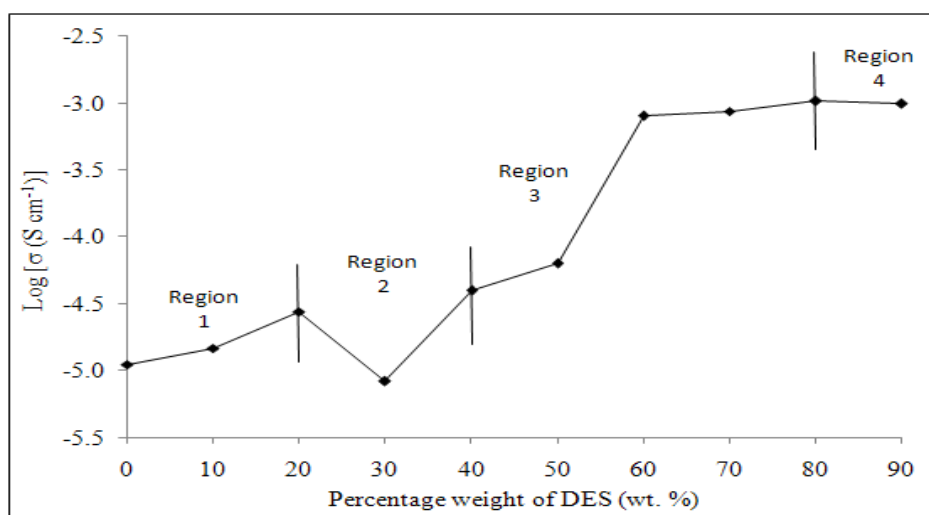


Figure 4.1: The dependence of log ionic conductivity (σ) values of CS: LiTFSI: DES polymer electrolytes at room temperature

From Figure 4.1, it can be understood that the ionic conductivity of CS: LiTFSI polymer electrolytes improved with the initial incorporation of DES. Further increase in the DES concentration contributes an appreciable enhancement in this property as revealed by sample DES-20. This was ascribed to the increase in the number of lithium conducting ions (Li^+) that

excessively migrates along the polymer backbone chain via forming coordination with the unoccupied oxygen atom. The unoccupied oxygen was obtained upon breaking of hydrogen bond in the hydroxyl (-OH) functional group in polymer backbone. The disruption in the hydrogen bond suppresses the crystallinity in CS matrix, allowing more amorphous region (disordered form that results in more free volume) to be available to ease the mobility of Li^+ ions that are responsible in enhancing the ionic conductivity (Uma *et al.*, 2003).

Besides that, the presence of chloride free ions (Cl^-) obtained upon dissociation of DES in the CS matrix provides an alternative pathway for ions motion by allowing the Li^+ ions to temporarily form coordination on its transit sites while the neighboring oxygen atom being vacated (Yahya *et al.*, 2006). This aids the hopping of Li^+ ions from one oxygen vacant site to another with ease and the increase in the capacity of ionic transfer enhances the ionic conductivity.

Further addition of DES above 20 wt. % (Region 2) induces an abrupt drop in the ionic conductivity. The reason for this slump was attributed to the possible conglomeration of excess DES particles forming neutral ion multiples (Ramesh and Lu, 2008). The ion aggregates will reduce the polymer-ionic mixture interface thereby blocking the existing conducting pathways (Winie *et al.*, 2009; Anantha and Hariharan, 2005). In accordance to this phenomenon, the extent of Li^+ ion transport will diminish due to the restriction on its mobility which subsequently decreases the ionic conductivity. As DES

concentration is increased to 40 wt. %, the conducting pathways are again created by the dissociation of ion aggregates into free ions, imparting greater availability of amorphous region and additional transit site to facilitate the Li⁺ ions mobility which aid in enhancing the ionic conductivity.

In Region 3, a considerable increase in the ionic conductivity was initially observed for sample DES-50 before a drastic increase accounted for the sample with 60 wt. % of DES. The increase in ionic conductivity shares a similar reason as in Region 1. The drastic increase in ionic conductivity provides an insight on the radical improvement in the structural disorderliness which induces to a very high concentration of amorphous fraction in the material. This significantly improves the ion transport mechanism. Further increase in the DES content contributes to an almost constant increase in the ionic conductivity. The maximum room temperature ionic conductivity of $1.04 \times 10^{-3} \text{ S cm}^{-1}$ is achieved by sample DES-80. Further incorporation of DES concentration accounts to a slight decrease in this property as observed in Region 4. The observed decline in ionic conductivity was attributed to the formation of neutral ion multiples that causes a decrease in the mobility of Li⁺ ions which are crucial in improving the ionic conductivity.

4.2 Scanning electron microscopy (SEM)

The exerted ionic conductivity trend in Region 2 can be further validated by relying on the SEM photographs that describes the surface morphology of the samples. The surface morphology of the polymer electrolytes has been presented in Figure 4.2 (a-c) with the magnification factor of 500 X.

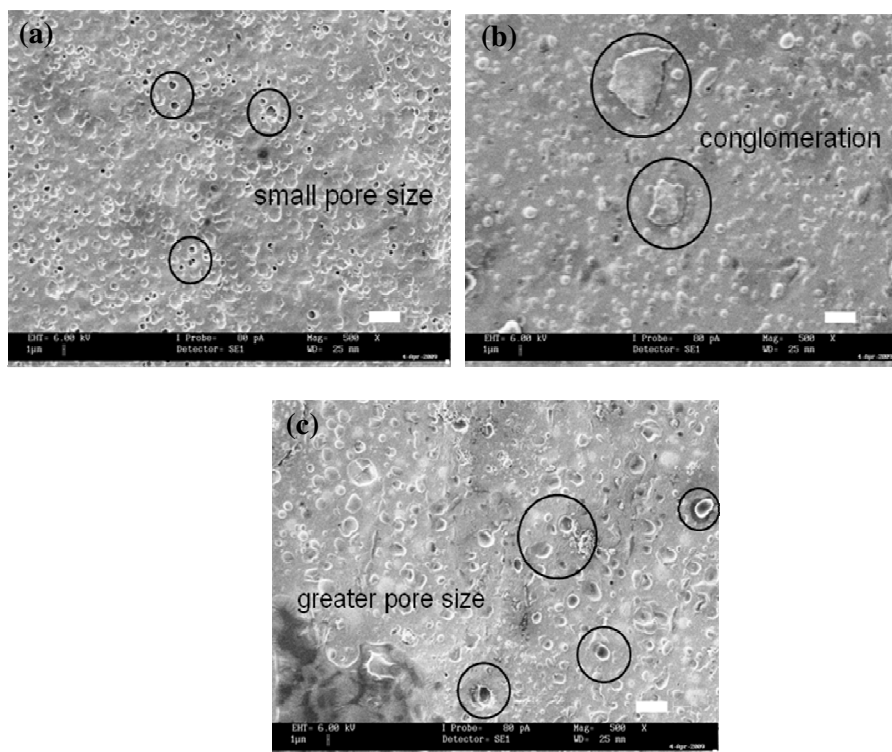


Figure 4.2: SEM micrographs of CS: LiTFSI: DES matrix when different concentration of DES is incorporated in (a) DES-20, (b) DES-30 and (c) DES-40, with the bar length of $1\ \mu\text{m} = 0.1\ \text{cm}$ for the image dimension $26.0\ \text{cm} \times 19.5\ \text{cm}$

Based on the SEM image in Figure 4.2 (a), it can be noted that the sample DES-20 is highly packed with small spheres having the diameter range of 4.0 to $7.0\ \mu\text{m}$, with some spheres embedded with small pores. These

spheres represent the crystalline region where it consists of a number of platelets or lamellae radiating from a nucleating centre, called spherulites (Paradhan *et al.*, 2008; Singh *et al.*, 2008). The regions between the neighboring lamellae show the existence of amorphous phase involved in ion conduction. This observation reveals the high order of atoms which makes it appear in a semi-crystalline nature.

Further addition of 30 wt. % of DES gradually modifies the porous microstructure to less porous membranes. This was attributed to the conglomeration of excess DES particles forming neutral ion aggregates (as circled in Figure 4.2 (b)) near the pores that consequently reduces the pore size and porosity (Deka and Kumar, 2009). This in turn, decreases the uptake of liquid electrolyte in the microporous membrane resulting in lower ionic conductivity.

Other plausible reason in explaining the drop in the ionic conductivity of sample DES-30 can be inferred from the placement of ion aggregates covering the amorphous phase which blocks the existing conducting pathways. Since ion migration is only allowed in amorphous regions thus the corresponding blockage restricts the ions mobility and causes an abrupt reduction in the ionic conductivity.

In Figure 4.2 (c), the disappearance of ion aggregates on the surface morphology upon addition of 40 wt. % DES reveals the dissociation of neutral ion multiples into charge carriers. Hence, conducting pathways are again

created for the Li^+ ion transport which would subsequently enhance the ionic conductivity. The neutral charge borne by the ion aggregates will make it be present in an unstable condition that easily disrupts upon the addition of small amount of free ions (from DES).

Another rationale to suggest the improvement in ionic conductivity was attributed to the increase in both the number of voids and pore size. The increase in the number of void correlates to the significant disruption in the crystalline region that enhances the amorphous fraction present between the spheres. Since the ion transport only occurs predominantly in amorphous phase thus an increase in ionic conductivity will be observed for sample DES-40. In addition, the increase in the pore size with the diameter range of 9.0 to 11.0 μm (Figure 4.2 (c)), reveals the increase in the porosity of the membrane which entraps large volumes of the liquid electrolyte in the cavities (Saikia *et al.*, 2008; Saikia *et al.*, 2009) accounting to the ease in the Li^+ ions mobility which then enhances the ionic conductivity.

4.3 Horizontal attenuated total reflectance-Fourier transform infrared (HATR-FTIR)

This analysis is a promising method to deduce the complexation between the chemical constituents present in both crystalline and amorphous phase. This was deduced by relying on the changes in cage peak in terms of the frequency shifting, relative intensity, shape, peak disappearance and also through the formation of new peaks. All the observable changes in cage peak attributed to the complexation have been reported.

The band assignments for respective pure substances were summarised in Table 4.1 (Ramesh and Lu, 2008; Ning *et al.*, 2009).

Table 4.1: Band assignments and wavenumbers exhibited by pure constituents namely CS, LiTFSI and DES

| Sample | Band assignments | Wavenumber (cm ⁻¹) |
|--------|--|--------------------------------|
| CS | δ (O-H) bending of H ₂ O | 1597 |
| | CH ₂ symmetric bending | 1432 |
| | CH ₂ wagging | 1326 |
| | C-O-C | 760-983 |
| LiTFSI | S-CH ₃ | 2979 & 2876 |
| | C-SO ₂ -N | 1356 |
| | -CF ₃ | 1193 |
| | C-F stretch | 1142 |
| | S=O | 1065 |
| DES | C-H stretching (CH ₃) | 2964 |
| | C-H stretching (CH ₂) | 2873 |
| | Ammonium ion | 1169 |

FTIR spectra of pure CS, pure LiTFSI, DES-0, pure DES and DES-80 were presented in Figure 4.3.

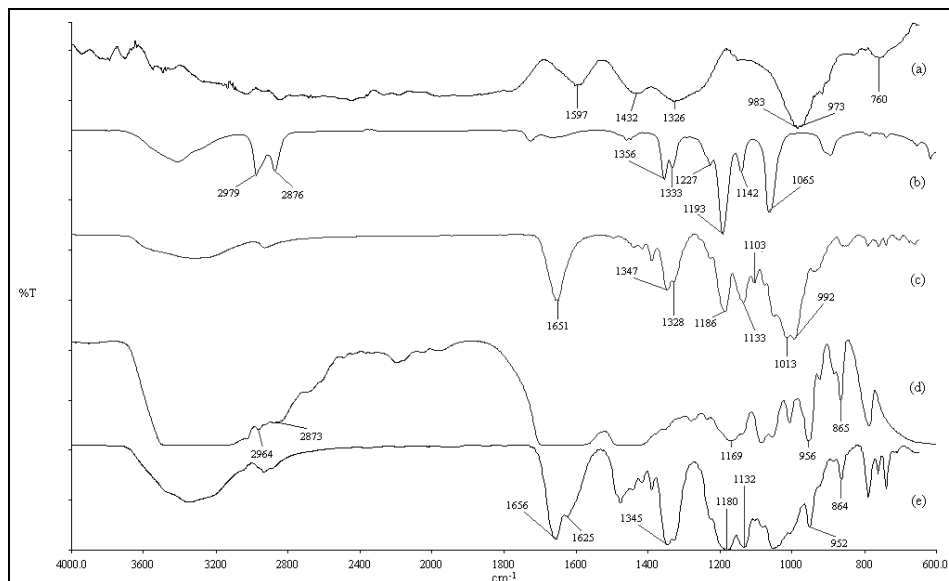


Figure 4.3: FTIR spectra of (a) pure CS, (b) pure LiTFSI, (c) DES-0, (d) pure DES and (e) DES-80

The complexation between pure CS and LiTFSI can be deduced based on the FTIR spectrum of DES-0 represented in Figure 4.3 (c). The first evidence to prove the complexation was based on new peaks formation at 1651 cm^{-1} and 1103 cm^{-1} in DES-0. This implies that some degree of complexation has occurred and new phase has formed between the LiTFSI and the oxygen atom of the hydroxyl (-OH) group.

Additionally, the peaks at 1356 cm^{-1} and 1333 cm^{-1} that corresponds to C-SO₂-N bonding in pure LiTFSI was shifted to lower frequency at 1347 cm^{-1} and 1328 cm^{-1} upon mixing with CS. This shows the coordination of free hydrogen atom with nitrogen at these frequencies. Besides that, the relative

intensity of this peak increases from 15 % (pure LiTFSI) to 18 % after complexation with pure CS as depicted in Figure 4.4.

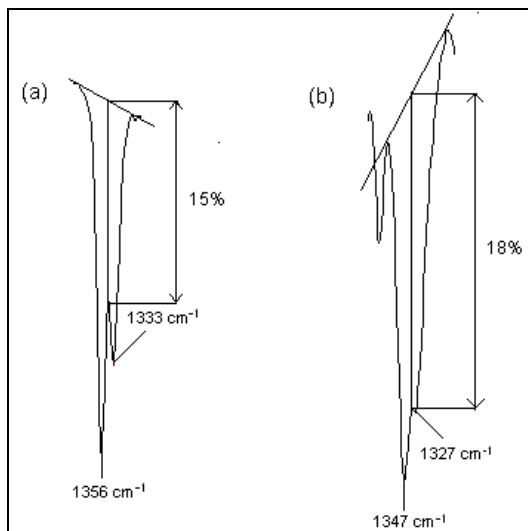


Figure 4.4: The changes in intensity of C-SO₂-N band for (a) pure LiTFSI and (b) DES-0

The characteristic peaks of CF₃ and C-F stretch that co-exist at 1193 and 1142 cm⁻¹, respectively in pure LiTFSI was shifted to lower frequency at 1186 and 1133 cm⁻¹ in DES-0 upon complexation with pure CS. Further evidence to prove the complexation was based on the peaks that fall in the range of 1100-1300 cm⁻¹ in pure LiTFSI which splits from 3 to 4 individual peaks and allocated at lower frequency in DES-0 upon complexation with pure CS. The final observable change proves the miscibility of LiTFSI in CS matrix was the two peaks at 983 and 973 cm⁻¹ in pure CS which was reallocated to higher frequency at 1013 and 992 cm⁻¹, respectively in DES-0. This frequency shifting illustrates the weaker interaction between Li⁺ ions and oxygen atom in C-O-C group.

The incorporation of DES in CS: LiTFSI matrix was believed to involve in complexation and this was evident based on the changes in cage peak that has been presented in Figure 4.3 (e). The peak at 1651 cm^{-1} in DES-0 underwent change in shape from one to two peaks and is consequently reallocated at higher frequency (1656 cm^{-1}) upon complexation with pure DES. Besides that, this particular peak also undergoes band broadening being effect of DES addition. Another evidence of complexation was the peak at 1347 cm^{-1} (DES-0) which shifted to lower frequency at 1345 cm^{-1} (DES-80) upon addition of DES. This shifting proves the substitution of initially bonded lithium to the nitrogen with hydrogen atom. The reference peak also underwent increase in relative intensity from 22 % (DES-0) to 66 % (DES-80) upon complexation.

The displacement of peak initially present at 1186 cm^{-1} in non-plasticised sample to 1180 cm^{-1} in DES plasticised sample also reveals possible interaction. The peak at 1133 cm^{-1} in DES-0 shifted to lower frequency at 1132 cm^{-1} upon addition of 80 wt. % of DES. The peaks present at 956 and 865 cm^{-1} in pure DES was shifted to lower frequency at 952 and 864 cm^{-1} , respectively in DES-80.

The observed changes in the cage peaks indicate that some degree of co-ordination or complexation had occurred between the constituents. The similarity between the FTIR spectra for each sample indicates that LiTFSI and DES are physically bonded with CS.

4.4 Frequency dependence of loss tangent studies

Figures 4.5 and 4.6 shed some light on the ionic transport mechanism in CS matrix when different concentration of DES is incorporated in CS: LiTFSI system.

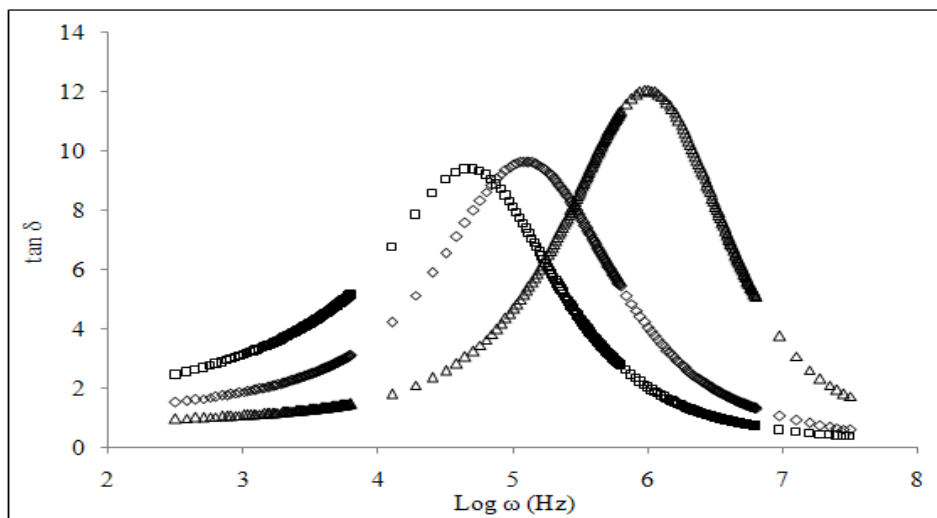


Figure 4.5: Variation of $\tan \delta$ as a function of angular frequency for samples DES-20 (\square), DES-40 (\diamond) and DES-60 (Δ) at room temperature

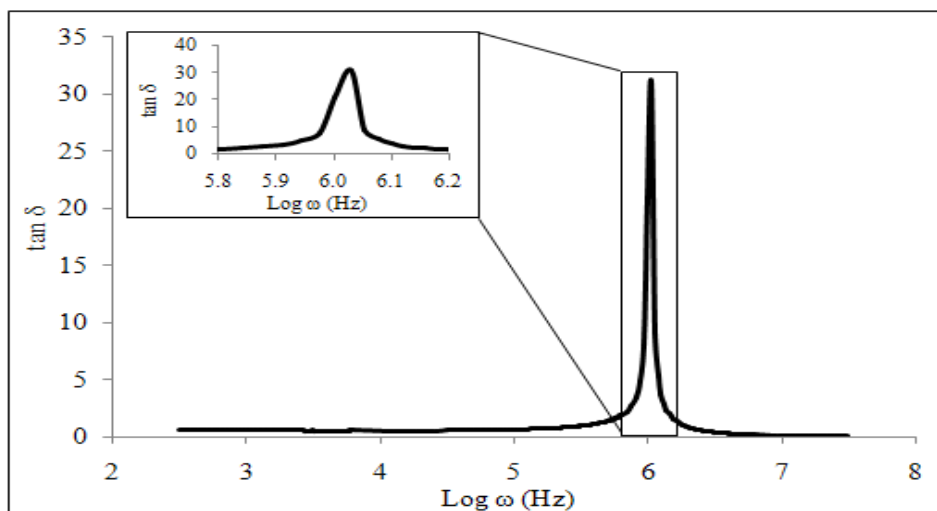


Figure 4.6: Variation of $\tan \delta$ as a function of angular frequency for sample DES-80 at room temperature

From Figure 4.5 it can be observed that the loss tangent peaks were found to have shifted towards the higher frequency upon increase in DES content similar to sample DES-80 in Figure 4.6. The increase in the relaxation frequency ($\log_{\max} \omega$) as a function of DES content is summarised in Table 4.2.

Table 4.2: Relaxation frequencies of samples with different DES content

| Sample | Relaxation frequency, $\log \omega_m$ (Hz) |
|--------|--|
| DES-20 | 4.70 |
| DES-40 | 5.10 |
| DES-60 | 6.00 |
| DES-80 | 6.03 |

The observation illustrates the reduction in the relaxation time of Li^+ ions due to greater acceleration on its mobility with increase in DES concentration (Paradhan *et al.*, 2008). As more DES is incorporated into the CS: LiTFSI matrix, more amorphous region will be available and facilitates the mobility of Li^+ ions in the matrix. Hence, enhancement in the ionic conductivity is observed.

Other plausible reasons for the displacement of loss tangent peaks to higher frequency may correlate to the increase in the number of non-bridging ions in DES (Cl⁻) that act as a transit site for the mobility of Li^+ ions. This transit site shorten the distance for Li^+ ions to hop from one oxygen atom to another in polymer chain acquiring less energy loss for the mobility of ion.

Hence, frequent migrations of mobile ions are expected to occur that crucial in enhancing the ionic conductivity.

The magnitude of $\tan \delta$ also provides an informative insight on the number of Li^+ ions that participate in ion conduction (Azizi Samir *et al.*, 2004). The increase in the magnitude of $\tan \delta$ upon increase in DES concentration inferred to an increase in the area under the loss factor peak. This was ascribed to the increase in the number of Li^+ ions that participates in the relaxation process to assist the ionic conductivity. The increase in Li^+ ions concentration evidence the efficiency of DES in overcoming the Coulombic force in LiTFSI, making more Li^+ ions to be available in enhancing the ionic conductivity. Sample DES-80 exhibits the highest magnitude of $\tan \delta$ compared to the rest of the tested samples attributed to the greater presence of Li^+ ions.

The increase in the DES content in polymer electrolyte speeds up the segmental motion by increasing the amorphous elastomeric phase. Thus, more free volume will be available which predominantly increases the Li^+ ion transport mechanism and enhances the ionic conductivity as a function of DES content. Sample DES-80 obtained the highest ionic conductivity due to the relatively fast segmental motion coupled with vast number of mobile Li^+ ions.

4.5 Temperature dependent conductivity studies

Figure 4.7 shows the variation of log ionic conductivity as a function of reciprocal temperature for plasticised polymer electrolytes with the DES content of 20, 40, 60 and 80 wt. %. The regression values (R^2) that lie close to unity reveal the linear relationship that co-exists between these two parameters. It can be verified that all the tested samples obey Arrhenius theory where the conductivity mechanism is thermally assisted (Shriver *et al.*, 1981).

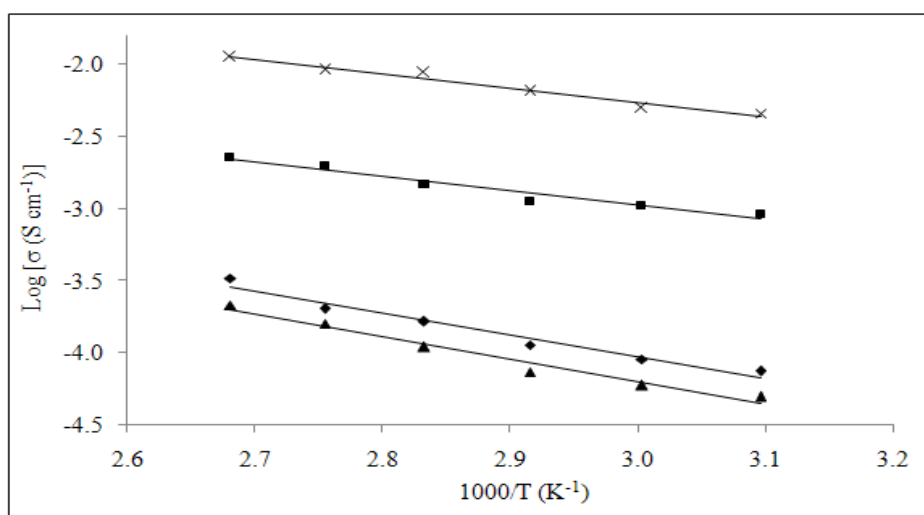


Figure 4.7: Arrhenius plots of log ionic conductivity against reciprocal temperature for samples DES-20 (▲), DES-40 (◆), DES-60 (■) and DES-80 (x)

The nature of cation transport in the DES plasticised samples are quite similar to that in ionic crystals, where ions jump into neighbouring vacant sites (Armand, 1986).

This model explains that when the temperature of polymer electrolytes are increased, the polymer chain acquires faster internal modes in which bond

rotations produce segmental motion. Thus, favours inter or intra-chain ion hopping and accordingly, the ionic conductivity of the polymer electrolyte will be improved with rise in temperature from 323 to 373 K.

All the tested samples obey Arrhenius theory revealing that there is no phase transition in the plasticized polymer electrolytes matrix in the temperature range studied. The ion transport mechanism in polymer electrolytes can effectively be expressed as below:

$$\sigma = \sigma_0 \exp (-E_a/kT) \quad (4.1)$$

where σ_0 is a pre-exponential factor, E_a is the activation energy in kJ mol^{-1} , k is Boltzmann constant and T is the absolute temperature in K.

Table 4.3 summarises the activation energy (E_a) of polymer electrolytes with different DES concentration calculated from the slope of the Arrhenius plot. Based on the tabulated results, it was found that E_a decreases with increase in DES concentration.

Table 4.3: Activation energies of samples calculated using Arrhenius equation

| Sample | Activation energy, E_a (kJ mol^{-1}) |
|--------|---|
| DES-20 | 13.16 |
| DES-40 | 12.55 |
| DES-60 | 8.25 |
| DES-80 | 8.22 |

This was attributed to the increase in the amorphous elastomeric fraction in the CS: LiTFSI: DES matrix that facilitates fast Li^+ ion motion in polymer network upon increase in temperature (Armand, 1986; Ratner and Shriver, 1988). The sample with lowest E_a value will exhibit the highest ionic conductivity due to greater migration of Li^+ ions.

4.6 Thermogravimetric Analysis

Knowledge on the influence of both LiTFSI and DES concentration on the CS matrix thermal properties was evaluated by the overlay thermogravimetric curves of pure CS, DES-0, DES-20 and DES-80 as represented in Figure 4.8.

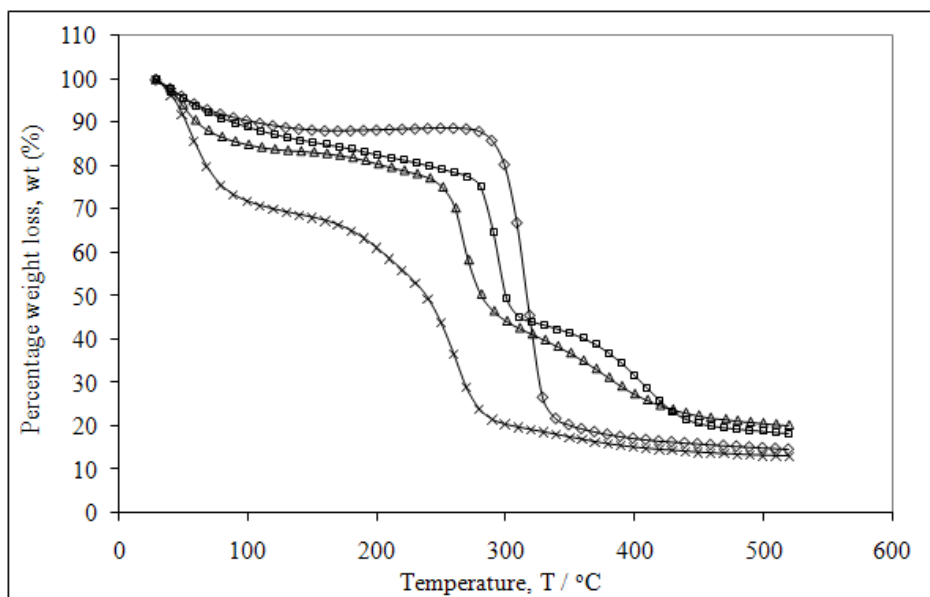


Figure 4.8: Thermogravimetric curves for pure CS (\diamond), DES-0 (\square), DES-20 (Δ) and DES-80 (\times)

The maximum decomposition temperature and total weight loss being obtained from Figure 4.8 has been recapitulated in Table 4.4.

Table 4.4: The maximum decomposition temperatures and percentages of total weight loss for pure CS, DES-0, DES-20 and DES-80

| Sample | Maximum decomposition temperature, T_d ($^{\circ}\text{C}$) | Total weight loss, wt (%) |
|---------|---|---------------------------|
| Pure CS | 317.56 | 86 |
| DES-0 | 406.67 | 82 |
| DES-20 | 382.50 | 80 |
| DES-80 | 261.45 | 88 |

Based on the thermogravimetric curve of DES-0, an improvement in both the heat-resistivity and thermal stability of pure CS were observed upon incorporation of LiTFSI. The observed enhancement in heat-resistivity was correlated to the decomposition of the organic part in LiTFSI which induces the displacement of the maximum decomposition temperature to a higher level. Since it is heat stable thus less monomer will be detached from the complex structure, hence lower the total weight loss.

Thermal properties are further altered upon addition of DES in polymer electrolytes. It can be observed that the DES plasticised polymer electrolytes exhibited weight loss starting at temperature $100\text{ }^{\circ}\text{C}$, which was almost $200\text{ }^{\circ}\text{C}$ lower than those experienced by non-plasticised sample as in Figure 4.8. These reveal that the crystalline structures of the plasticised samples were not sustained due to the good miscibility of DES in CS: LiTFSI matrix.

The displacement of the maximum decomposition temperature of sample DES-20 to lower temperature reveals the decline in the samples heat-resistivity. The diminishing heat-resistivity explains the possible structural disorderness in CS matrix that leads to the existence of vast free volume between the connected molecules which result in weaker bonding. Apparently, small amount of heat is sufficient to overcome the weak interactions between the connected molecules present in the amorphous region and hence decomposed at lower temperature. This incorporation improves the thermal stability of the polymer electrolytes which is evidenced by the reduction in total weight loss.

Further increase in DES content leads to the decline in both the heat-resistivity and thermal stability. This was associated with the presence of greater amorphous phase in the polymer electrolytes making it more heat sensitive. Hence, reduction in heat-resistivity will be observed accompanied by an increase in total weight loss as more DES particles are eliminated from the polymer electrolytes matrix upon the heating process (Mohamad and Arof, 2007).

CHAPTER 5

RESULTS AND DISCUSSION: SYSTEM II

5.1 Conductivity studies at room temperature

The dependence of ionic conductivity on DES concentration is clearly illustrated in Figure 5.1 in the plotted $\log \sigma$ versus percentage weight of DES at ambient temperature. The ionic conductivity of the polymer electrolytes significantly improved from 10^{-7} to 10^{-3} S cm^{-1} as the amount of DES is increased from 0 wt. % to 60 wt. % before a drop in the ionic conductivity is observed at the highest DES content.

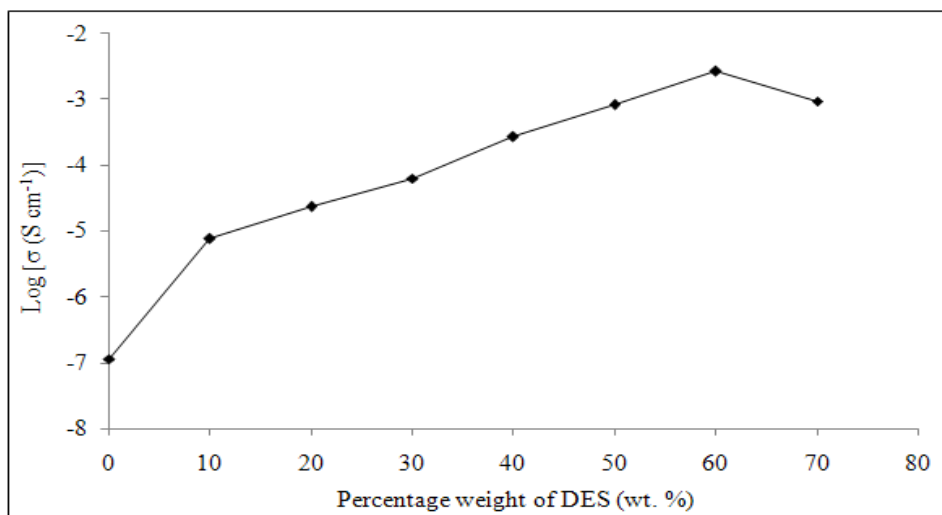


Figure 5.1: Variation of log ionic conductivity (σ) as a function of DES concentration at room temperature

The continuous increase in the ionic conductivity was accounted due to the increase in the mobility of lithium conducting ions (Li^+) in the polymer

matrix. The mobility of Li^+ ions take place by forming coordination with the unoccupied oxygen atom in polymer backbone, obtained upon breaking the bond in $-\text{OAc}$ functional group. The breaking of bond suppresses the high degree of crystallinity in CA matrix and allows the presence of very high concentration of amorphous phase (disordered arrangement). This condition permits a large number of Li^+ ions to move between the polymer chains without restrictions and consequently increase the ionic conductivity.

Another rationale to support the enhancement of ionic conductivity was discussed in terms of the increase in the non-bridging chloride ions (Cl^-) upon the miscibility of DES in the polymer matrix. This allows more number of transit sites to be available for the Li^+ ions to hop from one oxygen vacant site to another with ease through an alternative pathways created by the ionised DES particles (Yahya *et al.*, 2006). The increase in the capacity of ionic transfer enhances the ionic conductivity of the polymer electrolytes.

A drop in the ionic conductivity was observed when 70 wt. % of DES was incorporated in the polymer electrolytes. At this stage the presence of a large number of ionised DES particles tends to conglomerate forming neutral ion multiples which reduces the polymer-ionic mixture interface (Winie *et al.*, 2009; Anantha and Hariharan, 2005). Thus, the existing conducting pathways will be blocked and this restricts the movement of Li^+ mobile ions that crucial in enhancing the ionic conductivity.

The results show that sample CA-60 appears as the highest ion conducting sample with the calculated ionic conductivity value of $2.61 \times 10^{-3} \text{ S cm}^{-1}$ at ambient temperature. This is due to the immense presence of Li^+ ions that effectively interacts with the unoccupied oxygen in the polymer backbone. This complexation in turn facilitates the mobility of Li^+ ions for the purpose of enhancing the ionic conductivity.

5.2 Relative viscosity studies

This selected scrutiny was performed to determine the relative viscosity (η_{rel}) and fluidity (ϕ) possessed by a set of DES plasticised polymer electrolytes at room temperature. Theoretically, samples with low relative viscosity exhibits high ionic conductivity due to greater ion fluidity (Sharma and Sekhon, 2007). The identified low relative viscosity correlates with greater structural disorderness in the polymer matrix which offers vast free volume for Li^+ ions to move with immense ion fluidity and hence tempt high ionic conductivity.

Figure 5.2 exemplifies the dependence of relative viscosity and fluidity with change in the DES concentration in polymer electrolytes at room temperature.

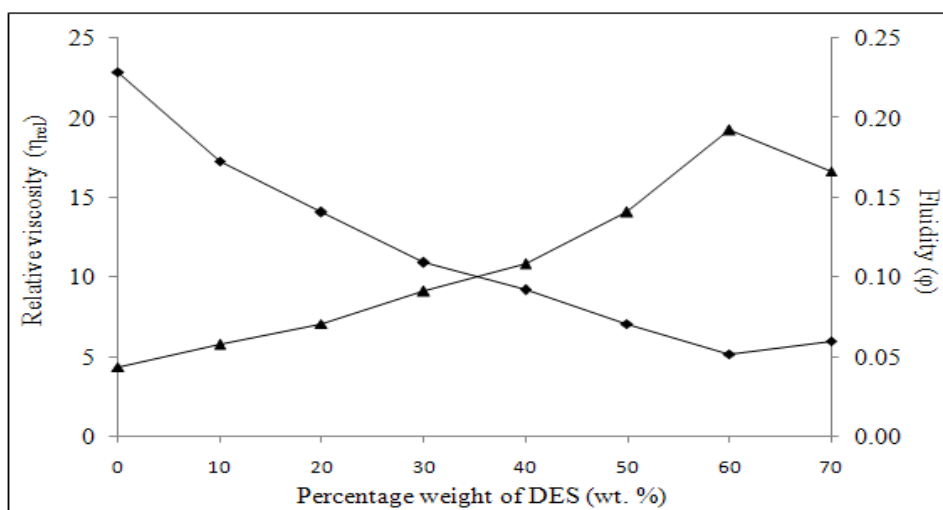


Figure 5.2: The dependence of relative viscosity (η_{rel} , \blacklozenge) and fluidity (ϕ , \blacktriangle) upon DES concentration at room temperature

Based on the collected results, it was found that an increase in DES concentration from 0 wt. % to 60 wt. % contributes to a continuous decline in the relative viscosity from 22.91 to 5.2. The continuous diminution was basically with increase in the concentration of free chloride ions (Cl⁻) as more DES particles dissociates in CA: LiTFSI matrix, which responsible in collapsing the crystalline network in CA matrix. This then leads to more dominant structural disorderliness making more availability of amorphous region. Hence, the greater free volume promotes rapid Li⁺ ions mobility within the polymer chains without restriction and consequently contributes to greater ionic conductivity. The increase in the Li⁺ ions mobility as increase in DES concentration well fitted the fluidity results, observed through an increase in the fluidity value from 0.04 (CA-0) to 0.19 (CA-60).

Further addition of DES above 60 wt. % results in a slightly increase in relative viscosity. This was solely due to the aggregation of excess DES particles forming neutral ion multiples (Zhang, 2009; Winie *et al.*, 2009; Anantha and Hariharan, 2005) at high DES concentration. This aggregation blocks the existing conducting pathways and consequently restricts the mobility of Li⁺ ions within the CA: LiTFSI matrix. The observed phenomenon was double confirmed based on the reduction in ions fluidity value at 70 wt. % of DES which successively contributes to a decline in ionic conductivity.

In view of the results, it was found that the sample containing 60 wt. % of DES possesses the lowest relative viscosity and the highest fluidity value.

This implies that CA-60 seized the highest ionic conductivity due to its highly amorphous nature which provides greater free volume for high Li^+ ions mobility.

5.3 Frequency dependence of loss tangent studies

This analysis provides detailed information on the movement of Li^+ ions in the CA: LiTFSI: DES matrix formed by different DES concentration. The respective loss tangent plot is represented in Figure 5.3 for samples CA-0, CA-40, CA-50 and CA-60. The appearance of peak in both non-plasticised and plasticised samples reveal the presence of relaxation dipoles (Paradhan *et al.*, 2008) possessed by Li^+ ions even in the presence of DES in the matrix.

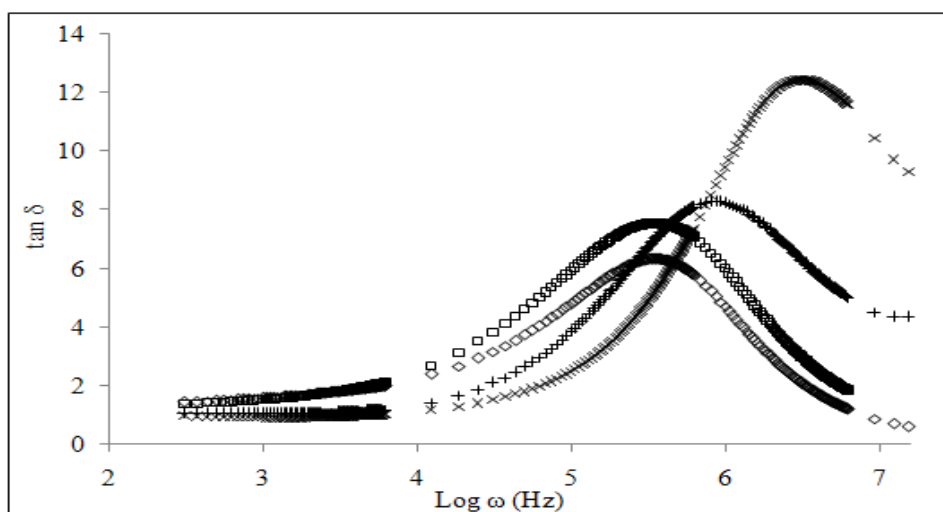


Figure 5.3: Variation of $\tan \delta$ as a function of angular frequency for samples CA-0 (\diamond), CA-40 (\square), CA-50 (+) and CA-60 (x)

Based on the results, it can also be visualised that the loss tangent peaks continuously shift towards the higher frequencies upon increase in DES content. The shift in peaks illustrate the reduction in the relaxation time of Li^+ ions due to greater acceleration on its mobility as more DES concentration is incorporated in the polymer electrolytes (Paradhan *et al.*, 2008).

Other rationale to support the shifting of peaks may correlate to the increasing number of non-bridging ions in DES (Cl^-) as the DES content in polymer electrolytes increased. These non-bridging ions (Cl^-) obtained from the miscibility of DES in the polymer matrix acts as a transit site for the Li^+ ions. This transit site increases the capacity of the Li^+ ion transfer and at the same time shorten the distance for Li^+ ions to hop from one oxygen atom to another in polymer chain. The shorter distance for Li^+ ion migration makes it to acquire less energy loss. Hence, frequent migrations of Li^+ ions are expected to occur that crucial in enhancing the ionic conductivity. The displacement of peaks leads to an understanding on the increase in the amorphous elastomeric fraction as more DES is incorporated into the matrix which provides greater free volume to ease Li^+ ions mobility which would consequently increase ionic conductivity.

The magnitude of the $\tan \delta$ also provides an informative insight on the number of Li^+ ions participating in ion conduction (Azizi Samir *et al.*, 2004). It was found that as the magnitude of the sample increases, the resulting area under the loss factor peak also adequately increases upon increase in DES concentration. This was ascribed to the increase in the number of Li^+ ions that participates in the relaxation process. As the DES concentration in the polymer electrolytes increase, it effectively weakens the inter-coulombic force that connects the anions and cations in LiTFSI, making more Li^+ ions to be available. Thus, enhancement in ionic conductivity will be observed as increase in DES content.

It can be concluded that increase in DES content would mean more mobile free ions from the DES to be available to speed up the segmental motion by increasing the available free volume through structural conversion. This increase would also be beneficial for the ease in Li^+ ion transfer. Sample CA-60 exhibits the highest ionic conductivity due to the relatively fast segmental motion coupled with greater presence of Li^+ ions.

5.4 Scanning electron microscopy (SEM)

The structural disorderliness in CA: LiTFSI matrix upon different addition of DES concentration was visualised based on the SEM photographs. The surface morphology of sample CA-0, CA-40, CA-50 and CA-60 were presented in Figure 5.4 (a-d) with the magnification factor of 1000 X.

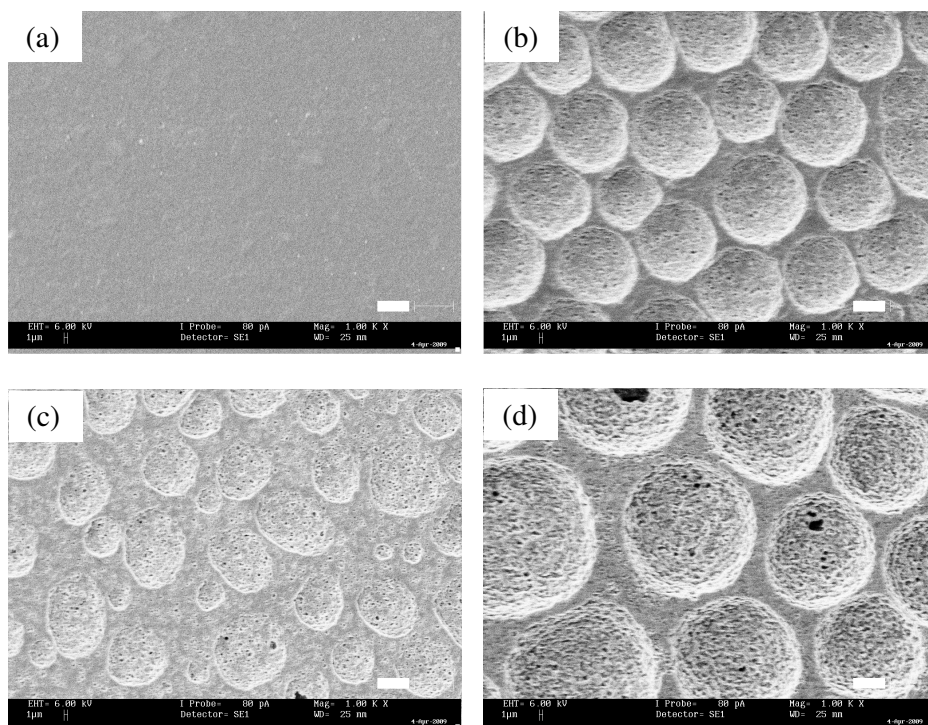


Figure 5.4: SEM micrographs of samples (a) CA-0, (b) CA-40, (c) CA-50 and (d) CA-60 obtained at room temperature, with the bar length of $1 \mu\text{m} = 0.2 \text{ cm}$ for the image dimension $27.0 \text{ cm} \times 20.3 \text{ cm}$

The SEM image in Figure 5.4 (a) illustrates that sample CA-0 is highly crystalline in nature based on the observation of smooth gray surface. This indicates the high order of the polymer chains in localised regions which exhibits low ionic conductivity.

Upon addition of DES in the polymer electrolytes, spheres, as in Figure 5.4 (b-d) are observed. These spheres represent the crystalline region which consists of a number of platelets or lamellae radiating from a nucleating centre, called spherulites (Paradhan *et al.*, 2008; Singh *et al.*, 2008). The regions between the neighboring lamellae show the existence of amorphous phase which are crucial for the ion conduction. The observation of spheres evident the disruption of formerly ordered coils (crystalline region) in CA-0 to a disordered form (less regular arrangement of the coils) in DES plasticised samples (Singh *et al.*, 2008), which improves the ionic conductivity.

Based on the previous analysis, greater structural conversion occurs as the DES content is increased from 0 wt. % to 60 wt. %. This statement can be proved by referring to Figure 5.4 (b-d). Initial observation of spheres having the diameter ranging between 24 to 29 μm in CA-40 was disrupted to the diameter range of 16 to 23 μm and become more diffuse upon addition of DES as shown in sample CA-50. This clearly indicates the reduction in the overall crystallinity of the sample with further doping of DES that crucial in enhancing the ionic conductivity.

Further addition of DES induce to the observation of spheres with greater diameter and reduction in the number of spheres that is visible on the surface of CA-60 as observed in Figure 5.4 (d). The greater diameter of spheres was obtained upon the clustering of small spheres in sample CA-50 whereas the decline in the number of spheres evident the increase in the free void as viewed by the increase in the region between the sphere boundaries in

Figure 5.4 (d). This composition appears as the highest conducting sample owing to the increase in the free void, ignoring the effect of the increasing diameter of spheres. The increase in the free void improves the charge transfer mechanism and hence increases the ionic conductivity.

5.5 Horizontal attenuated total reflectance-Fourier transform infrared (HATR-FTIR)

FTIR spectroscopy is a reliable and well recognised fingerprinting technique used in detecting the complexation between the constituents that present in both crystalline and amorphous phase. The occurrence of complexation can be deduced by relying on the alternations in the cage peaks in terms of the frequency shifting, shape, relative intensity, disappearance of existing peak and even through the formation of new peaks. The FTIR spectra of polymer electrolytes vary according to their compositions and it is independent of concentration.

The band assignments of pure substances are summarized in Table 5.1 (Ramesh *et al.*, 2008; da Conceição *et al.*, 2003).

Table 5.1: Band assignments and wavenumbers of some important peaks in FTIR spectra exhibited by pure CA, pure LiTFSI and pure DES

| Sample | Band assignments | Wavenumber (cm ⁻¹) |
|--------|------------------------------------|--------------------------------|
| CA | O-H stretching | 3445 |
| | C-H stretching (CH ₃) | 2932 |
| | C-H stretching (CH ₂) | 2879 |
| | C=O symmetric | 1734 |
| | C=O asymmetric | 1656 |
| | CH ₂ bending | 1436 |
| | δ C-H bending | 1369 |
| | C-O-C asymmetric bridge stretching | 1158 |

Table 5.1 continued: Band assignments and wavenumbers of some important peaks in FTIR spectra exhibited by pure CA, pure LiTFSI and pure DES

| Sample | Band assignments | Wavenumber (cm ⁻¹) |
|--------|-------------------------------------|--------------------------------|
| CA | C-O-C stretching of the pyrose ring | 1032 |
| | δ C-H | 901 |
| LiTFSI | O-H | 3419 |
| | S-CH ₃ | 2979 & 2876 |
| | C-SO ₂ -N | 1356 |
| | -CF ₃ | 1193 |
| | C-F stretch | 1142 |
| | S=O | 1065 |
| DES | C-H stretching (CH ₃) | 2964 |
| | C-H stretching (CH ₂) | 2873 |
| | Ammonium ion | 1169 |

The occurrence of complexation between pure CA and pure LiTFSI was confirmed based on the alternations in CA-0 spectrum as depicted in Figure 5.5.

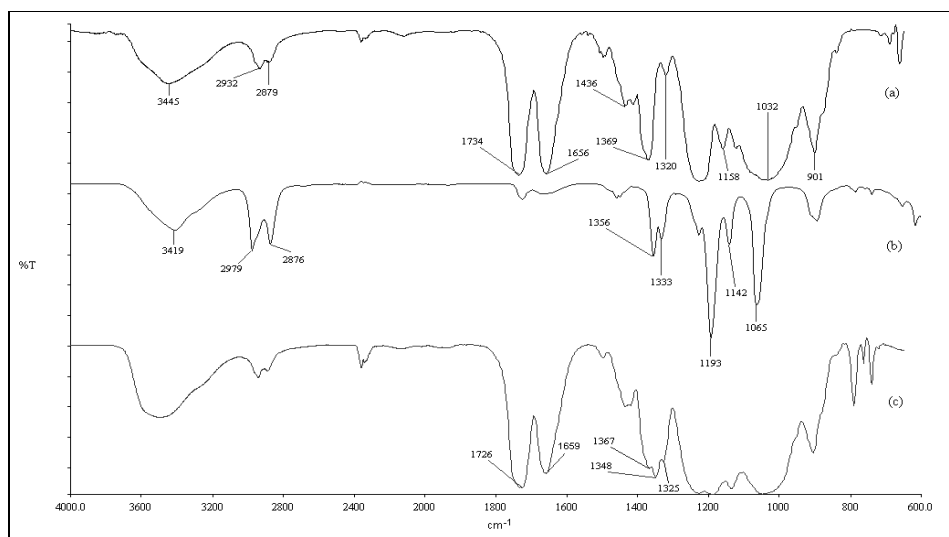


Figure 5.5: FTIR spectra of (a) pure CA, (b) pure LiTFSI and (c) CA-0

In Figure 5.5 (a), the peak at 1734 cm^{-1} was shifted to lower frequency at 1726 cm^{-1} in CA-0 after complexation with LiTFSI. This evident the dissociation of lithium from LiTFSI, which then forms coordination with the electron donor oxygen atoms in polymer backbone. This interaction consequently results in the reduction in peak relative intensity from 64 % (pure CA) to 55 % (CA-0) as shown in Figure 5.6.

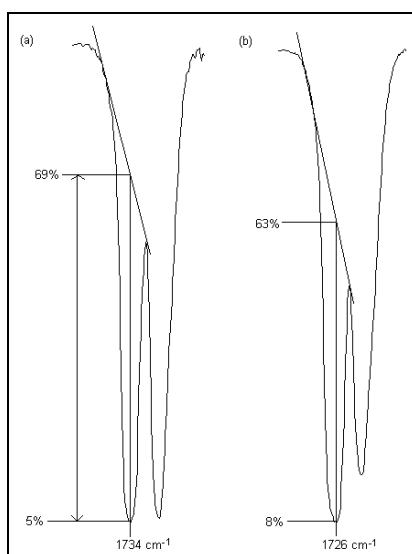


Figure 5.6: The changes in intensity of C=O symmetric band for (a) pure CA and (b) CA-0

The complexation between these two pure constituents was further supported by the absence of peak at 1320 cm^{-1} in pure CA upon addition of LiTFSI. The disappearance of peak proves the breaking of -Ac from the -OAc functional group, allowing the oxygen to be unoccupied in order to behave as a transit site for the mobility of Li^+ ions.

A simple peak overlapping between a single intense peak at 1369 cm^{-1} in pure CA with two peaks at 1356 and 1333 cm^{-1} in pure LiTFSI (Figure 5.5 (b)) results in three peaks formation at 1367 , 1348 and 1325 cm^{-1} in CA-0.

The observed change in the shape of peak was one of the evidence to prove the complexation. The peak that co-exists at 1656 cm^{-1} in pure CA was displaced to higher frequency at 1659 cm^{-1} in CA-0 upon complexation with LiTFSI. Besides that, the relative intensity of this peak gradually decreases from 61 % (pure CA) to 47 % (CA-0) after interaction with LiTFSI. The occurrence of complexation between CA and LiTFSI was further been verified by the band broadening effect at the frequency range of $1030\text{-}1250\text{ cm}^{-1}$ (Figure 5.5 (c)) which results from the overlapping of peaks. The change in the cage peaks discussed indicates the occurrence of complexation between CA and LiTFSI.

The incorporation of DES in CA: LiTFSI matrix also induces the occurrence of complexation. This can be clearly observed from the FTIR spectrum of sample CA-40 and CA-60 in Figure 5.7.

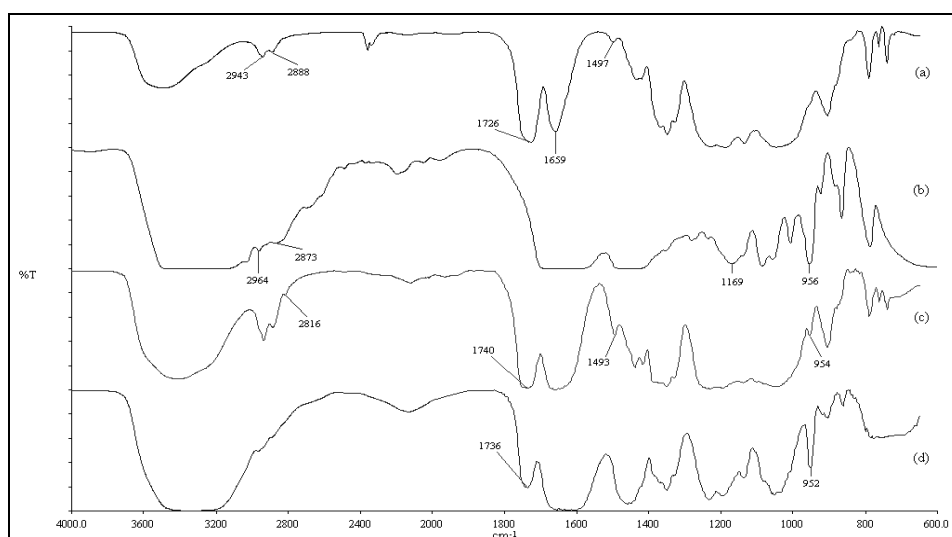


Figure 5.7: FTIR spectra of (a) CA-0, (b) pure DES, (c) CA-40 and (d) CA-60

In Figure 5.7 (a), the peak present at 1497 cm^{-1} was displaced to a lower frequency at 1493 cm^{-1} upon incorporation of 40 wt. % DES (Figure 5.7 (c)) and further addition of 60 wt. % of DES (Figure 5.7 (d)) in the polymer electrolytes gave rise to the disappearance of this particular peak. These observations suggest that there are some degree of complexation occurred when DES is incorporated in CA: LiTFSI polymer electrolytes.

The occurrence of complexation can further be proved by relying on the C=O characteristic peak present at 1726 cm^{-1} in CA-0. This peak shifted to 1740 cm^{-1} and 1736 cm^{-1} , respectively in CA-40 and CA-60 upon complexation with different DES content. Besides that, the relative intensity of this particular peak decreases from 55 % (CA-0) to 45 % (CA-40) and finally to 38 % (CA-60). The two moderate peaks that co-exist at 2943 cm^{-1} and 2888 cm^{-1} in CA-0 become more intense and a shoulder forms at 2816 cm^{-1} after 40 wt. % of DES is added in non-plasticised sample. The cage peaks were found to flatten at high concentration of DES (CA-60).

Other evidence to prove the complexation was from peak at 956 cm^{-1} in Figure 5.7 (b). This peak was found to have shifted to a lower frequency with the value of 954 cm^{-1} (CA-40) and 952 cm^{-1} (CA-60) as more DES particles interact with CA: LiTFSI matrix. This continuous shifting to lower frequencies evidence the increasing amount of nitrogen atom that actively participates in forming coordination with Li^+ ions. The peak at 1659 cm^{-1} in CA-0 subsequently broadens as DES concentration is increased in CA-0, implying the greater involvement of oxygen atom (C=O asymmetric) in

forming coordination with increasing amount of Li^+ ions.

The observed changes on the cage peak suggest that some degree of co-ordination or complexation has occurred between CA, LiTFSI and DES. The similarity between the FTIR spectrums for each sample indicates that LiTFSI and DES are physically bonded with CA.

5.6 X-ray diffractometry (XRD)

X-ray diffraction analysis was executed in order to monitor the changes in the structural properties of the polymer electrolytes as different amount of DES is incorporated in the CA: LiTFSI system. This is a versatile technique used for phase identification of a material available in both crystalline and amorphous region that aids in explaining the exerted ionic conductivity.

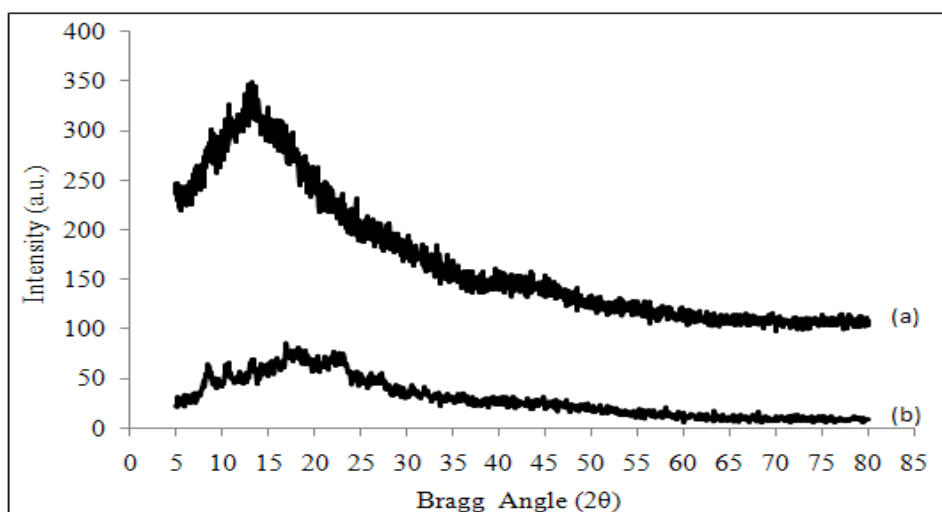


Figure 5.8: XRD patterns of pure CA that present in two different states (a) powder and (b) thin film forms

Figure 5.8 depicts the diffraction patterns of pure CA present in two different forms, powder and thin film. Based on Figure 5.8 (a), observation of an intense diffraction peak centered at $2\theta = 13.5^\circ$ reveals the crystalline nature of CA powder. This peak become less prominent after the CA powder was processed into thin film as seen in Figure 5.8 (b). The initial degree of crystallinity possessed by CA was suppressed and allowed to be present in

semi-crystalline nature. This evidence through the observation of moderate intense peaks within the hump diffraction peak that co-exist at the angles $2\theta = 8.5^\circ$, 10.5° , 13.5° , 17.5° and 23.5° . Based on the above, it was clear that the first structural disorderness occurs when the CA powder was dissolved in the organic solvent to process it into thin film.

In order to further understand the structural conversion that takes place in CA: LiTFSI: DES system, a few selected samples with different DES content was subjected to this analysis. Figure 5.9 depicts the diffraction patterns of pure CA (thin film), pure LiTFSI, CA-0, CA-40 and CA-60 at room temperature.

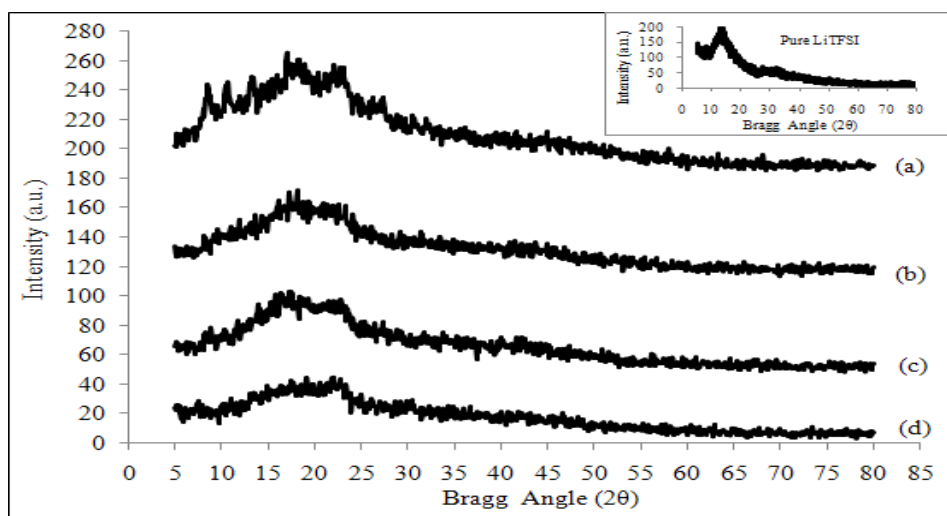


Figure 5.9: XRD patterns of (a) pure CA-thin film, (b) CA-0, (c) CA-40 and (d) CA-60

The inset graph that represents the XRD pattern of pure LiTFSI reveals the crystalline nature of this compound based on the existence of single intense diffraction peak centered at $2\theta = 13.5^\circ$. This particular peak was

found to be absent in CA-0 which correlates to the complete dissolution of LiTFSI in the CA matrix (Sharma and Sekhon, 2007). The complete dissolution induces an increase in the amorphous region of CA matrix based on the absence of the moderate intense peak ($2\theta = 8.5^\circ$, 10.5° and 13.5°) and a substantial broadening in the CA-0 diffraction peak.

The diffractograms in Figure 5.9 (c–d) clearly indicate the fact that the semi-crystalline nature in CA: LiTFSI matrix was further being disrupted by the addition of DES. This was confirmed by the substantial broadening in the diffraction peak at the angle ranging from 5° to 30° in the DES plasticised samples. It was noted that as the percentage of DES in the polymer electrolyte increases from 40 to 60 wt. % the diffraction peak substantially decreased in intensity accompanied by an increase in broadness. This observation marks the decline in the degree of crystallinity in CA matrix as more DES is incorporated in the CA: LiTFSI: DES system.

The two diffraction peaks assigned at $2\theta = 17.5^\circ$ and 23.5° in CA-40 further illustrates the suppression of crystalline region. Further incorporation of 20 wt. % DES in CA-40 alters the shape of diffraction peak at $2\theta = 17.5^\circ$ (CA-40) to a slight shoulder as shown in CA-60. This observation suggests that further structural conversion had taken place at that particular angle and more free volume were available for the movement of Li^+ ions. Some degree of crystallinity in CA still persists even till the highest conducting composition, as observed from the distinct peak at $2\theta = 23.5^\circ$. This reveals that the system is not fully amorphous yet attains high ionic conductivity due

to the reduction in the intensity of the CA crystallization peak from a hump shape (in CA powder) to a broadening shape upon addition of LiTFSI and DES. The observed changes on the diffraction peak also provide an insight on the occurrence of complexation between CA, LiTFSI and DES that takes place in the amorphous region (Ramesh *et al.*, 2010).

The associated reduction in crystallinity was caused by the significant structural reorganisation by the presence of DES that induces greater structural disorderness. The observed increase subsequently cause a decline in the energy barrier to the segmental motion of the polymer electrolytes (Baskaran *et al.*, 2006) which will enable the Li⁺ ions to accelerate and induce greater ionic conductivity. It can be concluded that the sample CA-60 experiences greatest structural conversion from crystalline to amorphous region enabling it to possess greater free volume for the movement of Li⁺ ions. Thus, CA-60 will be the highest conducting sample concurrent with earlier findings.

5.7 Temperature dependent conductivity studies

Figure 5.10 represents the temperature-dependent ionic conductivity of sample CA-40 and CA-60. The regression values of all the tested samples are close to unity, revealing that the conductivity mechanism is in agreement with Arrhenius rule.

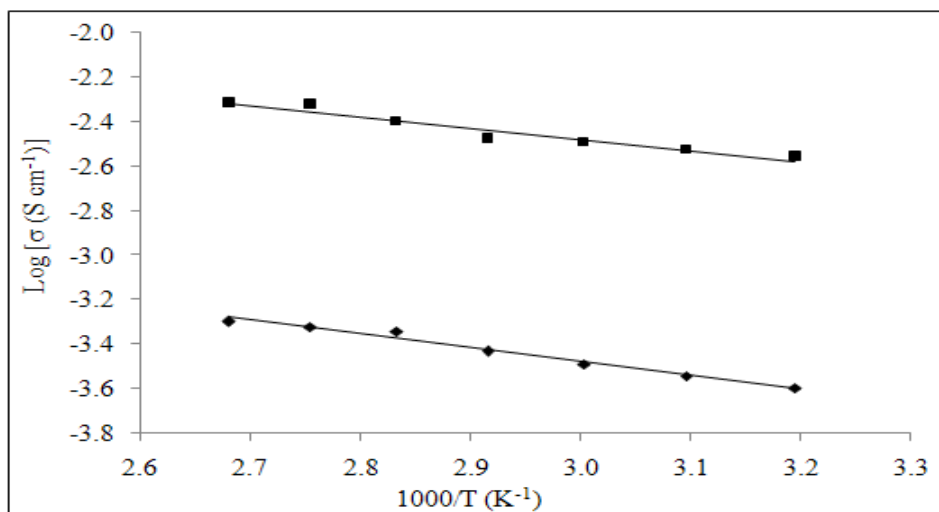


Figure 5.10: Arrhenius plots of log ionic conductivity (σ) against reciprocal temperature for samples CA-40 (♦) and CA-60 (■)

According to the Arrhenius behavior, the nature of cation transport is quiet similar to that in ionic crystals, where ions jump into neighbouring vacant sites (Ramesh *et al.*, 2002).

These types of samples will experience an enhancement in the ionic conductivity with increase in temperature. This signifies that the ion transport mechanism is thermally assisted (Ramesh *et al.*, 2002), whereby when a sample is subjected to a certain temperature rise, the polymer chain acquires

faster internal modes in which bond rotations produce segmental motion. Thus, favours inter or intra-chain ion hopping, and hence the degree of ionic conductivity being enhanced by the free paths (Kumar *et al.*, 2009).

It was noted that there is no phase transition in the DES plasticised polymer electrolytes in the temperature range studied since all the tested samples obey a common rule. The ion transport mechanism in polymer electrolytes was correlated with the equation below:

$$\sigma = \sigma_0 \exp (-E_a/kT) \quad (5.1)$$

where σ_0 is a pre-exponential factor, E_a is the activation energy in kJ mol^{-1} , k is Boltzmann constant and T is the absolute temperature in K.

The activation energy (E_a) for all the tested samples were calculated by using the slope of the graph and the values are 5.16 and 4.23 kJ mol^{-1} for CA-40 and CA-60, respectively. It was found that the E_a decreases with increase in DES content. This was attributed to the increase in the flexibility of polymer backbone promoted by the decrease in the crystallinity of CA matrix. Thus, greater amorphous fraction will be available which consequently increases the migration of lithium mobile ions. Hence, sample with low E_a value will possess high ionic conductivity which in this case refers to sample CA-60.

5.8 Conductivity retained studies

Incorporation of DES in polymer electrolytes is believed to improve the aging effect. In order to justify the mentioned statement, the ionic conductivity of selected samples was monitored at room temperature for the duration of 30 days. The collected results were plotted in Figure 5.11 (a-d) which depicts the variation of ionic conductivity values as a function of storage time for samples CA-0, CA-20, CA-40 and CA-60, respectively at room temperature.

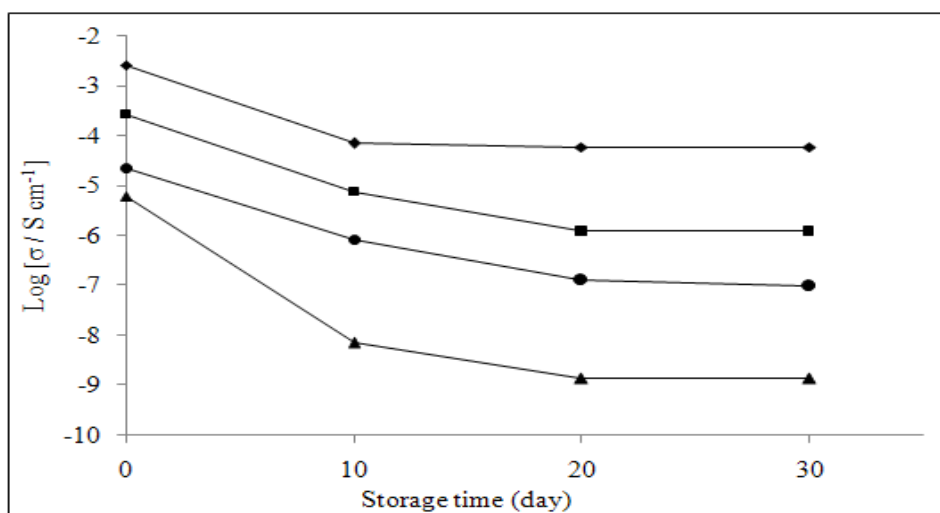


Figure 5.11: Variation of log ionic conductivity as a function of storage time for samples CA-0 (▲), CA-20 (●), CA-40 (■) and CA-60 (◆) at room temperature

It is clearly observed from Figure 5.11 that the sample CA-0 experience greatest decrease in ionic conductivity as compared to the DES plasticised polymer electrolytes. This concludes that CA-0 does not have the tendency to retain ionic conductivity for a longer duration. This may be due to the high crystallinity of CA-0 that does not have the ability to hold the liquid

component within the membrane structure. Thus, the ionic conductivity decreases over time caused by the dissipation of liquid component from the matrix.

In view of the results for CA-20, CA-40 and CA-60, the ionic conductivity was further retained as increase in DES concentration. This was due to the increase in the polar functional groups that have higher liquid retention capabilities (Ramesh and Arof, 2009). Thus, more liquid component will be trapped within the CA membrane structure providing a dilute medium to ease the lithium conducting ions (Li^+) motion and hence, retain the ionic conductivity over the entire storage time (Ramesh and Arof, 2009). Additionally, there is no significant change was observed in the ionic conductivity for all the tested samples after 10 days. This reveals that the samples retain high chemical integrity overcoming the liquid leakage limitation over the storage time.

The increase in DES concentration in the polymer electrolytes considerably enhances the stability of CA: LiTFSI: DES matrix evident by its capability in retaining the integrity over the storage time. Sample CA-60 appears as the highest conducting sample which has high tendency in retaining the ionic conductivity from $2.61 \times 10^{-3} \text{ S cm}^{-1}$ (after casting) to $5.89 \times 10^{-5} \text{ S cm}^{-1}$ after the storage time of 30 days. This was due to the presence of high concentration of polar functional groups that have high liquid retention capabilities.

5.9 Thermogravimetric analysis

Thermogravimetric curves were obtained for selected polymer electrolytes to give an insight on the thermal properties governed by CA: LiTFSI: DES matrix with different DES content. Figure 5.12 represents the overlay of all four thermogravimetric curves for pure CA, CA-0, CA-40 and CA-60.

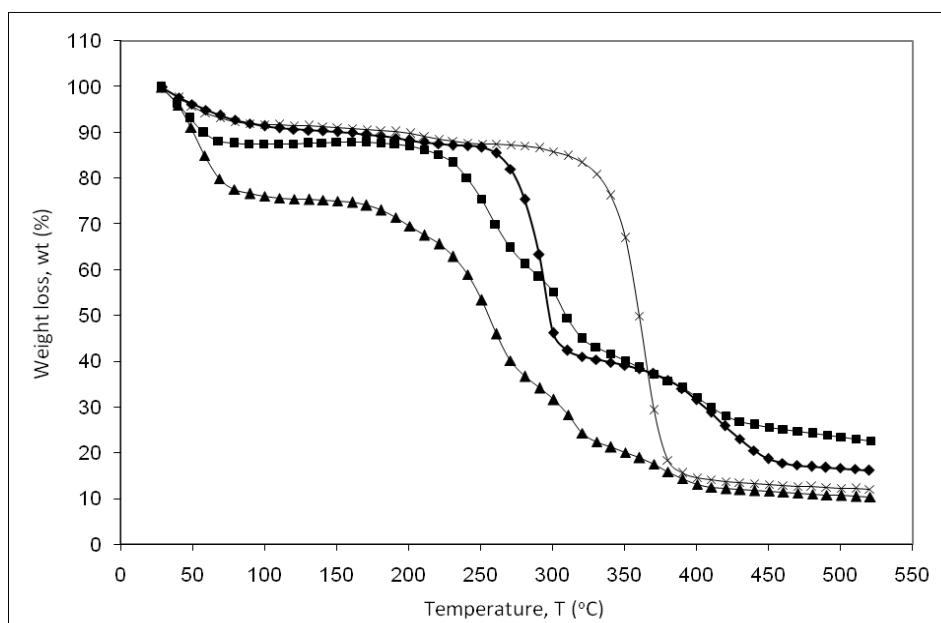


Figure 5.12: Thermogravimetric curves of pure CA (x), CA-0 (◆), CA-40 (■) and (d) CA-60 (▲)

The maximum decomposition temperature and percentage total weight loss of the same samples are listed in Table 5.2.

Table 5.2: Maximum decomposition temperatures and percentages of total weight loss for pure CA, CA-0, CA-40 and CA-60 by TGA analysis

| Sample | Maximum decomposition temperature, T_d ($^{\circ}$C) | Total weight loss, wt. (%) |
|---------------|---|-----------------------------------|
| Pure CA | 363.40 | 88 |
| CA-0 | 414.01 | 84 |
| CA-40 | 407.19 | 77 |
| CA-60 | 377.81 | 90 |

In view of the results in Table 5.2, it can be understood that the incorporation of LiTFSI in CA matrix successfully increased both the heat-resistivity and thermal stability of pure CA. The enhancement in the heat-resistivity was attributed to the decomposition of the organic part in LiTFSI which causes the displacement of the maximum decomposition temperature to a higher level. The reduction in the total weight loss experienced by CA-0 was an evidence to support the increase in its thermal stability.

The reduction in the maximum decomposition temperature was observed upon addition of 40 wt. % DES, which deduces the occurrence of structural disorderness in CA matrix that leads to very high concentration of free volume between the connected molecules and results in weaker bonding. Thus, a small amount of heat is sufficient to disrupt the interaction between the molecules present in the amorphous region cause it to decompose at lower

temperature. Therefore, this sample tends to lose its heat resistivity. Improvement in the thermal stability was accounted for the same sample owing to its lowest weight loss among the selected samples.

Further addition of DES, lead to a decline in both heat-resistivity and thermal stability. The sample tends to lose its heat resistivity due to the presence of vast free volume between the connected atoms in amorphous region making it to be more heat sensitive. On the other hand, the thermal stability diminishes due to the elimination of DES particles from the polymer electrolytes matrix upon the heating process (Mohamad and Arof, 2007).

Based on Figure 5.12, it can be notified that all the DES plasticised samples experiences decomposition stage at the temperature beyond 370 °C which was greater than the one observed for pure CA. Thus, it can be concluded that the presence of an appropriate amount of DES in CA: LiTFSI matrix is capable in exerting an appreciable thermal properties that suits the electronic device application.

CHAPTER 6

RESULTS AND DISCUSSION: SYSTEM III

6.1 Conductivity studies at room temperature

Figure 6.1 shows the variation of log ionic conductivity (σ) values of CS: LiTFSI: [Amim] Cl polymer electrolytes as a function of [Amim] Cl concentration. For the simplicity in explaining the ionic conductivity trend, the collected data was divided into two major stages which are stage 1 and stage 2 and further three sub regions were divided under stage 1.

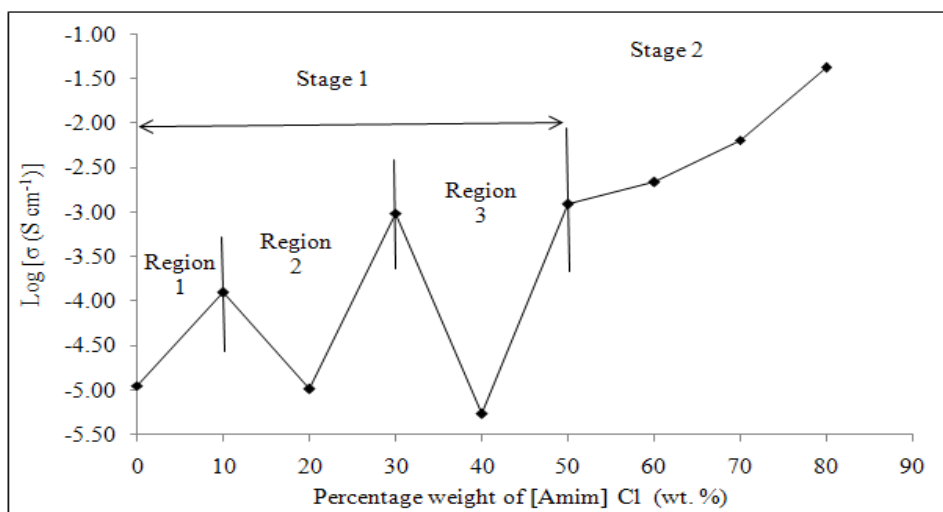


Figure 6.1: Variation of log ionic conductivity (σ) values of CS: LiTFSI: [Amim] Cl polymer electrolytes as a function of [Amim] Cl concentration

The first region in stage 1 reveals that the ionic conductivity of CS-0 was improved with the addition of [Amim] Cl. This is due to the disruption in the crystalline region which provides free volume for the mobility of lithium

conducting ions (Li^+). Further addition of [Amim] Cl in the polymer electrolytes contributes to an abrupt decrease in the ionic conductivity. This initial drop in ionic conductivity was attributed to the blocking of existing conducting pathways due to the possible conglomeration of the excess [Amim] Cl, which reduces the polymer-ionic liquid interface and hence reduces the availability of conducting pathways (Ramesh and Lu, 2008). As the [Amim] Cl concentration is increased to 30 wt. %, the conducting pathways are again created by the dissociation of ion aggregates which leads to an increase in the ionic conductivity as observed in Region 2. Since the ionic conductivity trend in Region 2 and 3 are similar thus both of it shares the same reasons.

In stage 2, the ionic conductivity increases with the addition of [Amim] Cl up to 80 wt. % of [Amim] Cl. The enhancement was attributed to the increase in the concentration of free mobile ions upon dissolution of [Amim] Cl in CS matrix, which are responsible in increasing the amorphous phase (highly disordered) through favorable free volume between the polymer chains. Thus, Li^+ ions migration will take place easily and consequently increases the ionic conductivity. Other plausible reason for the noted enhancement in the ionic conductivity may relate to the increase in the non-bridging ions from [Amim] Cl (Cl^-) in the matrix. These chloride (Cl^-) ions acts as transit site to further ease the mobility of Li^+ ions, which then improves the ionic conductivity. The highest ionic conductivity was achieved for sample CS-80, with the calculated value of $4.18 \times 10^{-2} \text{ S cm}^{-1}$ at room temperature.

At low concentration of [Amim] Cl, no greater free volume will be available in the polymer electrolytes for the movements of Li^+ ions thus at this point the low dielectric constant of [Amim] Cl exerts a significant impact on the ionic conductivity trend. In some extent, this property dominates the free volume effect by leading to the formation of neutral ion multiples that reduces the ionic conductivity. A slight increase in [Amim] Cl concentration will enhance the ionic conductivity. At this stage the free volume effect dominates the low dielectric constant behavior. It can clearly be seen that at low concentration of [Amim] Cl, its low dielectric constant and the free volume effect adequately influences the ionic conductivity until leads to the rapid fluctuation as observed in stage 1. Whereas in stage 2 the ionic conductivity trend was dominated by the free volume effect and as a result no fluctuations in ionic conductivity is observed.

6.2 Relative viscosity analysis

The ionic conductivity of polymer electrolytes depends upon two major factors and those are the concentration of charge carriers (n) and the relative viscosity (η_{rel}) (Sharma and Sekhon, 2007). Since the relative viscosity of polymer electrolytes have significant impact on the ionic conductivity thus this supporting analysis is crucial to double confirm the ionic conductivity trend. Both of these parameters are inversely proportional. The relative viscosity of polymer electrolytes strongly depends on the structural conversion from crystalline to amorphous phase. This means that, a highly crystalline sample possesses greater relative viscosity and exhibits

lower ionic conductivity due to the restriction in Li^+ ions movements.

Figure 6.2 depicts the effect of [Amim] Cl concentration in the relative viscosity (η_{rel}) of the polymer electrolytes at room temperature. This plot was divided into few different sections for easier comparison.

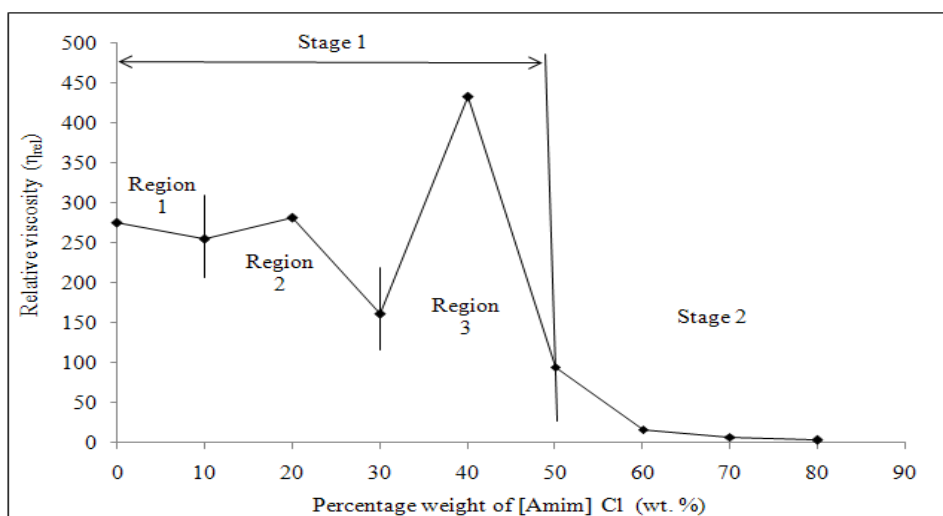


Figure 6.2: Variation of relative viscosity (η_{rel}) of CS: LiTFSI: [Amim] Cl polymer electrolytes as a function of [Amim] Cl concentration at room temperature

Based on the Region 1 in Figure 6.2, it can be seen that the addition of [Amim] Cl in CS-0 reduces the relative viscosity from 275.89 to 254.73 due to the increase in the structural disorderness that promotes greater Li^+ ions migration that responsible in increasing the ionic conductivity. Further addition of [Amim] Cl exhibits an increase in the polymer electrolytes relative viscosity as been observed in Region 2. At this stage the presence of large number of ionised [Amim] Cl particles tend to conglomerate forming neutral ion aggregates which increases the samples relative viscosity and hence reduces the ionic conductivity. The same explanation fits for the trend in Region 3.

Reference to stage 2, the incorporation of [Amim] Cl above 60 wt. % exhibits a continuous decline in the relative viscosity till it reaches 80 wt. % with the calculated value from 16.82 to 3.98. This reduction was due to greater structural conversion from crystalline to amorphous phase which results in greater free volume. This condition allows a large number of Li⁺ ions to move between the polymer chains without restrictions and hence contributes to greater ionic conductivity.

6.3 Frequency dependence of loss tangent studies

Figure 6.3 shows the variation in the displacement of tangent loss peak when the concentration of [Amim] Cl is increased from 20 to 80 wt. %. This characterisation provides an insight on the extent of Li^+ ions transportation in CS: LiTFSI: [Amim] Cl matrix upon increase in [Amim] Cl concentration by relying on the maximum angular frequency ($\log_{\max} \omega$) value whereas the area under the peak correlates to the number of Li^+ ions that participates in the relaxation process.

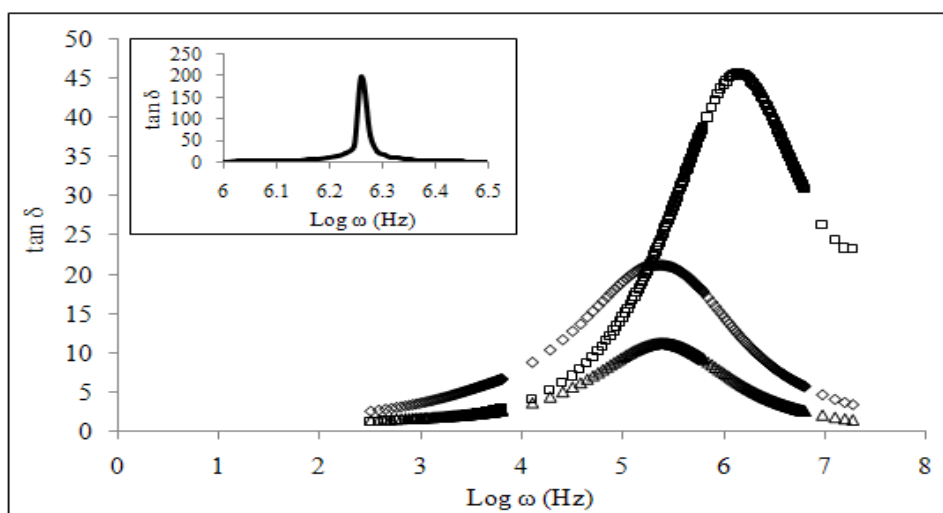


Figure 6.3: Variation of $\tan \delta$ with angular frequency at room temperature for samples CS-20 (Δ), CS-40 (\diamond), CS-60 (\square) and CS-80 (in the inset)

Based on Figure 6.3, the tangent loss peak for CS-40 was slightly displaced to lower frequency in reference to CS-20. This observation correlates an increase in the relaxation time of Li^+ ions upon reduction on its mobility with further increase in [Amim] Cl concentration. The restriction in the Li^+ ions mobility was due to the formation of neutral ion aggregates that blocks the

existing conducting pathways and consequently decreases the ionic conductivity. The variation in the displacement of relaxation frequency ($\log_{\max} \omega$) upon different addition of [Amim] Cl concentration is summarised in Table 6.1.

Table 6.1: Relaxation frequencies for samples with different [Amim] Cl content

| Sample | Relaxation frequency, $\log \omega_m$ (Hz) |
|--------|--|
| CS-20 | 5.4 |
| CS-40 | 5.3 |
| CS-60 | 6.15 |
| CS-80 | 6.26 |

Further increase in [Amim] Cl concentration provokes the tangent loss peak to shift at higher frequencies as observed for sample CS-60 and CS-80. This shifting illustrates the increase in the Li^+ ions mobility upon reduction in the relaxation time. As the concentration of [Amim] Cl is increased from 60 to 80 wt. %, continuous enhancement in the amorphous fraction occur attribute to an increase in the segmental motion. The availability of free volume in the matrix formed eases the mobility of Li^+ ions hence, improves the ionic conductivity. Other plausible reason for the displacement of loss tangent peaks to higher frequencies may correlate to an increase in the number of non-bridging ions in [Amim] Cl (Cl⁻) that increases the capacity of the cation (Li^+) transfer.

The magnitude of $\tan \delta$ also appears as an informative source since the area under the peak inferred to the concentration of mobile Li^+ ions that participate in ion conduction (Azizi Samir *et al.*, 2004). As clearly depict the magnitude of $\tan \delta$ increases as increase in the concentration of [Amim] Cl. This evidence the effectiveness of [Amim] Cl in overcoming the inter-coulombic force in LiTFSI, making more availability of Li^+ ions to assist in enhancing the ionic conductivity.

An enhancement in the ionic conductivity always coupled with two major factors, the prominent influence comes from the greater mobility of Li^+ ions and subsequently followed by the concentration of conducting Li^+ ions. Although the sample CS-40 possess greater concentration of Li^+ ions yet its lower mobility causes the sample to exhibit low ionic conductivity as compared to sample CS-20. From here it is clear that the ionic conductivity is mainly dependent on the mobility of Li^+ ions.

Reference to the plot, sample CS-80 exhibits the highest ionic conductivity attributed to the greater Li^+ ions mobility coupled with vast number of conducting ions that participates in the ion conduction.

6.4 Temperature dependent conductivity studies

An understanding on the mechanism of ion transport in polymer electrolytes was established by relying on temperature dependent ionic conductivity measurement. This measurement was carried out at the temperature ranging from 313 K to 363 K. The variation of ionic conductivity with the reciprocal temperature was represented in Figure 6.4.

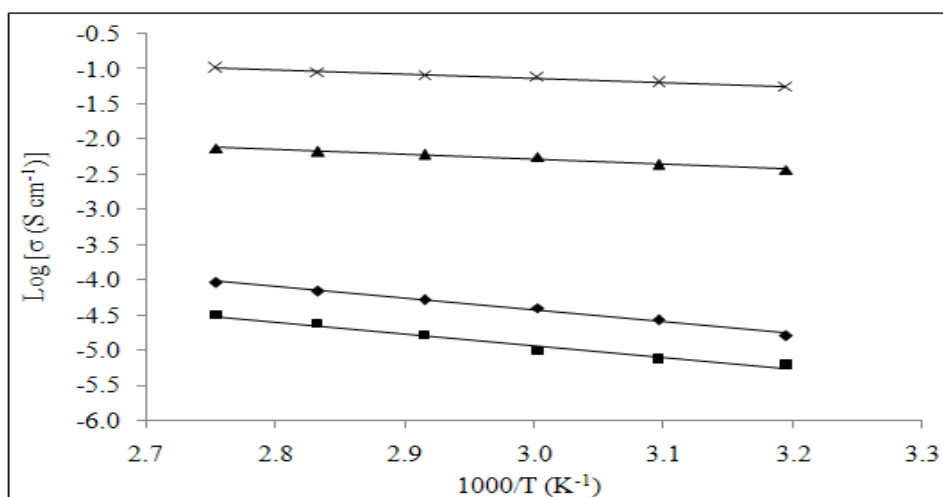


Figure 6.4: Arrhenius plots of log ionic conductivity (σ) against reciprocal temperature for samples CS-20 (\blacklozenge), CS-40 (\blacksquare), CS-60 (\blacktriangle) and CS-80 (\times)

The regression values (R^2) that lies close to unity indicates the linear relationship between log ionic conductivity and reciprocal temperature. This finding reveals that all the tested samples obey Arrhenius theory, indicating that the conductivity mechanism is thermally assisted (Yahya and Arof, 2003). According to this theory, the nature of cation transport in the polymer electrolytes is quite similar to that in ionic crystals, where the ionic conductivity is enhanced through continuous jumping of Li^+ mobile ions into neighbouring vacant sites (Ramesh *et al.*, 2002).

As the temperature increases, the polymer chain acquires faster internal modes in which bond rotations produce segmental motion. This in turn, favours inter or intra-chain ion hopping and accordingly, the ionic conductivity of the polymer electrolyte will be improved with rise in temperature. Since all the tested samples obey a common theory, there is no phase transition in plasticized polymer electrolytes matrix in the temperature range studied. The ionic conductivity of samples that comply with Arrhenius rule can be expressed as below:

$$\sigma = \sigma_0 \exp (-E_a/kT) \quad (6.1)$$

where σ_0 is a pre-exponential factor, E_a is the activation energy in kJ mol^{-1} , k is Boltzmann constant and T is the absolute temperature in K.

Apart from the above discussed point, the activation energy (E_a) values evaluated from the slope of the Arrhenius plot also contribute some relevant information. The variation of E_a for polymer electrolytes with different [Amim] Cl concentration is summarised in Table 6.2 and the result reveal that the E_a decreases effectively with the increase in ionic conductivity value.

Table 6.2: The activation energies (E_a) exhibited by polymer electrolytes with different [Amim] Cl concentration

| Sample | Activation energy, E_a (kJ mol^{-1}) |
|--------|---|
| CS-20 | 13.87 |
| CS-40 | 14.22 |
| CS-60 | 5.79 |
| CS-80 | 4.86 |

This is because the increase in the structural disorderness facilitates fast Li⁺ ion motion in polymer network upon the increase in temperature (Ramesh *et al.*, 2002; Winie *et al.*, 2009). Since the ion transfer is greatly affected by the polymer segmental motion, sample with the lowest E_a value will possess the highest ionic conductivity. In this case it refers to sample CS-80.

6.5 Horizontal attenuated total reflectance-Fourier transform infrared (HATR-FTIR)

FTIR spectroscopy is a powerful tool in detecting the occurrence of possible complexation between the constituents that present in both crystalline and amorphous phase. This was evident via changes in cage peak in terms of shifting in frequency, relative intensity, shape, disappearance of peak and through the formation of new peaks. The FTIR spectra of polymer electrolytes vary according to their compositions and it is independent on the concentration. FTIR spectra of pure CS, pure LiTFSI and CS-0 were presented in Figure 6.5.

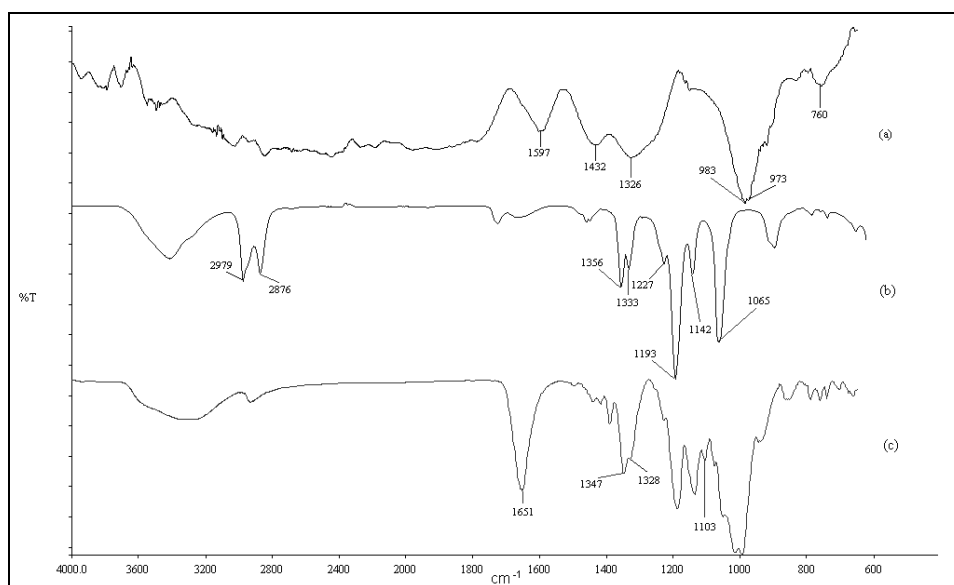


Figure 6.5: FTIR spectra of (a) pure CS, (b) pure LiTFSI and (c) CS-0

The band assignments for pure substances were summarised in Table 6.3 (Ramesh and Lu, 2008; Ning *et al.*, 2009; Ranga Rao *et al.*, 2009).

Table 6.3: Band assignments and wavenumbers exhibited by pure CS, pure LiTFSI and pure [Amim] Cl

| Sample | Band assignments | Wavenumber (cm ⁻¹) |
|-----------|--|--------------------------------|
| CS | δ (O-H) bending of | 1597 |
| | CH ₂ symmetric bending | 1432 |
| | CH ₂ wagging | 1326 |
| | C-O-C | 760-983 |
| LiTFSI | S-CH ₃ | 2979 & 2876 |
| | C-SO ₂ -N | 1356 |
| | -CF ₃ | 1193 |
| | C-F stretch | 1142 |
| | S=O | 1065 |
| [Amim] Cl | H ₂ O in materials | 3369 |
| | Alkyl C-H stretching | 2962, 2941 & 2873 |
| | O-H bending | 1645 |
| | Imidazole ring stretching | 1573 |
| | Imidazole H-C-C & H-C-N bending | 1168 |
| | In-plane Imidazole ring bending | 849 |
| | Out – of – plane C-H bending of imidazole ring | 764 |

Figure 6.5 clearly displays the occurrence of complexation between pure CS and pure LiTFSI by the presence of new peaks at 1651 cm^{-1} and 1103 cm^{-1} in CS-0. This implies that some degree of complexation has occurred and result in new phase formation between LiTFSI and the oxygen atom of the hydroxyl (-OH) group in the polymer backbone. In Figure 6.5 (b), the peak at 1356 cm^{-1} an 1333 cm^{-1} that corresponds to C-SO₂-N bonding in pure LiTFSI was shifted to lower frequency at 1347 cm^{-1} and 1328 cm^{-1} in CS-0. Besides that, the relative intensity of this peak increases from 15 % (pure LiTFSI) to 18 % after complexation with pure CS as shown in Figure 6.6.

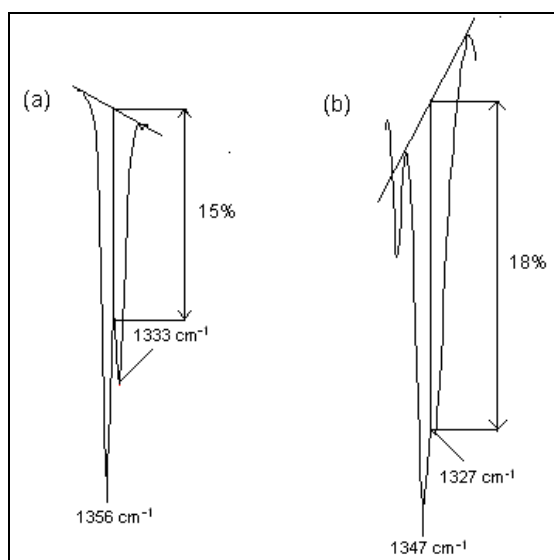


Figure 6.6: The changes in intensity of C-SO₂-N band for (a) pure LiTFSI and (b) CS-0

Apart from that, it also can be seen that the peaks at the range of $1100\text{-}1300\text{ cm}^{-1}$ split from 3 to 4 individual peaks and shifted to lower frequency in CS-0 after complexation with pure CS.

Further evidence on the miscibility of LiTFSI in CS matrix was identified from the shifting of peaks at 1193 (CF_3) and 1142 cm^{-1} (C-F stretch) to lower frequency at 1186 and 1133 cm^{-1} , respectively in CS-0. The shifting of two peaks at 983 and 973 cm^{-1} in pure CS to higher frequency at 1013 and 992 cm^{-1} , respectively in CS-0 proves the complexation. The peaks that fall in the range of 1100-1300 cm^{-1} in pure LiTFSI splits from 3 to 4 individual peaks and allocated at lower frequency in CS-0 upon the complexation with pure CS.

The same technique was relied to identify the possible complexation when different concentration of [Amim] Cl is added in CS: LiTFSI matrix. The FTIR spectra of pure [Amim] Cl, CS-40 and CS-80 were presented in Figure 6.7.

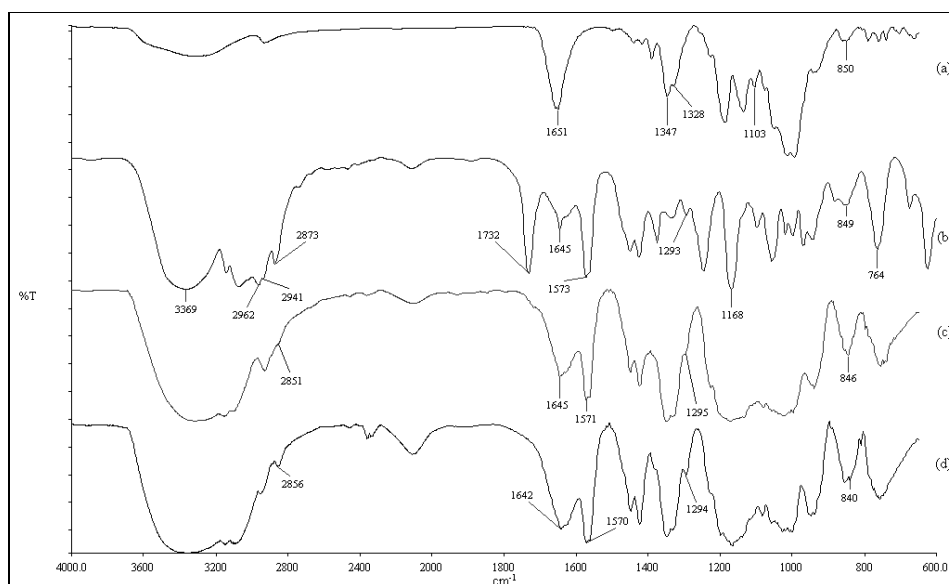


Figure 6.7: FTIR spectra of (a) CS-0, (b) pure [Amim] Cl, (c) CS-20 and (d) CS-80

The peaks that falls in the wavenumber range of 2800-3600 cm^{-1} in pure [Amim] Cl was broaden in Figure 6.7 (c) and (d) due to the overlapping with hydroxyl (-OH) band in CS-0 (Figure 6.7 (a)). This depicts that complexation

occurs at this range. Incorporation of [Amim] Cl leads to an observation of a small shoulder at 2851 cm^{-1} in CS-40 and further addition of [Amim] Cl in the polymer electrolytes leads to the formation of a moderate peak at 2856 cm^{-1} in CS-80. The absence of peak at 1732 cm^{-1} (Figure 3(b)) in the polymer electrolytes containing [Amim] Cl assured the complexation.

A simple overlapping between the peaks at 850 cm^{-1} and 849 cm^{-1} respectively in CS-0 and pure [Amim] Cl results in an intense peak that was shifted to lower frequency as been observed in CS-40 and CS-80 at 846 cm^{-1} and 840 cm^{-1} , respectively. The peak at 1573 cm^{-1} that corresponds to imidazole ring stretching in pure [Amim] Cl interacts with the non-bridging oxygen in CS and as a result this peak was shifted to 1571 cm^{-1} and 1570 cm^{-1} , respectively in CS-40 and CS-80. The occurrence of complexation between CS-0 and pure [Amim] Cl can be further proved by the formation of a shoulder at 1295 cm^{-1} in CS-40. This observation was attributed due to the overlapping with the moderate peak at 1293 cm^{-1} originated from pure [Amim] Cl. Further addition of [Amim] Cl leads to the formation of small peak at 1294 cm^{-1} in CS-80.

The observed changes in the cage peaks indicate that some degree of co-ordination or complexation had occurred between the constituents. The similarity between the FTIR spectra for each sample indicates that LiTFSI and [Amim] Cl are physically bonded with CS.

6.6 Thermogravimetric analysis

Thermogravimetric analysis (TGA) is a reliable technique used to identify the thermal properties of polymer electrolytes in terms of the heat-resistivity and thermal stability based on the maximum decomposition temperature and total weight loss, respectively. Table 6.3 summarises the decomposition temperature and percentage of total weight loss of the selected polymer electrolytes. Figure 6.8 represents the overlay of all four thermogravimetric curves of pure CS, CS-0, CS-20 and CS-80.

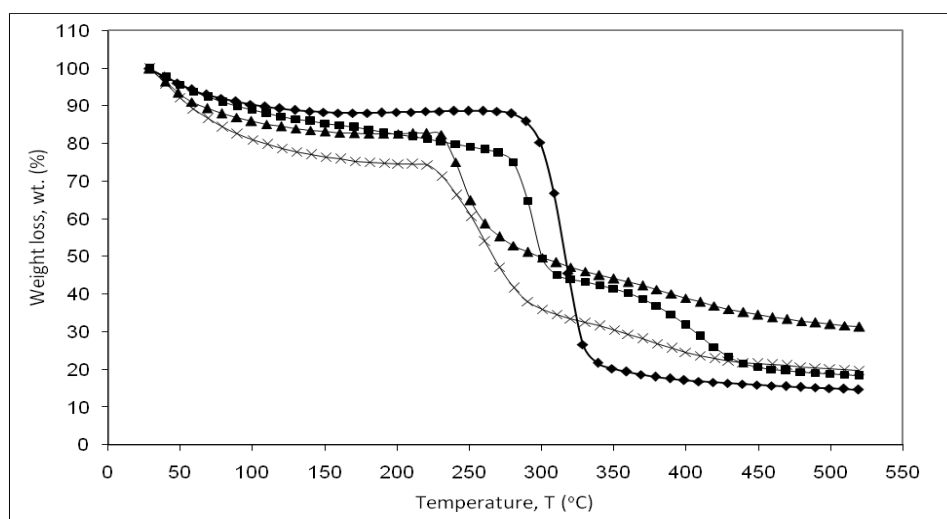


Figure 6.8: Thermogravimetric curves for pure CS (◆), CS-0 (■), CS-20 (▲) and CS-80 (x)

Dehydration and decomposition are the main processes associated with the degradation mechanism of starch. Based on Figure 6.8, an initial weight loss experienced by all the tested samples are quite constant up to 100 °C due to the evaporation of residual solvent and moisture from the samples (Mohamad and Arof, 2007). Further increase in the temperature leads to the

depolymerisation of the polymer electrolytes. According to the results, it can be observed that pure CS decomposed at temperature around 300 °C. At this temperature, the glucose monomers that initially built up the CS will tend to detach from the long polymer chain. Subsequent heating of samples beyond the decomposition temperature will result in carbonisation and ash formation (Mano *et al.*, 2003).

The maximum decomposition temperature of pure CS was displaced to higher temperature above 360 °C upon incorporation of both LiTFSI and [Amim] Cl, this evidences the possible interaction between the constituents. The displacement was due to the decomposition of the organic part both in LiTFSI and [Amim] Cl.

Table 6.4 depicts that the maximum decomposition temperature of pure CS increases upon addition of LiTFSI. This observation reveals the improvement in the heat-resistivity, but this property was found to diminish with the incorporation of [Amim] Cl.

Table 6.4: The maximum decomposition temperatures and percentages of total weight loss for pure CS, CS-0, CS-20 and CS-80

| Sample | Maximum decomposition temperature, T_d (°C) | Total weight loss, wt (%) |
|---------|---|---------------------------|
| Pure CS | 317.56 | 86 |
| CS-0 | 406.67 | 82 |
| CS-20 | 399.09 | 69 |
| CS-80 | 370.99 | 80 |

This is because addition of [Amim] Cl will cause an immense increase in the structural disorderness, thus a small amount of heat will be sufficient to decompose the polymer electrolytes. This explains the decreasing trend in the maximum decomposition temperature with an increase in [Amim] Cl concentration.

In addition, it was found that the thermal stability of the polymer electrolytes improved with the incorporation of LiTFSI and [Amim] Cl. This can be concluded by referring to the decrease in total weight loss experience by the polymer electrolytes as in Table 6.3. Pure CS experienced the highest total weight loss compared to the rest of the plasticised samples and the incorporation of LiTFSI lessens this amount and formulates it to be more thermally stable. This property was further improved with the addition of [Amim] Cl. Upon comparing the thermal stability among [Amim] Cl containing samples, it can be concluded that an increase in [Amim] Cl concentration will result in a decrease in the thermal stability. The observable reduction in this property was attributed to the removal of [Amim] Cl through heating (Mohamad and Arof, 2007). Other plausible reasoning may be due to increase in the structural disorderliness that subsequently weakens the interaction between the connected molecules present in amorphous region. Thus, highly amorphous sample can easily decompose at lower temperature.

CHAPTER 7

RESULTS AND DISCUSSION: SYSTEM IV

7.1 Conductivity studies at room temperature

Figure 7.1 represents the variation of ionic conductivity as a function of [Amim] Cl concentration at room temperature. The results clearly illustrate that the ionic conductivity of the polymer electrolytes significantly improved from 10^{-7} to 10^{-2} S cm^{-1} with increase in [Amim] Cl concentration up to the maximum addition of 80 wt. % of [Amim] Cl.

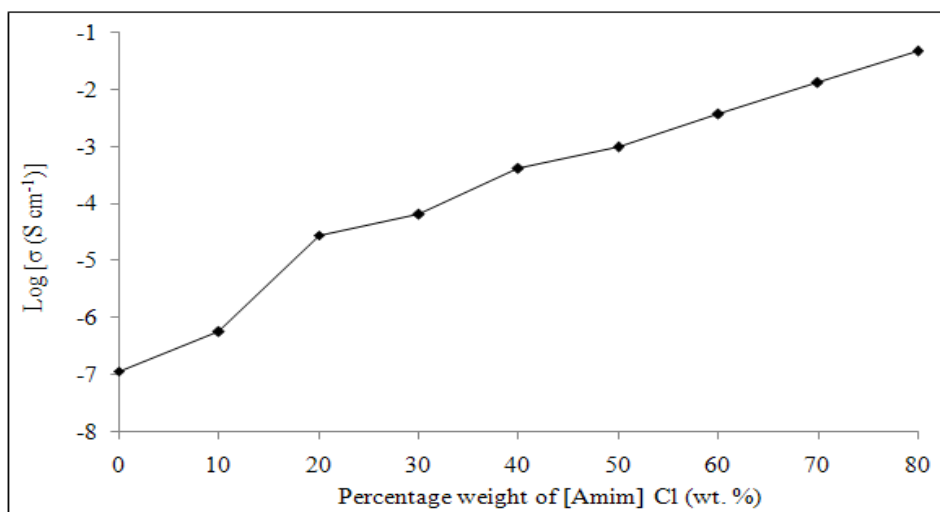


Figure 7.1: The variation of ionic conductivity as a function of [Amim] Cl concentration at room temperature

This observation was accounted to the efficiency of [Amim] Cl in dissociating LiTFSI in CA matrix by weakening the inter-ion Coulomb force between the anions and cations, making more availability of lithium

conducting ions (Li^+) that increases with increase in plasticisation. Besides that, the addition of [Amim] Cl reduces the crystallinity of CA matrix by breaking the bond in $-\text{OAc}$, allowing the oxygen atom to be unoccupied. The unoccupied oxygen was then forms temporary coordination with the mobile Li^+ ions, which enables the free conducting ions to move along the flexible polymer chain. The disruption in crystallinity increases the amorphous phase (disordered arrangement) in the polymer matrix allowing more free volume to be present between the polymer chains and permits a large number of Li^+ ions to move without restrictions and consequently increases the ionic conductivity.

The continuous improvement in the ionic conductivity with increase in [Amim] Cl concentration also can be validated in terms of the increase in the non-bridging ions in [Amim] Cl (Cl^-) after dissociates in the CA matrix. As more [Amim] Cl are added into the CA matrix, the number of transit sites for the Li^+ ions to hop increases. This is because, [Amim] Cl provides an alternative pathway for the conducting ions to hop from one oxygen vacant site to another with ease (Yahya *et al.*, 2006). This in turn, increases the capacity of the ionic transfer which subsequently increases the room temperature ionic conductivity. The highest ionic conductivity was achieved by sample IL-80, with the calculated value of $4.68 \times 10^{-2} \text{ S cm}^{-1}$ at room temperature.

There is no anomalies in the ionic conductivity is observed through out the sample composition owing to the absence of conglomeration within the matrix formed that would cause a decrease in ionic conductivity. This

evidence the effectiveness of the ionised [Amim] Cl particles in consistently increases the amorphous region in the matrix as increase in [Amim] Cl content, providing sufficient free volume for the free mobile ions to resides without having the tendency to form neutral ion multiples.

7.2 Relative viscosity analysis

Figure 7.2 depicts the variation on relative viscosity (η_{rel}) when the ratio of [Amim] Cl is varied in CA: LiTFSI: [Amim] Cl polymer electrolytes at room temperature. This selective scrutiny was performed to provide an insight on the influence of [Amim] Cl concentration on the ionic conductivity based on the relative viscosity which is inversely proportional with each other. The relative viscosity of polymer electrolyte strongly depend on the structural arrangement, where structural disorderness produces greater presence of amorphous phase will gives a lower value for relative viscosity and tempt high ionic conductivity owing to the ease in the Li^+ ions mobility (Sharma and Sekhon, 2007).

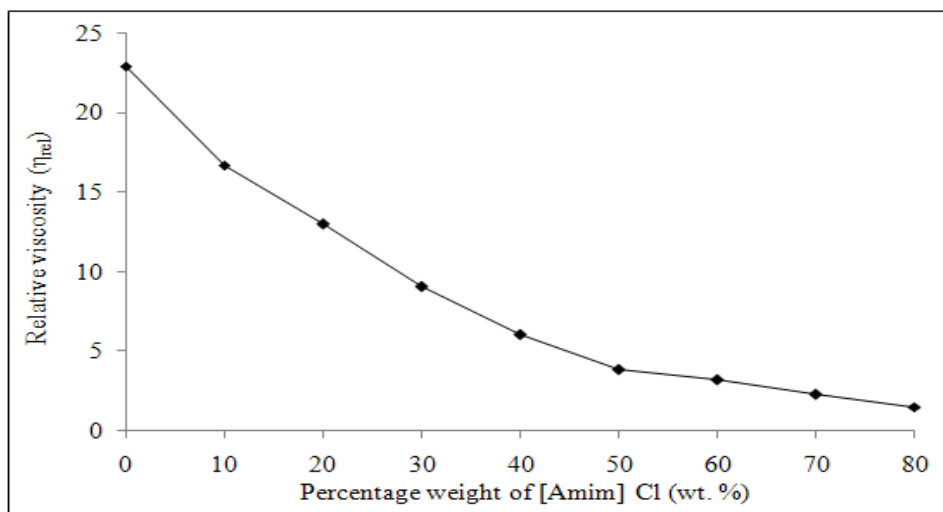


Figure 7.2: Variation of relative viscosity (η_{rel}) as a function of [Amim] Cl concentration at room temperature

With reference to Figure 7.2, it is noted that the initial addition of [Amim] Cl in the CA: LiTFSI system reduces the relative viscosity from 22.91

to 16.69, respectively in IL-0 and IL-10. This intense drop reveals the disruption in the crystalline region of CA: LiTFSI matrix by the presence of free mobile ions (from the ionised [Amim] Cl) which improves the amorphous nature in the polymer electrolytes. This enhances the ion transport mechanism and exhibits an increase in the ionic conductivity. This observation reveals the effectiveness of [Amim] Cl in plasticising the CA: LiTFSI matrix.

Further addition of [Amim] Cl above 20 wt. % exhibits continuous decrease in the polymer electrolytes relative viscosity till the highest addition of 80 wt. % from 12.96 to 1.49. This continuous reduction can be attributed to the increase in the concentration of free ions as more [Amim] Cl particles in polymer electrolytes dissociates. Hence, greater disruption in the crystalline phase will occur that consequently increases the free volume in between the polymer chains. This permits a large number of Li^+ ions to move between the polymer chains, which would contribute to greater ionic conduction (Sharma and Sekhon, 2007). Based on the plot, it can be justified that sample IL-80 is the highest conducting sample since it possesses the lowest relative viscosity.

7.3 Atomic force microscopy (AFM)

AFM analysis was performed to identify the influence of different [Amim] Cl concentration incorporated in CA: LiTFSI matrix in terms of the surface morphology. Figure 7.3 (a-d) shows the AFM images of IL-40, IL-50, IL-60 and IL-80, respectively.

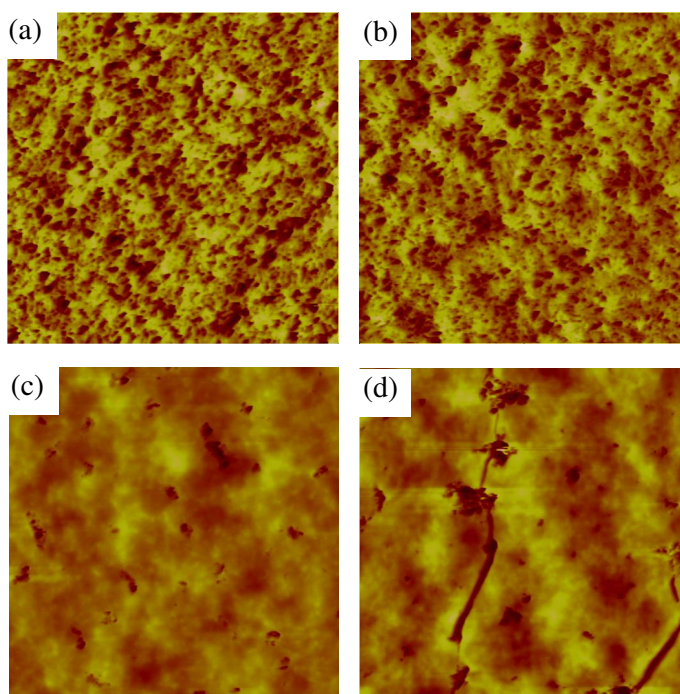


Figure 7.3: AFM images for samples (a) IL-40, (b) IL-50, (c) IL-60 and (d) IL-80

Figure 7.3 (a) illustrates that the sample is highly crystalline based on the compact arrangement of spherulites that contribute to rough surface with the root mean square (Rms) roughness value of 153.78 nm. This rough surface indicates the highly packed arrangement of the atoms (Paradhan *et al.*, 2008) whereas the boundary between the spherulites shows the existence of amorphous phase which is the region concerned in the ion conduction (Paradhan *et al.*, 2008).

The surface roughness in Figure 7.3 (b) was found to diminish upon incorporation of [Amim] Cl in CA: LiTFSI matrix, identified from the reduction in the Rms value to 132.57 nm in sample IL-50 in reference with the Rms value of IL-40. Further increase in [Amim] Cl concentration in the polymer electrolyte contributes to a continuous decrease in the Rms value from 112.36 nm to 105.01 nm respectively in IL-60 and IL-80. This finding verifies the possible disruption of crystalline structure in CA: LiTFSI matrix upon increase in [Amim] Cl content, which enhances the amorphous nature. The increase in the amorphous fraction co-exist between the spherulites boundary (represented by the bright yellowish region) was obvious after the addition of 80 wt. % [Amim] Cl. This reveals that greater structural disorderness took place at this composition, inducing an immense increase in the amorphous region which is potential in improving the ion transfer mechanism.

The changes observed on the surface morphology upon plasticising with increasing [Amim] Cl concentration evident the reduction in the crystallinity of CA matrix. This in turn, enhances the overall amorphous fraction in the materials which ultimately results in the appearance of smooth texture of the surface and followed by a subsequent enhancement in the ionic conductivity.

7.4 Temperature dependent conductivity studies

Figure 7.4 depicts the influence of ionic conductivity exerted by polymer electrolytes with selective composition of [Amim] Cl when varying the reciprocal temperature. This scrutiny sheds some light on the mechanism of ion transport in polymer electrolytes which being performed at the temperature ranging from 313 K to 373 K.

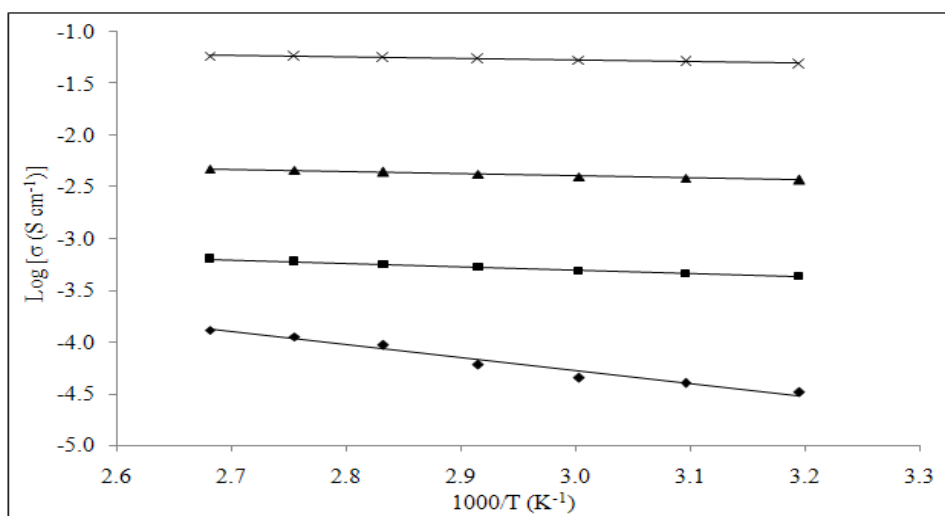


Figure 7.4: Arrhenius plots of log ionic conductivity (σ) against reciprocal temperature for samples IL-20 (\blacklozenge), IL-40 (\blacksquare), IL-60 (\blacktriangle) and IL-80 (\times)

The regression values (R^2) that lies close to unity identifies that a linear relationship co-exists between log ionic conductivity and reciprocal temperature. The observable fact reveals that the conductivity mechanism of all the tested samples is thermally assisted which obeys Arrhenius theory (Yahya and Arof, 2003).

This theory states that as the polymer electrolytes being subjected to a continuous increase in temperature, the polymer chain acquires faster internal modes in which bond rotations produce segmental motion and hence increases the chain flexibility. The resultant flexibility either endorses the mobility of Li^+ ions from one vacant site to another as similar in ionic crystal (Ramesh *et al.*, 2002) or provides the pathway for ions to move. The hopping inter-chain and intra-chain ion movements are responsible in improving the ionic conductivity with rise in temperature.

The Arrhenius behavior possessed by all the tested samples reveal that there is no phase transition in plasticised polymer matrix in the temperature range studied. The ionic conductivity of samples that comply with Arrhenius rule can be expressed as below:

$$\sigma = \sigma_0 \exp(-E_a/kT) \quad (7.1)$$

where σ_0 is a pre-exponential factor, E_a is the activation energy in kJ mol^{-1} , k is Boltzmann constant and T is the absolute temperature in Kelvin (K).

The amorphous nature of the solvent treated CA: LiTFSI matrix provides a greater free volume in the plasticised polymer electrolyte upon increasing in temperature. The highest plasticised sample of IL-80 was displayed at the highest range in the Arrhenius plot revealing the greater presence of amorphous elastomeric phase. This fraction increases gradually with rise in temperature evident from the continuous enhancement in the ionic conductivity.

The slope of the graph is fruitful in calculating the activation energy (E_a) values borne by the tested samples. The variation of E_a for polymer electrolytes with different [Amim] Cl concentration is summarised in Table 7.1 and the result reveals that the E_a decreases effectively with an increase in [Amim] Cl ratio.

Table 7.1: The activation energies (E_a) exhibited by polymer electrolytes with different [Amim] Cl concentration

| Sample | Activation energy, E_a (kJ mol ⁻¹) |
|--------|--|
| IL-20 | 10.49 |
| IL-40 | 2.82 |
| IL-60 | 1.78 |
| IL-80 | 1.25 |

The observed finding correlates to an increase in the concentration of free mobile ions as more [Amim] Cl particles been ionised in the polymer matrix which then contributes to greater structural disorderliness that increases the flexibility of the polymer backbone. Therefore, facilitates fast Li^+ ion motion in the polymer network upon the increase in temperature. A wise comparative between the E_a values of samples with different [Amim] Cl content reveals that the sample with lowest E_a value will possess the highest ionic conductivity as in this case it refers to sample IL-80.

7.5 Conductivity retained studies

This study focused on investigating the influence of [Amim] Cl concentration on the aging effect govern by CA: LiTFSI: [Amim] Cl system. In order to accomplish this, the ionic conductivity of samples IL-0, IL-40 and IL-80 were monitored for the period of 30 days at room temperature and the results are as represented in Figure 7.5. In general, addition of [Amim] Cl improves the aging effect in immense proportion.

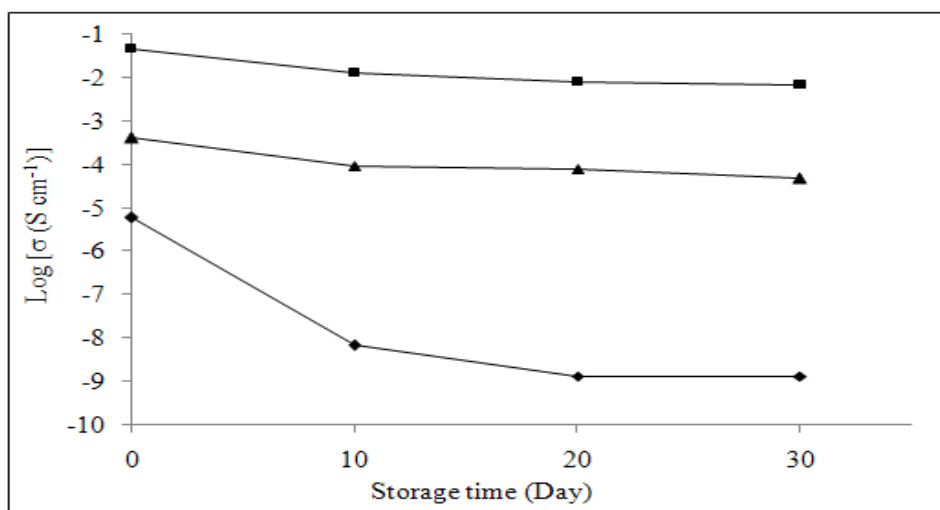


Figure 7.5: Variation of log ionic conductivity with storage time for samples IL-0 (◆), IL-40 (▲) and IL-80 (■) at room temperature

With reference to Figure 7.5, it can be understood that the sample IL-0 experience greater aging effect that is evident through an enormous decline in the ionic conductivity compared to the [Amim] Cl plasticised samples, IL-40 and IL-80. This reveals that IL-0 does not have the ability to retain ionic conductivity for a longer storage time ascribed to high crystallinity which has low liquid retention ability. Thus, the ionic conductivity of the sample will

diminish over time due to the dissipation of liquid component from the matrix.

Incorporation of [Amim] Cl in the polymer electrolytes considerably retains the ionic conductivity over the entire storage time, making it more aging resistant. This is due to the increase in the polar functional groups that exhibits higher liquid retention capability (Ramesh and Arof, 2009). Therefore, more traces of liquid component will be trapped between the CA matrix providing a dilute medium to ease the Li^+ ions motion and hence retaining the ionic conductivity over the storage time (Ramesh and Arof, 2009).

On the other hand, it can also be found that all the tested polymer electrolytes do not exhibit any dramatic change in ionic conductivity after 10 days. This proves that the samples retain high chemical integrity overcoming the solvent leakage limitation over storage time. In view of the results, it can be established that the increase in [Amim] Cl concentration in CA: LiTFSI matrix continuous improves the stability of polymer electrolytes by retaining their integrity over the storage time.

7.6 Horizontal attenuated total reflectance-Fourier transform infrared (HATR-FTIR)

FTIR spectroscopy is a well recognized fingerprinting technique used in perceiving the occurrence of complexation between the constituents present in both crystalline and amorphous phase. The complexation between the constituents were deduced by relying on the changes in the cage peak in terms of the frequency shifting, relative intensity, shape, disappearance of existing peak and even through the formation of new peaks. The FTIR spectra of polymer electrolytes vary according to their compositions and it is independent of concentration.

The band assignments for pure substances are summarised in Table 7.2 (da Maria *et al.*, 2003; Ramesh and Lu, 2008; Ranga Rao *et al.*, 2009).

Table 7.2: Band assignments and wavenumbers exhibited by pure CA, pure LiTFSI and pure [Amim] Cl

| Sample | Band assignments | Wavenumber (cm ⁻¹) |
|--------|------------------------------------|--------------------------------|
| CA | O-H stretching | 3445 |
| | C-H stretching (CH ₃) | 2932 |
| | C-H stretching (CH ₂) | 2879 |
| | C=O symmetric | 1734 |
| | C=O asymmetric | 1656 |
| | CH ₂ bending | 1436 |
| | C-H bending | 1369 |
| | C-O-C asymmetric bridge stretching | 1158 |

Table 7.2 continued: Band assignments and wavenumbers exhibited by pure CA, pure LiTFSI and pure [Amim] Cl

| Sample | Band assignments | Wavenumber (cm⁻¹) |
|------------------|--|-------------------------------------|
| CA | C-O-C stretching of the pyrose ring | 1032 |
| | δ C-H | 901 |
| LiTFSI | O-H | 3419 |
| | S-CH ₃ | 2979 & 2876 |
| | C-SO ₂ -N | 1356 |
| | -CF ₃ | 1193 |
| | C-F stretch | 1142 |
| | S=O | 1065 |
| | H ₂ O in materials | 3369 |
| [Amim] Cl | Alkyl C-H stretching | 2962, 2941 & 2873 |
| | O-H bending | 1645 |
| | Imidazole ring stretching | 1573 |
| | Imidazole H-C-C & H-C-N bending | 1168 |
| | In-plane Imidazole ring bending | 849 |
| | Out – of – plane C-H bending of imidazole ring | 764 |

The occurrence of complexation between pure CA and pure LiTFSI was confirmed based on the alternations in IL-0 spectrum as portrayed in Figure 7.6.

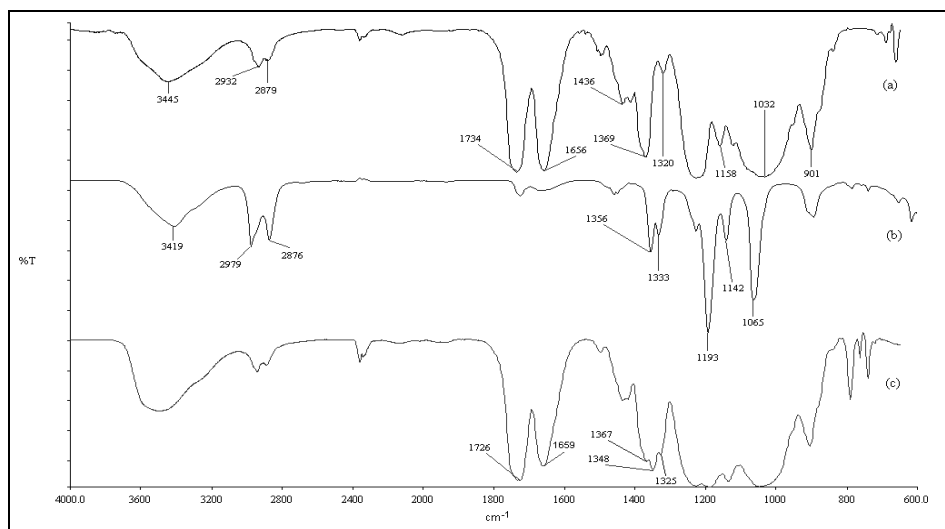


Figure 7.6: FTIR spectra of (a) pure CA, (b) pure LiTFSI and (c) IL-0

The first evidence of complexation was based on the characteristic peak of C=O symmetric present at 1734 cm^{-1} in pure CA which shifted to lower frequency at 1726 cm^{-1} in IL-0 after complexation with LiTFSI. The shifting of this characteristic peak proves the occurrence of complexation at this frequency range between the Li^+ ions and oxygen atoms in polymer backbone. The relative intensity of the interacted band was found to reduce from 64 % (pure CA) to 55 % (IL-0) upon complexation as represented in Figure 7.7.

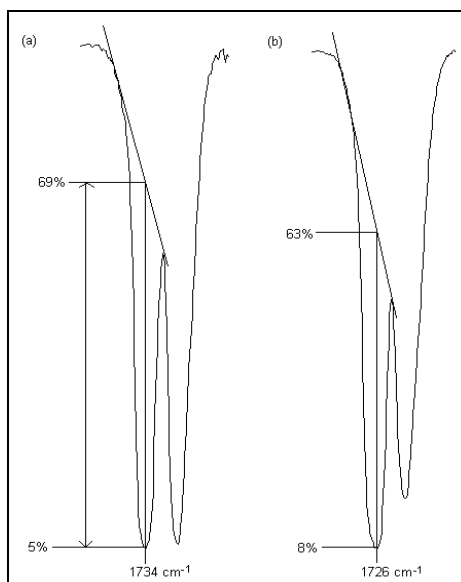


Figure 7.7: The changes in intensity of C=O symmetric band for (a) pure CA and (b) IL-0

The occurrence of complexation between CA and LiTFSI was further verified by the band broadening effect at the frequency range of 1030-1250 cm^{-1} which results from the simple peak overlapping. The disappearance of peak at 1320 cm^{-1} in pure CA upon addition of LiTFSI reveals the detachment of acetate (-Ac) from the -OAc functional group via occurrence of complexation. A simple peak overlapping between a single intense peak at 1369 cm^{-1} in Figure 7.6 (a) with two peaks at 1356 and 1333 cm^{-1} in Figure 7.6 (b) results in a three peaks formation at 1367, 1348 and 1325 cm^{-1} in Figure 7.6 (c). The observed change in the shape of peak was one of the evidence to prove the complexation. The initial relative intensity of the peak that co-exists at 1656 cm^{-1} in pure CA was 61 % and upon complexation with LiTFSI this peak was displaced to higher frequency at 1659 cm^{-1} with reduced relative intensity (47 %) in IL-0. The shifting to higher frequency evidence weaker interaction between Li^+ ions and oxygen

atom in C=O asymmetric.

The same technique was relied to deduce the possible complexation between different concentrations of [Amim] Cl in CA: LiTFSI matrix. The dominant interest to find out the possible complexation was gained by sample IL-40 and IL-80 whereby the respective spectra are presented in Figure 7.8 together with IL-0 and pure [Amim] Cl.

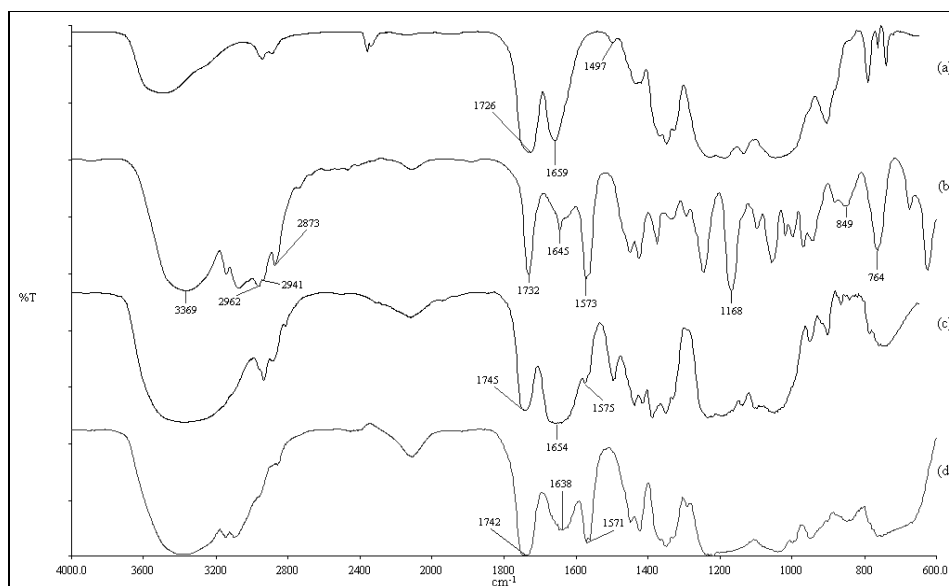


Figure 7.8: FTIR spectra of (a) IL-0, (b) pure [Amim] Cl, (c) IL-40 and (d) IL-80

The first evidence to prove the complexation was based on the displacement of C=O characteristic peak initially present at 1726 cm^{-1} in Figure 7.8 (a) and 1732 cm^{-1} in Figure 7.8 (b). The C=O peak was shifted to higher frequency at 1745 cm^{-1} in Figure 7.8 (c) upon complexation and further addition of [Amim] Cl induce the displacement at lower frequency in Figure 7.8 (d) with the value of 1742 cm^{-1} . The observed reduction in frequency with further

addition of [Amim] Cl suggests greater interaction between increasing amount of Li^+ ions and oxygen atom. Apart from this, the respective peak also experienced an increase in the relative intensity with further addition of [Amim] Cl with the calculated value from 54 % in IL-40 to 70 % in IL-80. The increase in the relative intensity evidence the increase in number of Li^+ ions that form complexation with the oxygen atom at this frequency, upon increase in [Amim] Cl concentration that effectively overcomes the inter-coulombic force between the different charged of ions in LiTFSI making more availability of Li^+ ions.

Other evidence to prove the complexation was focused on the peak at 1573 cm^{-1} in pure [Amim] Cl. This intense peak was changed to a small peak (1575 cm^{-1}) as in IL-40 upon the complexation with CA and LiTFSI and further addition of [Amim] Cl in the polymer electrolytes induce to an increase in the relative intensity as in IL-80 (1571 cm^{-1}). The small peak that co-exist at 1497 cm^{-1} in IL-0 becomes more intense without no change in its frequency upon the complexation with [Amim] Cl and consequently absent at higher [Amim] Cl containing sample, IL-80.

A simple overlapping between the peak at 1659 cm^{-1} and 1645 cm^{-1} , respectively in IL-0 and pure [Amim] Cl is able to deduce the complexation. The result of this overlapping is the presence of broader peak both in IL-40 and IL-80, respectively at 1654 and 1638 cm^{-1} . The broad peak at 1654 cm^{-1} in IL-40 was shifted to lower wavelength at 1638 cm^{-1} in IL-80, showing greater extent of interaction between the Li^+ ions and oxygen atom. This

reference peak was found to decline in broadness as more [Amim] Cl is incorporated which would attribute to the decrease in the number of Li^+ ions that forms complexation with the oxygen atom at this frequency. This was attributed to the high concentration of nitrogen atom in [Amim] Cl which have higher tendency to form coordination with Li^+ ions than the oxygen owing to its better electron donating feature.

7.7 X-ray diffractometry (XRD)

X-ray diffraction measurements were performed on polymer electrolytes plasticised with different [Amim] Cl ratio to deduce the degree of amorphocity at room temperature. The diffraction patterns of pure CA (thin film), pure LiTFSI, IL-0, IL-40 and IL-80 are represented in Figure 7.9.

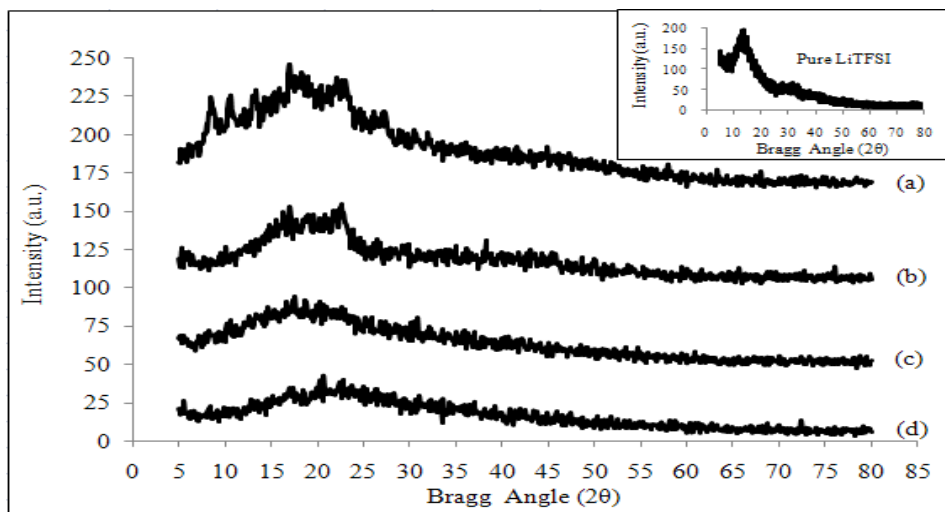


Figure 7.9: The diffraction patterns of (a) pure CA (thin film), (b) IL-0, (c) IL-40, (d) IL-80 and pure LiTFSI in the inset

In view of the inset graph in Figure 7.9, the appearance of a single intense diffraction peak centered at $2\theta = 13.5^\circ$ shows the typical characteristic of a crystalline microstructure of pure LiTFSI. This intense peak was found to be absent in sample IL-0 associated to the complete dissolution of the LiTFSI in CA matrix which further suppresses the crystalline phase. This was validated through the disappearance of the moderate intense peak at $2\theta = 8.5^\circ$, 10.5° and 13.5° in pure CA and accompanied by a substantial broadening in the IL-0 diffraction peak. Additionally, the peaks that remained undisturbed upon

addition of LiTFSI at $2\theta = 17.5^\circ$ and 23.5° in IL-0 were found to disrupt after the addition of [Amim] Cl and a substantial broadening in the diffraction peak occurs in the angle range between 5° to 30° with increase in [Amim] Cl concentration.

It also been observed that the diffraction peak substantially increased in broadness and decreased in intensity with the increase in [Amim] Cl concentration in the polymer electrolytes. This observation indicates the considerable decrease in the degree of crystallinity of CA matrix as more [Amim] Cl particles are being incorporated in the polymer electrolytes. The associated reduction in crystallinity was caused by the significant structural reorganisation imposed by [Amim] Cl that induces greater structural disorderness. Hence, the increase in amorphous region will cause a decline in the energy barrier to the segmental motion of the polymer electrolytes (Baskaran *et al.*, 2006) which undeniably improves the charge transfer mechanism and induces greater ionic conductivity.

With reference to the results, it can be clarified that greater structural conversion occurs predominantly in the highest [Amim] Cl containing sample, IL-80 allowing it to present in highly amorphous morphology which provides greater free volume for the movement of Li^+ ions. Thus, this polymer electrolyte composition appears as the highest conducting sample.

7.8 Frequency dependence of loss tangent studies

This scrutiny was performed in order to understand the Li^+ ions transport mechanism when different concentration of [Amim] Cl was incorporated in CA: LiTFSI matrix. Figure 7.10 represents the plot of $\tan \delta$ versus frequency for samples IL-0, IL-40 and IL-80.

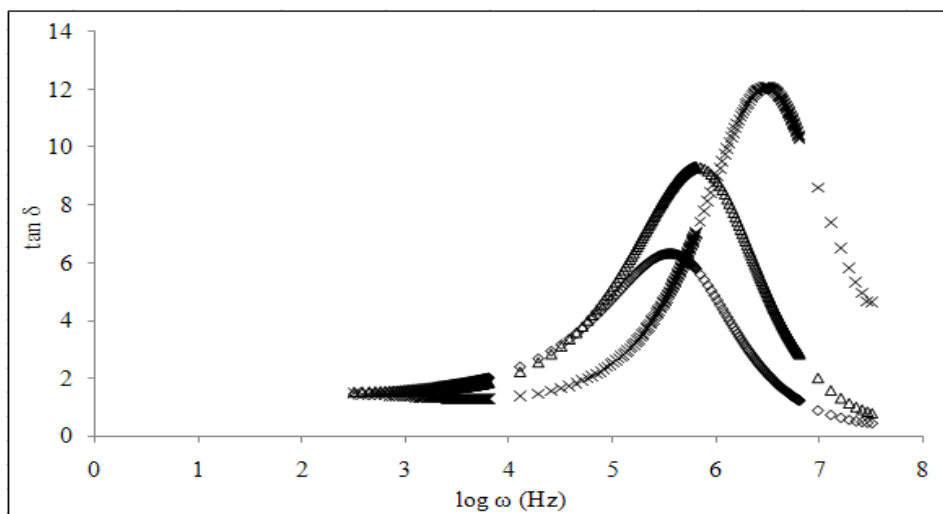


Figure 7.10: Variation of $\tan \delta$ with angular frequency for IL-0 (\diamond), IL-40 (Δ) and IL-80 (x) at room temperature

In view of the plot, it was found that the appearance of peak both in non-plasticised and plasticised samples discloses the presence of relaxation dipoles in Li^+ ions in all the tested samples (Paradhan *et al.*, 2008). This confirms that the presence of [Amim] Cl in the matrix still persist the mobility of Li^+ ions in enhancing the ionic conductivity.

Apart from the earlier discussed point, this plot also provides an insight on the Li^+ ions mobility upon presence of different [Amim] Cl content. It can

be visualised that the loss tangent peaks was continuously shifted towards higher frequencies upon increase in the [Amim] Cl content based on the relaxation frequency ($\log_{\max} \omega$) values as tabulated in Table 7.3.

Table 7.3: Relaxation frequencies of samples with different [Amim] Cl content

| Sample | Relaxation frequency, $\log \omega_m$ (Hz) |
|--------|--|
| IL-0 | 5.60 |
| IL-40 | 5.80 |
| IL-80 | 6.50 |

This shifting phenomenon illustrates the reduction in the relaxation time of Li^+ ions, which speed up its mobility as more amorphous elastomeric region available with increase in [Amim] Cl concentration in the polymer electrolytes matrix (Paradhan *et al.*, 2008).

The increase in the number of non-bridging ions in [Amim] Cl (Cl^-) increases the capacity of the Li^+ ions transfer which may contribute to such findings. This non-bridging ions act as an additional transit site that permits the mobility of Li^+ ions through polymer backbone. The presence of the transit site shorten the distance for the Li^+ ions to hop from one unoccupied oxygen to another in polymer chain acquiring less energy loss for the mobility of ion. Hence, frequent migrations of mobile ions are expected to occur that crucial in enhancing the ionic conductivity.

The influence of different addition of [Amim] Cl concentration on the number of Li^+ ions that participate in ion conduction can be determined based on the magnitude of the $\tan \delta$ (Azizi Samir *et al.*, 2004). The magnitude of the $\tan \delta$ increases upon increase in [Amim] Cl concentration which indicates the increase in the number of Li^+ ions that participates in the relaxation process to assist the ionic conductivity as ascribed by the area under the loss factor peak. The increase in Li^+ ions concentration evidence the efficiency of [Amim] Cl in overcoming the inter-coulombic force in LiTFSI, making more Li^+ ions to be available in enhancing the ionic conductivity.

As the concentration of [Amim] Cl in polymer electrolytes is increased, more mobile free ions (obtained from the dissolution of [Amim] Cl in the CA matrix) will exist and accelerate the segmental motion by increasing the available free volume through structural conversion. The resultant increment will be beneficial for the ease in Li^+ ion transfer that significantly exerts high ionic conductivity. The highest conducting sample was achieved by IL-80 which had relatively fast segmental motion coupled with greater presence of Li^+ ions.

7.9 Thermogravimetric analysis

Figure 7.11 shows the normalized TGA thermograms of CA: LiTFSI: [Amim] Cl polymer electrolytes with different amount of [Amim] Cl.

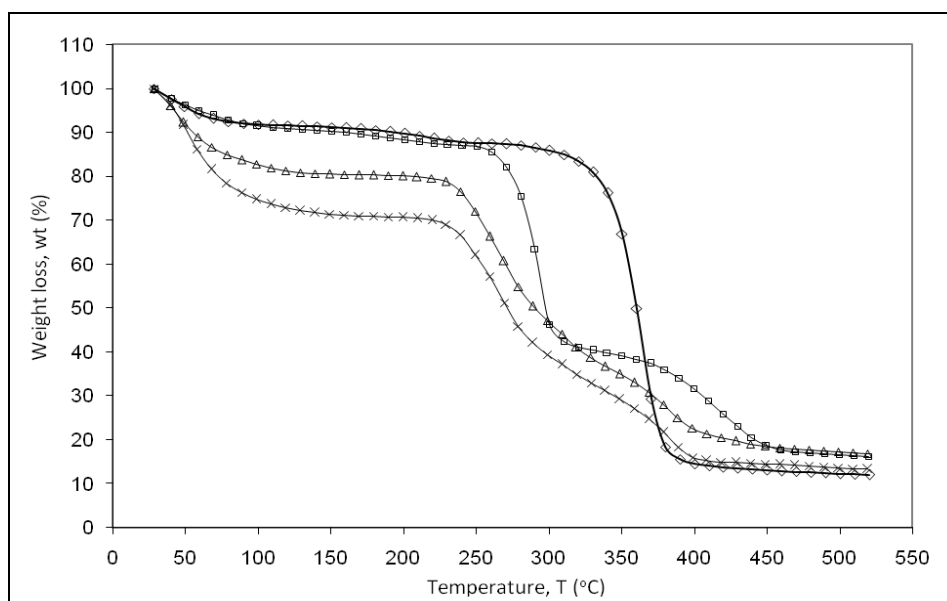


Figure 7.11: Thermogravimetric curves for pure CA (◇), IL-0 (□), IL-40 (Δ) and IL-80 (x)

The change in the thermal properties of the CA: LiTFSI: [Amim] Cl system with increasing [Amim] Cl concentration is shown in Table 7.4.

Table 7.4: Maximum decomposition temperature and percentage of total weight loss for pure CA, IL-0, IL-40 and IL-80 by TGA analysis

| Sample | Maximum decomposition temperature, T_d ($^{\circ}\text{C}$) | Total weight loss, wt. (%) |
|---------|---|----------------------------|
| Pure CA | 363.40 | 88 |
| IL-0 | 414.01 | 84 |
| IL-40 | 380.96 | 85 |
| IL-80 | 380.93 | 87 |

The tabulated results prove that the heat-resistivity and thermal stability of pure CA is improved upon addition of LiTFSI. The increase in heat-resistivity was attributed to the decomposition of the organic part in LiTFSI giving rise to the displacement of the maximum decomposition temperature to a higher level. The decrease in the total weight loss evident the improvement in the thermal stability of IL-0.

In addition, the incorporation of [Amim] Cl does exert significant alteration in the thermal properties. It was found that the samples tend to lose both the heat-resistivity and thermal stability once plasticised with increasing concentration of [Amim] Cl. The decline in maximum decomposition temperature was attributed to the diffusion of atoms in the amorphous region results in weaker bond which can easily decompose at lower temperature with a minimum amount of energy. Whereas the reduction in the thermal stability

was attributed to the removal of [Amim] Cl upon the heating process (Mohamad and Arof, 2007).

The plasticised samples experience decomposition at the temperature above 375 °C which was higher than the one observed for pure CA. Hence it can be concluded that the presence of an appropriate amount of [Amim] Cl in CA: LiTFSI matrix enhances the thermal properties making it suitable in electronic device application.

CHAPTER 8

RESULTS AND DISCUSSION: COMPARISON

8.1 Comparison of CS: LiTFSI matrix plasticised with DES and [Amim] Cl

Figure 8.1 shows the variation of logarithm ionic conductivity when the CS: LiTFSI matrix is plasticised with different DES and [Amim] Cl concentration.

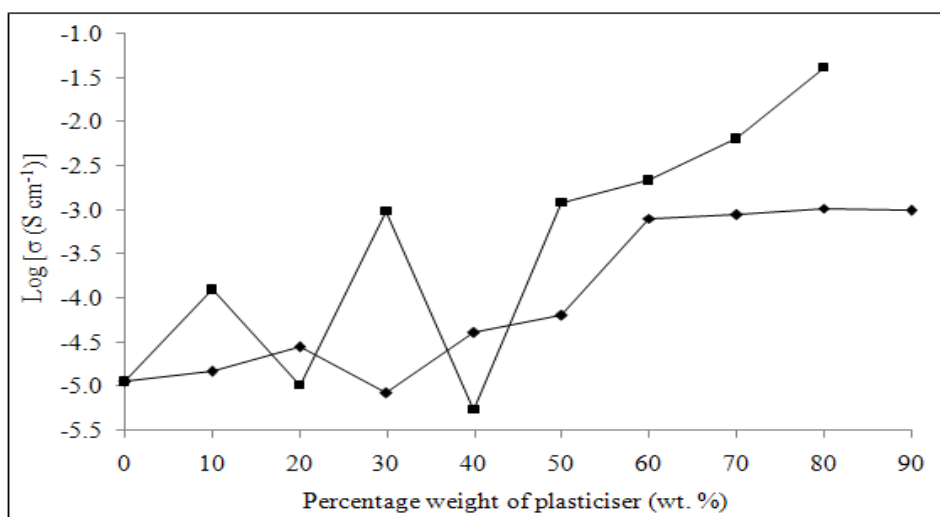


Figure 8.1: Variation of logarithm ionic conductivity of CS: LiTFSI matrix as a function of plasticiser content for DES (♦) and [Amim] Cl (■)

In view of the plot, rapid fluctuations occur at lower concentration of ionic solvent and more consistent increasing trend was obtained at higher plasticization. The fluctuation in [Amim] Cl system is greater than the compared system. In DES containing system, the high viscosity of DES inhibits dramatic fluctuations in ionic conductivity at lower concentration owing to the low mobility of the ionized DES particles.

At higher [Amim] Cl plasticisation, almost uniform increase in ionic conductivity is accounted whereas in DES containing system almost constant rise is obtained. The uniform increase evidence the greater ionic mobility own by [Amim] Cl in excessively suppresses the crystalline region and increases the ion transport mechanism. The almost constant trend in ionic conductivity was obtained upon achieving the maximum collapse in CS crystallinity even at 60 wt. % of DES and enhancement in the ionic conductivity is still observed due to the mobility of Li^+ ions along the DES transit site.

8.2 Comparison of CA: LiTFSI matrix plasticised with DES and [Amim] Cl

Figure 8.2 shows the variation of logarithm ionic conductivity when the CA: LiTFSI matrix is plasticised with different DES and [Amim] Cl concentration.

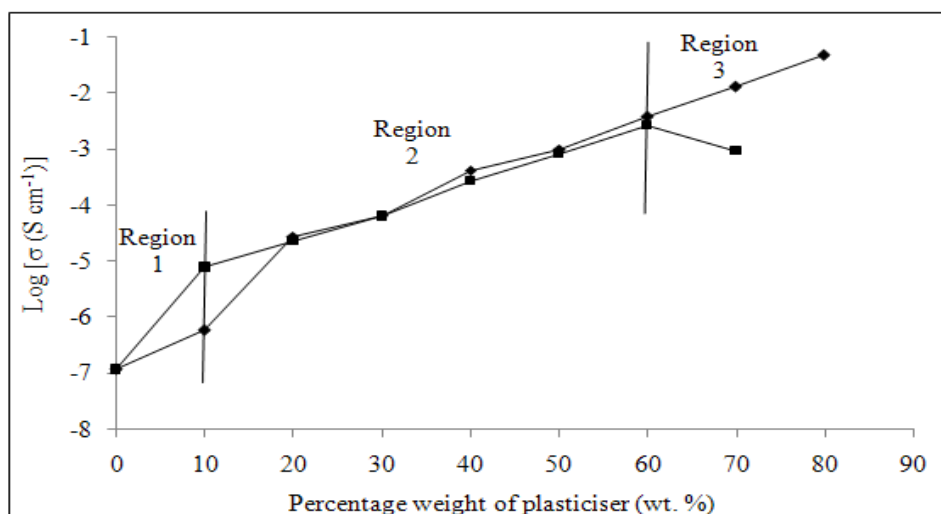


Figure 8.2: Variation of logarithm ionic conductivity of CA: LiTFSI matrix as a function of plasticiser content for DES (■) and [Amim] Cl (◆)

Based on the Region 1, it can be rectified that a dramatic increase in ionic conductivity was observed for system containing DES at initial incorporation nevertheless a slight increase in [Amim] Cl plasticised sample. The observed increase in ionic conductivity evidence the collapse in the crystallinity of CA and the extent of disruption was prominently induced by DES compared to [Amim] Cl. This is because DES contains greater number of transit site for lithium coordination that eases its mobility to enhance the ionic conductivity.

In Region 2, continuous increase in ionic conductivity is observed in both systems attributed to the increase in the mobility of Li^+ ions. The highest ionic conductivity of DES sample in Region 1 is overrode by [Amim] Cl containing samples as increase in the plasticiser content. This is due to the high viscosity of DES which may form small aggregates in the matrix when the amount is increased, which consequently restricts the Li^+ ions mobility. The low viscosity of [Amim] Cl allows the ionic species to possess greater mobility which then involves in ion conduction.

At higher plasticisation (Region 3), anomaly was identified in DES system accounting to the presence of larger aggregates that suppresses the Li^+ ions mobility owing to the high viscosity of DES. Whereas a consistent increase in ionic conductivity was observed for the matrix plasticised with [Amim] Cl. This holds to the low viscosity feature of [Amim] Cl that does not have the tendency to form neutral ion multiples upon conglomeration.

The highest ionic conductivity value of DES system ($10^{-3} \text{ S cm}^{-1}$) is only lower in one order compared to the [Amim] Cl plasticised system ($10^{-2} \text{ S cm}^{-1}$) which far higher for application practice. This meant DES may serve as an alternative in tailoring the insulating properties of natural polymer owing to its low cost and non-toxic nature, which are the lacking properties in pure ionic liquid, [Amim] Cl.

8.3 Comparison between CS and CA based polymer electrolytes

A wise comparison between the two utilised host polymers in developing separators bring to light the profound properties of CA based polymer electrolytes. Reference to the conductivity plot in Figure 8.1 and 8.2, no fluctuation in ionic conductivity is observed at lower plasticiser content as compared to CS based polymer electrolytes. This is due to greater structural disorderness in CA matrix that provides sufficient free volume for the free ions to reside in the matrix without conglomerating.

Besides that, the ionic conductivity of CA based polymer electrolytes are higher than the CS based when compared with similar plasticiser type. This is attributed to the low crystallinity in CA ascribed to the larger acetate (-Ac) group that connected to oxygen, which can easily detach from the polar functional group. Whereas in CS the oxygen atom is connected to hydrogen which is smaller in radius compared to -Ac, thus it well fit into the lattice forming high crystalline structure. The ease in obtaining the vacant oxygen in CA matrix promises greater migration of lithium conducting ions (Li^+) that subsequently enhances the ionic conductivity. The good mechanical stability of CA thin film promises its utilisation as a separator in batteries.

CHAPTER 9

CONCLUSION

Four different series of biodegradable polymer electrolytes were fabricated by plasticising the matrix formed by either CS or CA in the combination of LITFSI with either DES or [Amim] Cl by solution casting technique. The incorporation of DES/[Amim] Cl in plasticising the CS/CA: LiTFSI matrix was valued primarily due to its capability in increasing the amorphous elastomeric phase that crucial in enhancing the ionic transport mechanism for better conductivity enhancement. The highest conducting sample with the respective composition for all the four systems were identified as $1.04 \times 10^{-3} \text{ S cm}^{-1}$ (14 wt. %: 6 wt. %: 80 wt. %), $2.61 \times 10^{-3} \text{ S cm}^{-1}$ (28 wt. %: 12 wt. %: 60 wt. %), $4.18 \times 10^{-2} \text{ S cm}^{-1}$ (14 wt. %: 6 wt. %: 80 wt. %) and $4.68 \times 10^{-2} \text{ S cm}^{-1}$ (14 wt. %: 6 wt. %: 80 wt. %), respectively in system I, II, III and IV at room temperature. The conductivity-temperature plots for all four developed systems obey Arrhenius theory in which the conductivity enhancement is thermally assisted. The ionic conductivity of polymer electrolytes was found to retain over a storage time as increase in plasticisation. The occurrence of some degree of co-ordination between the chemical constituents was revealed by the FTIR spectra and the resultant structural disorderliness was evident by the XRD, relative viscosity, fluidity and surface morphology analysis. The variation in the mobility of Li^+ ions upon increase in the plasticisation was revealed by the placement of tangent loss peak. The thermal properties of plasticised polymer electrolytes were

found to diminish as increase in either DES or [Amim] Cl concentration. All four developed polymer electrolytes well fit as a separator in electronic devices owing to its high ionic conductivity and biodegradable nature.

REFERENCES

- Abbott, A. P., Capper, G., Davies, D. L., Rasheed, R. K. & Shikotra, P. (2005). Selective extraction of metals from mixed oxide matrixes using choline-based ionic liquids. *Inorganic Chemistry*, 44 (19), 6497 – 6499.
- Abbott, A. P., Capper, G., Davies, D. L., Rasheed, R. K. & Tambyrajah, V. (2003). Novel solvent properties of choline chloride/urea mixtures. *Chemical Communications*, 39 (1), 70 – 71.
- Abbott, A. P., Capper, G., McKenzie, K. J & Ryder, K. S. (2006). Voltammetric and impedance studies of the electropolishing of type 316 stainless steel in a choline chloride based ionic liquid. *Electrochimica Acta*, 51 (21), 4420 – 4425.
- Abbott, A. P., Capper, G., McKenzie, K. J & Ryder, K. S. (2007). Electrodeposition of zinc–tin alloys from deep eutectic solvents based on choline chloride. *Journal of Electroanalytical Chemistry*, 599 (2), 288 – 294.
- Abraham, K. M. & Alamgir, M. (1994). Room temperature polymer electrolytes and batteries based on them. *Solid State Ionics*, 70-71 (1), 20 – 26.

- Ahmad, S., Saxena, T. K., Ahmad, S. & Agnithotry, S. A. (2006). The effect of nanosized TiO₂ addition on poly (methylmethacrylate) based polymer electrolytes. *Journal of Power Sources*, 159 (1), 205 – 209.
- Anantha, P. S. & Hariharan, K. (2005). Physical and Ionic transport studies on poly (ethylene oxide) NaNO₃ polymer electrolyte system. *Solid State Ionics*, 176 (1-2), 155 – 162.
- Appetecchi, G. B. & Passerini, S. (2000). PEO-carbon composite lithium polymer electrolyte. *Electrochimica Acta*, 45 (13), 2139 – 2145.
- Armand, M. B. (1986). Polymer electrolytes. *Annual Review of Materials Science*, 16, 245 – 261.
- Atwell, W. A., Hood, L. F., Lineback, D. R., Varriano- Marston, E. & Zobel, H. F. (1988). The terminology and methodology associated with basic starch phenomena. *Cereal Foods World*, 33 (3), 306 – 311.
- Azizi Samir, M. A. S., Alloin, F., Sanchez, J. –Y., Gorecki, W., & Dufresne, A. (2004). Nanocomposite polymer electrolytes based on poly(oxyethylene) and cellulose nanocrystals. *The Journal of Physical Chemistry B*, 108 (30), 10845 – 10852.

- Bakkar, A. & Neubert, V. (2007). Electrodeposition onto magnesium in air and water stable ionic liquids: From corrosion to successful plating. *Electrochemistry Communications*, 9 (9), 2428 – 2435.
- Baskaran, R., Selvasekarapandian, S., Kuwata, N., Kawamura, J. & Hattori, T. (2006). Conductivity and thermal studies of blend polymer electrolytes based on PVAc-PMMA. *Solid State Ionics*, 177 (26-32), 2679 – 2682.
- Beninca, C., Demiate, I. M., Lacerda, L. G., Carvalho Filho, M. A. S., Ionashiro, M. & Schnitzler, E. (2008). Thermal behavior of corn starch granules modified by acid treatment at 30 and 50°C. *Eclética Química*, 33 (3), 13 – 18.
- Berthier, C., Gorecki, W., Minier, M., Armand, M. B., Chabagno, J. M. & Rigaud, P. (1983). Microscopic investigation of ionic conductivity in alkali metals salts-poly (ethylene oxide) adducts. *Solid State Ionics*, 11 (1), 91 – 95.
- Croce, F., Sacchetti, S. & Scrosati, B. (2006). Advanced, lithium batteries based on high-performance composite polymer electrolytes. *Journal of Power Sources*, 162 (1), 685 – 689.

- Cuissinat, C., Navard, P. & Heinze, T. (2008). Swelling and dissolution of cellulose. Part IV: Free floating cotton and wood fibres in ionic liquids. *Carbohydrate Polymer*, 72 (4), 590 – 596.
- da Conceição, M., Lucena, C., de Alencar, A.E.V., Mazzeto, S.E. & de Soares, S. (2003). The effect of additives on the thermal degradation of cellulose acetate. *Polymer Degradation Stability*, 80 (1), 149 – 155.
- Dale, P. J., Samantilleke, A. P., Shivagan, D. D. & Peter, L. M. (2007). Synthesis of cadmium and zinc semiconductor compounds from an ionic liquid containing choline chloride and urea. *Thin Solid Films*, 515 (15), 5751 – 5754.
- Deka, M. & Kumar, A. (2009). Ionic transport in P(VdF–HFP)–PEO based novel microporous polymer electrolytes. *Bulletin of Material Science*, 32 (6), 627 – 632.
- Fenton, D. E., Parker, J. M. & Wright, P. V. (1973). Complexes of alkali metal ions with poly (ethylene oxide). *Polymer*, 14 (11), 589- 589.
- Feuillade, G. & Perche, P. (1975). Ion-conductive macromolecular gels and membrane for solid lithium cells. *Journal of Applied Electrochemistry*, 5 (1), 63 – 69.

- Finkenstadt, V. & Willett, J. L. (2005). Preparation and characterization of electroactive biopolymers. *Macromolecular Symposia*, 227 (1), 367 – 371.
- Fischer, F., Rigacci, A., Pirard, R., Berthon-Fabry, S. & Achard, P. (2006). Cellulose-based aerogels. *Polymer*, 47 (22), 7636 – 7645.
- Foropoulos, Jr. J. & DesMarteau, D. D. (1984). Synthesis, properties, and reactions of bis((trifluoromethyl)sulfonyl) imide, $(\text{CF}_3\text{SO}_2)_2\text{NH}$. *Inorganic Chemistry*, 23 (23), 3720 – 3723.
- Forsyth, S. A. & MacFarlane, D. R. (2003). 1-Alkyl-3-methylbenzotriazolium salts: Ionic solvents and electrolytes. *Journal of Materials Chemistry*, 13 (10), 2451 – 2456.
- Furasawa, S., Kamiyama, A. & Tsurui, T. (2008). Fabrication and ionic conductivity of amorphous lithium meta-silicate thin film. *Solid State Ionics*, 179 (15-16), 536 – 542.
- Hou, Y., Gu, Y., Zhang, S., Yang, F., Ding, H. & Shan, Y. (2008). Novel binary eutectic mixtures based on imidazole. *Journal of Molecular Liquids*, 143 (2-3) 154 – 159.
- Jhong, H. -R., Wong, D. S. -H., Wan, C. -C., Wang, Y. -Y. & Wei, T. -C. (2009). A novel deep eutectic solvent-based ionic liquid used as

- electrolyte for dye-sensitized solar cells. *Electrochemistry Communications*, 11 (1), 209 – 211.
- Kim, D. W. & Sun, Y. K. (2001). Electrochemical characterization of gel polymer electrolytes prepared with porous membranes. *Journal of Power Sources*, 102 (1-2), 41 – 45.
- Kumar, G. G., Kim, P., Kim, A. R., Nahm, K. S. & Elizabeth, R. N. (2009). Structural, thermal and ion transport studies of different particle size nanocomposite fillers incorporated PVDF–HFP hybrid membranes. *Materials Chemistry Physics*, 115 (1), 40 – 46.
- Low, S. P., Ahmad, A. & Rahman, M. Y. A. (2010). Effect of ethylene carbonate plasticizer and TiO₂ nanoparticles on 49 % poly (methyl methacrylate) grafted natural rubber-based polymer electrolyte. *Ionics*, 16 (9), 821 – 826.
- Maccallum, J. R., Tomlin, A. S., Tunstall, D. P. & Vincent, C. A. (1988). A mixed-salt polyether electrolyte: PEO-LiCF₃SO₃-NaI. *British Polymer Journal*, 20 (3), 203 – 206.
- Mano, J. F., Koniarova, D. & Reis, R. L. (2003). Thermal properties of thermoplastic starch/synthetic polymer blends with potential biomedical capability. *Journal of Materials Science Materials in Medicine*, 14 (2), 127 – 135.

- Minier, M., Berthier, C. & Gorecki, W. (1984). Thermal analysis and NMR study of poly (ethylene oxide) complex electrolyte: PEO (LiCF₃SO₃). *Journal de Physique*, 45 (4), 739 –744.
- Mohamad, A. A. & Arof, A. K. (2007). Plasticized alkaline solid polymer electrolyte system. *Materials Letters*, 61 (14-15), 3096 – 3099.
- Morita, M., Tanaka, H., Ishikawa, M. & Matsuda, Y. (1996). Effects of crown ethers on the electrochemical properties of polymeric solid electrolytes consisting of poly (ethylene oxide)-grafted poly(methyl methacrylates). *Solid State Ionics*, 86 – 88 (1), 401 – 405.
- Naoi, K., Mori, M., Naruoka, Y., Lamanna, W. M. & Atanasoski, R. (1999). The surface film formed on a lithium metal electrode in a new imide electrolyte, lithium bis(perfluoroethylsulfonylimide) [LiN(C₂F₅SO₂)(2)]. *Journal of the Electrochemical Society*, 146 (2), 462 – 469.
- Ning, W., Xingxiang, Z., Haihui, L., & Benqiao, H. (2009). 1-Allyl-3-methylimidazolium chloride plasticized-corn starch as solid biopolymer electrolytes. *Carbohydrate Polymers*, 76 (3), 482 – 484.
- Osada, Y. & Kajiwara, K. (2001). The Fundamentals. *Gels Handbook Volume 1*. (pp. 65 – 85). San Diego, CA: Academic Press.

- Paradhan, D. K., Choudhary, R. N. P. & Samantaray, B. K. (2008). Studies of dielectric relaxation and AC conductivity behavior of plasticized polymer nanocomposite electrolytes. *International Journal of Electrochemical Science*, 3 (5), 597 – 608.
- Pradhan, D. K., Samantaray, B. K., Choudhary, R. N. P. & Thakur, A. K. (2005). Effect of plasticizer on structure–property relationship in composite polymer electrolytes. *Journal of Power Sources*, 139 (1-2), 384 – 393.
- Rajendran, S. & Uma, T. (2000). Effect of ZrO₂ on conductivity of PVC-LiBF₄-DBP polymer electrolytes. *Materials Letter*, 44 (3-4), 208 – 214.
- Rajendran, S., Kannan, R. & Mahendran, O. (2001). Ionic conductivity studies in PMMA–PEO hybrid polymer electrolytes with lithium salts. *Journal of Power Sources*, 96 (2), 406 – 410.
- Rajendran, S., Sivakumar, M. & Subadevi, R. (2004). Investigations on the effect of various plasticizers in PVA-PMMA solid polymer blend electrolytes. *Materials Letters*, 58 (5), 641 – 649.
- Ramesh, S. & Arof, A. K. (2000). Electrical conductivity studies of polyvinyl chloride-based electrolytes with double salt system. *Solid State Ionics*, 136 – 137 (1 – 2), 1197 – 1200.

- Ramesh, S. & Arof, A. K. (2001). Structural, thermal and electrochemical cell characteristics of poly (vinyl chloride)-based polymer electrolytes. *Journal of Power Sources*, 99 (1-2), 41 – 47.
- Ramesh, S. & Arof, A. K. (2009). A study incorporating nano-sized silica into PVC-blend-based polymer electrolytes for lithium batteries. *Journal of Materials Science*, 44 (23), 6404 – 6407.
- Ramesh, S. & Lu, S. -C. (2008). Effect of nanosized silica in poly (methyl methacrylate)-lithium bis(trifluoromethanesulfonyl)imide based polymer electrolytes. *Journal of Power Sources*, 185 (2), 1439 – 1443.
- Ramesh, S., Teh, G. B., Louh, R. -F., Hou, Y. K., Sin, P. Y. & Yi, L. J. (2010). Preparation and characterization of plasticized high molecular weight PVC based polymer electrolytes. *Sadhana*, 35 (1), 87 – 95.
- Ramesh, S., Yahya, A. H. & Arof, A. K. (2002). Dielectric behavior of PVC based polymer electrolytes. *Solid State Ionics*, 152-153, 291 – 294.
- Ranga Rao, G., Rajkumar, T. & Babu Varghese (2009). Synthesis and characterization of 1-butyl 3-methylimidazolium phosphomolybdate molecular salt. *Solid State Sciences*, 11 (1), 36 – 42.
- Ratner, M. A. & Shriver, D. F. (1988). Ion transport in solvent-free polymers. *Chemical Reviews*, 88 (1), 109 – 124.

Reverchon, E. & Cardea, S. (2007). Production of controlled polymeric foams by supercritical CO₂. *The Journal of Supercritical Fluids*, 40 (1), 144 – 152.

Rodrigues Filho, G., Monteiro, D. S., Meireles, C. d. de., Assuncao, R. M. N., Cerqueira, D. A., Barud, H. S., Ribeiro, S. J. L. & Messadeq, Y. (2008). Synthesis and characterization of cellulose acetate produced from recycled newspaper. *Carbohydrate Polymers*, 73 (1), 74 – 82.

Saikia, D., Chen-Yang, Y. W., Chen, Y. T., Li, Y. K. & Lin, S. I. (2008). Investigation of ionic conductivity of composite gel polymer electrolyte membranes based on P(VDF-HFP), LiClO₄ and silica aerogel for lithium ion battery. *Desalination*, 234 (1-3), 24 – 32.

Saikia, D., Chen-Yang, Y. W., Chen, Y. T., Li, Y. K. & Lin, S. I. (2009). ⁷Li NMR spectroscopy and ion conduction mechanism of composite gel polymer electrolyte: A comparative study with variation of salt and plasticizer with filler. *Electrochimica Acta*, 54 (4), 1218 – 1227.

Selvakumar, M. & Krishna Bhat, D. (2008). LiClO₄ doped cellulose acetate as biodegradable polymer electrolyte for supercapacitors. *Journal of Applied Polymer Science*, 110 (1), 594 – 602.

- Sharma, J. P. & Sekhon, S. S. (2007). Nanodispersed polymer gel electrolytes: Conductivity modification with the addition of PMMA and fumed silica. *Solid State Ionics*, 178 (5-6), 439 – 445.
- Shriver, D. F., Papke, B. L., Ratner, M. A., Dupon, R., Wong, T. & Brodwin, M. (1981). Structure and ion transport in polymer-salt complexes. *Solid State Ionics*, 5, 83 – 88.
- Singh, P. K., Kim, K. -W. & Rhee, H. -W. (2008). Electrical, optical and photoelectrochemical studies on a solid PEO-polymer electrolyte doped with low viscosity ionic liquid. *Electrochemistry Communications*, 10 (11), 1769 – 1772.
- Siva Kumar, J., Subrahmanyam, A. R., Jaipal Reddy, M. & Subba Rao, U. V. (2006). Preparation and study of properties of polymer electrolyte system (PEO + NaClO₃). *Materials Letters*, 60 (28), 3346 – 3349.
- Song, J. Y., Wang, Y. Y. & Wan, C. C. (1999). Review of gel-type polymer electrolytes for lithium-ion batteries. *Journal of Power Sources*, 77 (2), 183 – 197.
- Subramaniam, C. K., Ramya, C. S. & Ramya, K. (2008). Performance of EDLCs using Nafion and Nafion composites as electrolyte. *Journal of Applied Electrochemistry*, 41 (2), 197 – 206.

- Swatloski, R. P., Spear, S. K., Holbrey, J. D. & Rogers, R. D. (2002). Dissolution of cellulose with ionic liquids. *Journal of American Chemical Society*, 124 (18), 4974 – 4975.
- Takeda, Y., Tomooka, S. & Hizukuri, S. (1993). Structures of branched and linear molecules of rice amylose. *Carbohydrate Research*, 246 (1), 267 – 272.
- Takegawa, A., Murakami, M. –a., Kaneko, Y. & Kadokawa, J. –i. (2010). Preparation of chitin/cellulose composite gels and films with ionic liquids. *Carbohydrate Polymers*, 79 (1), 85 – 90.
- Uma, T., Mahalingam, T. & Stimming, U. (2003). Mixed phase solid polymer electrolytes based on poly (methylmethacrylate). *Materials Chemistry and Physics*, 82 (2), 478 – 483.
- Vieira, D. F. & Pawlicka, A. (2010). Optimization of performances of gelatin/LiBF₄-based polymer electrolytes by plasticizing effects. *Electrochimica Acta*, 55 (4), 1489 – 1494.
- Vieira, D. F., Avellaneda, C. O. & Pawlicka, A. (2007). Conductivity study of a gelatin-based polymer electrolyte. *Electrochimica Acta*, 53 (4), 1404 – 1408.

- Wang, Y. J., Pan, Y., Wang, L., Pang, M. J. & Chen, L. S. (2005). Conductivity studies of plasticized PEO-Lithium chlorate-FIC filler composite polymer electrolytes. *Materials Letters*, 59 (24-25), 3021 – 3026.
- Webber, A. (1991). Conductivity and viscosity of solutions of LiCF_3SO_3 , $\text{Li}(\text{CF}_3\text{SO}_2)_2\text{N}$, and their mixtures. *Journal of the Electrochemical Society*, 138 (9), 2586 – 2590.
- Winie, T., Ramesh, S. & Arof, A. K. (2009). Studies on the structure and transport properties of hexanoyl chitosan-based polymer electrolytes. *Physica B: Condensed Matter*, 404 (21), 4308 – 4311.
- Wright, P. V. (1975). Electrical conductivity in ionic complexes of poly (ethylene oxide). *British Polymer Journal*, 7 (5), 319 – 327.
- Wu, R. -L., Wang, X. -L., Li, F., Li, H. -Z. & Wang, Y. -Z. (2009). Green composite films prepared from cellulose, starch and lignin in room-temperature ionic liquid. *Bioresource Technology*, 100 (9), 2569 – 2574.
- Xu, Y. X., Kim, K. M., Hanna, M. A. & Nag, D. (2005). Chitosan-starch composite film: preparation and characterization. *Industrial Crops and Products*, 21 (2), 185 – 192.

- Xu, Y., Miladinov, V. & Hanna, M. A. (2004). Synthesis and characterization of starch acetates with high degree of substitution. *Cereal Chemistry*, 81 (6), 735 – 740.
- Yahya, M. Z. A. & Arof, A. K. (2003). Effect of oleic acid plasticizer on chitosan–lithium acetate solid polymer electrolytes. *European Polymer Journal*, 39 (5), 897 – 902.
- Yahya, M. Z. A., Ali, A. M. M., Mohammat, M. F., Hanafiah, M. A. K. M., Mustaffa, M., Ibrahim, S. C., Darus, Z. M. & Harun, M. K. (2006). Ionic conduction model in salted chitosan membranes plasticized with fatty acid. *Journal of Applied Sciences*, 6 (6), 1287 – 1291.
- Yue, Z., McEwen, I. J. & Cowie, J. M. G. (2003). Novel gel polymer electrolytes based on a cellulose ester with PEO side chains. *Solid State Ionics*, 156 (1-2), 155 – 162.
- Zhang, J., Wu, T., Chen, S., Feng, P. & Bu, X. (2009). Versatile structure-directing roles of deep eutectic solvents and their implication in generation of porosity and open metal sites for gas storage. *Angewandte Chemie International Edition in English*, 48 (19), 3486 – 3490.
- Zhang, S. S. (2006). A review on the separators of liquid electrolyte Li-ion batteries. *Journal of Power Sources*, 164 (1), 351 – 364.

